Argonne NATIONAL LABORATORY

ANL/RERTR/TM-10-21

Feasibility Analyses for HEU to LEU Fuel Conversion of the Laue Langevin Institute (ILL) High Flux Reactor (RHF)

Nuclear Engineering Division

About Argonne National Laboratory

Argonne is a U.S. Department of Energy laboratory managed by UChicago Argonne, LLC under contract DE-AC02-06CH11357. The Laboratory's main facility is outside Chicago, at 9700 South Cass Avenue, Argonne, Illinois 60439. For information about Argonne and its pioneering science and technology programs, see www.anl.gov.

Availability of This Report

This report is available, at no cost, at http://www.osti.gov/bridge. It is also available on paper to the U.S. Department of Energy and its contractors, for a processing fee, from:

U.S. Department of Energy
Office of Scientific and Technical Information
P.O. Box 62
Oak Ridge, TN 37831-0062
phone (865) 576-8401
fax (865) 576-5728
reports@adonis.osti.gov

Disclaimer

This report was prepared as an account of work sponsored by an agency of the United States Government. Neither the United States Government nor any agency thereof, nor UChicago Argonne, LLC, nor any of their employees or officers, makes any warranty, express or implied, or assumes any legal liability or responsibility for the accuracy, completeness, or usefulness of any information, apparatus, product, or process disclosed, or represents that its use would not infringe privately owned rights. Reference herein to any specific commercial product, process, or service by trade name, trademark, manufacturer, or otherwise, does not necessarily constitute or imply its endorsement, recommendation, or favoring by the United States Government or any agency thereof. The views and opinions of document authors expressed herein do not necessarily state or reflect those of the United States Government or any agency thereof, Argonne National Laboratory, or UChicago Argonne, LLC.

ANL/RERTR/TM-10-21

Feasibility Analyses for HEU to LEU Fuel Conversion of the Laue Langevin Institute (ILL) High Flux Reactor (RHF)

by
A. Bergeron, A. Tentner, and J.G. Stevens
Nuclear Engineering Division, Argonne National Laboratory

July 31, 2010

Abstract

The High Flux Reactor (RHF) of the Laue Langevin Institute (ILL) based in Grenoble, France is a research reactor designed primarily for neutron beam experiments for fundamental science. It delivers one of the most intense neutron fluxes worldwide, with an unperturbed thermal neutron flux of 1.5×10^{15} n/cm^2/s in its reflector. The reactor has been conceived to operate at a nuclear power of 57 MW but currently operates at 52 MW. The reactor currently uses a Highly Enriched Uranium (HEU) fuel.

In the framework of its non-proliferation policies, the international community presently aims to minimize the amount of nuclear material available that could be used for nuclear weapons. In this geopolitical context, most worldwide research and test reactors have already started a program of conversion to the use of Low Enriched Uranium (LEU) fuel. A new type of LEU fuel based on a mixture of uranium and molybdenum (UMo) is expected to allow the conversion of compact high performance reactors like the RHF.

This report presents the results of reactor design, performance and steady state safety analyses for conversion of the RHF from the use of HEU fuel to the use of UMo LEU fuel. The objective of this work was to show that is feasible, under a set of manufacturing assumptions, to design a new RHF fuel element that could safely replace the HEU element currently used. The new proposed design has been developed to maximize performance, minimize changes and preserve strong safety margins.

Neutronics and thermal-hydraulics models of the RHF have been developed and qualified by benchmark against experiments and/or against other codes and models. The models developed were then used to evaluate the RHF performance if LEU UMo were to replace the current HEU fuel "meat" without any geometric change to the fuel plates. Results of these direct replacement analyses have shown a significant degradation of the RHF performance, in terms of both neutron flux and cycle length.

Consequently, ANL and ILL have collaborated to investigate alternative designs. A promising candidate design has been selected and studied, increasing the total amount of fuel without changing the external plate dimensions by relocating the burnable poison. In this way, changes required in the fuel element are reasonably small. With this new design, neutronics analyses have shown that performance could be maintained at a high level: 2 day decrease of cycle length (to 47.5 days at 58.3 MW) and 1-2% decrease of brightness in the cold and hot sources in comparison to the current typical operation. In addition, studies have shown that the thermal-hydraulic and shutdown margins for the proposed LEU design would satisfy technical specifications.

Table of Contents

Abstract i

Table of Contents ii

List of Figures v

List of Tables viii

I Introduction 1

II General Description of Facility and Reactor 2

III LEU Fuel & Manufacturing Assumptions 8

IV Neutronic Analyses 11

4.1 Description of Neutronic Codes, Model and Methodologies 11

4.2 Computational Model Credibility – HEU Core 15

4.2.1 k-effective of a Fresh Core with Critical Control Rod 15

4.2.2 Control Rod Worth 15

4.2.3 Safety Rod Worths 16

4.2.4 Heat Flux, Heat Generation and Fission Density 20

4.2.5 Cycle Length 22

4.2.6 Kinetic Parameters 24

4.2.7 Summary of ANL Codes and Model Performance 25

4.3 Evaluation of LEU Direct Replacement Core Performance 26

4.3.1 Cycle Length 26

4.3.2 Neutron Flux 27

4.3.3 Conclusions of LEU Direct Replacement Analysis 30

4.4 New LEU Plate Design 31

4.4.1 Ways to Optimize the Conversion 31

4.4.2 The Extended Meat Configuration 31

4.4.3 The Relocated Poison Configuration 33

4.4.3.1 Determination of the Maximum Heat Flux & Maximum Fission Density 34

4.4.3.2 Nature and Density of Poison 35

4.4.3.3 Dimensions of the Poison Belt 35

4.4.3.4 Cadmium and Gadolinium Foils 37

4.4.3.5 Optimal Boron Powder Poison Belt 37

4.4.3.6 Cycle Length 40

4.4.3.7 Safety and Control Rod Worths 42

4.4.3.8 Beta-effective 44

4.4.3.9 Brightness in the Beam Tubes 44

4.5 Summary of Neutronic Analyses 46

V Thermal-Hydraulic Analyses 48

5.0 Introduction 48

5.1 Review of RHF Geometry 48

5.2 The CFD Model of the HEU RHF Reactor 50

5.2.1 The CFD Computational Mesh 51

5.2.2 Material Properties 53

5.2.3 Boundary Conditions 53

5.2.4 Power Source 54

5.3 Preliminary CFD Analysis of the HEU RHF Reactor 55

5.3.1 Results of Preliminary HEU RHF Analysis.....55

5.3.2 Discussion of Preliminary HEU RHF Analysis Results 63

5.4 Preliminary CFD Analysis of the LEU RHF Reactor.....65

5.4.1 The CFD LEU Model 65

5.4.1.1 The Refined CFD Computational Mesh for the HEU and LEU Models.....65

5.4.1.2 Boundary Conditions 66

5.4.1.3 Power Source 67

5.4.2 Results of Preliminary LEU RHF Analysis 69

5.4.2.1 Coolant and Cladding Temperature Results 69

5.4.2.2 Predictions of Margin to Boiling 75

5.5 Thermal-Hydraulic Conclusions.....82

VI Summary of Differences between HEU and LEU Design 83

VII Conclusions 85

References..... 86

List of Figures

Figure [2.1]: General view of the ILL facility 2

Figure [2.2]: Picture of the reactor taken above the light water pool 3

Figure [2.3]: Cross section of the reactor.....4

Figure [2.4]: Top view of the reactor.....5

Figure [2.5]: RHF HEU fuel plate dimensions before and after bending.....6

Figure [2.6]: RHF fuel element dimensions 7

Figure [4.2]: Top view of the MCNP RHF heavy water tank model 13

Figure [4.3]: Two top views of the modeled fuel element.....14

Figure [4.4]: Cross section of the modeled heavy water tank.....14

Figure [4.5]: Deviation from Critical for the various HEU core CR and SR modeled 20

Figure [4.6]: Heat flux distribution in the hot channel obtained with MCNP for HEU ...22

Figure [4.7]: k-effective evolution obtained by REBUS-MCNP for an HEU core.....23

Figure [4.8]: Control rod motion evolution obtained by VESTA for an HEU core.....24

Figure [4.9]: Comparison of cycle length obtained for several LEU configurations 26

Figure [4.10]: Neutron spectrum for fresh HEU and LEU Direct Replacement Configuration 29

Figure [4.11]: Thermal neutron mapping in the median plane of an HEU core.....29

Figure [4.12]: Thermal neutron mapping in the median plane of an LEU Direct Replacement Configuration 29

Figure [4.13]: Scheme of HEU and extended meat LEU plates.....31

Figure [4.14]: Cycle length for extended meat LEU configuration.....32

Figure [4.15]: Heat flux in the hot strip for HEU and the LEU extended meat core.....33

Figure [4.16]: Maximum heat flux as a function of the thickness of the poison belt.....36

Figure [4.17]: Maximum heat flux as a function of the height of the poison belt.....37

Figure [4.18]: Evolution of the minimum boron density required to satisfy the limit of qualification. Control area of ~0.3x0.3cm².....38

Figure [4.19]: Evolution of the minimum boron density required to satisfy the limit of qualification. Asymptotic method....39

Figure [4.20]: Control rod motion evolution obtained by VESTA with the automatic critical search. LEU Relocated Poison Configuration....41

Figure [4.21]: k-effective evolution obtained by REBUS-MCNP using VESTA control rod positions. LEU Relocated Poison Configuration....41

Figure [4.22]: Safety rod worths for HEU and for LEU Relocated Poison Configuration where the control rod is fully inserted....42

Figure [4.23]: Safety rod worths for HEU and for LEU Relocated Poison Configuration where the control rod is fully withdrawn....43

Figure [4.24]: Brightness in the Horizontal Cold Source (HCS) evaluated for HEU and LEU Relocated Poison Configuration....45

Figure [4.25]: Brightness in the Horizontal Cold Source (VCS) evaluated for HEU and LEU Relocated Poison Configuration....45

Figure [5.1]: Fuel element overview....48

Figure [5.2]: HEU fuel plate dimensions....49

Figure [5.3]: Cross section through the coolant channels and fuel plates, viewed from the +z direction....50

Figure [5.4]: Cross section through the centerline of the HEU fuel plate, viewed from the -y direction....51

Figure [5.5]: CFD Computational mesh detail....52

Figure [5.6]: Coolant temperatures [K] at the center of cells adjacent to the fuel plate surface, view from the -y direction....56

Figure [5.7]: Coolant temperatures [K] at the fuel plate surface, view from the -y direction, from the -y direction....57

Figure [5.8]: Cladding temperature [K] at the center of cells at plate surface, (adjacent to coolant), view from the -y direction....58

Figure [5.9]: Temperature distribution [K] in a cross section at z = - 0.5 m from inlet....59

Figure [5.10]: Coolant temperature distribution [K] in a cross section at z = - 0.5 m from inlet....60

Figure [5.11]: Coolant axial velocity distribution, cross section at z = - 0.5 m from inlet....61

Figure [5.12]: Coolant transverse velocity distribution (v component, m/s), cross section at z = - 0.5 m from inlet 62

Figure [5.13]: Pressure distribution in the coolant channel (relative to PREF = 4.0 bar), view from the -y direction.....63

Figure [5.14]: Cross section through the centerline of the LEU fuel plate, viewed from the -y direction 66

Figure [5.15]: Axial power distribution in the LEU Relocated Poison Configuration at the outermost radial cell.....68

Figure [5.16]: Axial power distribution in the HEU fuel meat at the outermost radial cell.....69

Figure [5.17]: Coolant temperatures [K] at the center of cells adjacent to the LEU fuel plate surface, view from the -y direction 71

Figure [5.18]: Coolant temperatures [K] at the fuel plate surface, view from the -y direction 72

Figure [5.19]: Cladding temperature [K] at the center of cells at plate surface, (adjacent to coolant), view from the -y direction 73

Figure [5.20]: Axial distribution of cladding surface temperature at the radial location of T(wall surface, max) for the LEU fuel plate.....74

Figure [5.21]: Axial distribution of cladding surface temperature at the radial location of T(wall surface, max) for the HEU fuel plate 75

Figure [5.22]: Axial distribution of DTsat, DTong, and DTfnb for the LEU Relocated Poison Configuration 77

Figure [5.23]: Axial distribution of DTsat, DTonb, and DTfnb for the HEU fuel plate ...78

Figure [5.24]: Variation of the margins to saturation, ONB, and FNB with relative RHF power for the LEU Relocated Poison Configuration.....79

Figure [5.25]: Variation of the margins to saturation, ONB, and FNB with relative RHF power for the HEU fuel.....80

Figure [6.1]: Scheme and dimensions for HEU and LEU Relocated Poison plates 83

List of Tables

Table [3.1]: Isotopic description of the LEU UMo fuel as used in the calculations.....8

Table [4.1]: k-effective predictions by different codes/models for a fresh HEU core 15

Table [4.2]: Control rod worth predicted by different sources 16

Table [4.3]: Configuration studied during the June 24th 2006 experiment.....17

Table [4.4]: Configuration studied during the March 19th 2008 experiment.....18

Table [4.5]: k-effective for the different cases of the March 19th 2006 experiment.....18

Table [4.6]: Deviation from Critical for the different cases of the March 19th 2006 experiment.....19

Table [4.7]: k-effective for the different cases of the June 24th 2008 experiment.....19

Table [4.8]: Deviation from Critical for the different cases of the June 24th 2008 experiment.....19

Table [4.9]: Summary of heat flux, heat generation and fission density 21

Table [4.10] Summary of HEU Beff values obtained by different studies.....24

Table [4.11]: k-effective obtained for 5 accident configurations 44

Table [4.12]: Comparison of performance between an HEU core at 57 MW nuclear and the recommended LEU design at the same power.....46

Table [4.13] Comparison of performance between an HEU core at 52 MW nuclear and the recommended LEU design at 57 MW nuclear.....47

Table [5.1]: Comparison of LEU and HEU coolant and cladding surface temperatures ..70

Table [5.2]: Minimum margins to saturation, ONB, and FNB for the LEU and HEU nominal cases 78

Table [5.3]: Relative RHF core power levels at which the margins to saturation, ONB, and FNB become zero.....80

Table [5.4]: Absolute RHF core power levels at which the margins to saturation, ONB, and FNB become zero.....80

Table [5.5]: Margin to Saturation, ONB, and FNB relative to Scram Power, Vr, in% 81

Table [6.1]: Main characteristics of current HEU and recommended LEU design.....84

I Introduction

This report describes the neutronic and thermal-hydraulic analyses performed to study the feasibility of converting the High Flux Reactor (RHF) of the Laue Langevin Institute (ILL) from the use of Highly Enriched Uranium fuel (HEU) to the use of a Low Enriched Uranium (LEU) fuel.

Previous studies have shown that, due to its compact core design and high power density, the RHF could only be converted to an LEU fuel (enriched at <20%) if the fuel density was in a range of 7-9 g/cm^3 [Ref. 1] which was not possible with the existing fuel. However, the recent development of a new kind of high density (8-9 g/cm^3) fuel based on a mixture of uranium – molybdenum (UMo) could allow the RHF conversion.

ANL and ILL have collaborated to investigate alternative designs of the LEU fuel to minimize the fuel element design changes while maintaining the RHF performance in terms of both neutron flux and cycle length.

A promising candidate design has been selected and studied, increasing the total amount of fuel without changing the external plate dimensions by relocating the burnable poison. In this way, changes required in the fuel element design and fabrication are reasonably small. This report presents results of neutronics analyses of the selected LEU design that show that the LEU RHF performance can be maintained at a high level: 2 day decrease of cycle length (to 47.5 days at 58.3 MW) and 1-2% decrease of neutron flux of in comparison to the current typical HEU operation. The report also presents results of studies that show that the thermal-hydraulic and shutdown margins for the proposed LEU design remain sufficiently high to satisfy technical specifications.

II General Description of Facility and Reactor

As described in Reference 9, the institute Laue Langevin (ILL) is an international research centre which operates the most intense neutron source in the world, the ILL High Flux Reactor (RHF) with an unperturbed thermal neutron flux of 1.5×10^{15} n/cm²/s in the reflector. This high performance reactor feeds intense beams of neutrons to a suite of 40 high-performance instruments. Research carried out in this institute focuses primarily on fundamental science in a variety of fields: condensed matter physics, chemistry, biology, nuclear physics and materials science.

The ILL was founded on January 19th 1967 with the signing of an agreement between the governments of the French Republic and the Federal Republic of Germany. The friendship and influence of Louis Néel and Heinz Maier-Leibnitz brought this project to fruition in Grenoble, France. Figure 2.1 shows a general view of the ILL facility.

The ILL had the status of a service institute, offering the scientific community a hot, cold and ultra cold neutron source and ten neutron guides, each capable of serving three or four instruments. In January 1973 the United Kingdom decided to join ILL and officially became the institute's third Associate member. Ten countries have signed "Scientific Membership" agreements with ILL: Spain (1987), Switzerland (1988), Austria (1990), Russia (1996), Italy (1997), the Czech Republic (1999), Sweden and Hungary (2005), Belgium and Poland (2006).

Figure [2.1]: General view of the ILL facility. On the right, the reactor plant

The reactor has been conceived to operate continuously for 45 day cycles with a thermal power of 58.3 MW (nuclear power 57 MW). Nevertheless, in order to reduce the number of cycles per year, ILL has recently decreased the power of the reactor to a thermal power of 53.3 MW (nuclear power 52 MW) so that the reactor can operate for 49-50 day cycles. Figure 2.2 is a picture of the reactor taken above the light water pool. Currently, there are 4 cycles each year, providing neutrons for nearly 200 days of science. The neutrons are extracted from the pile using beam tubes and sent to the ILL instruments.

The reactor is cooled, moderated and reflected by heavy water. It has only one fuel element, based upon the Oak Ridge National Laboratory High Flux Isotope Reactor (HFIR) design. RHF is composed of three concentric regions. The heavy water tank contains the fuel element and has a diameter of 2.50 m. It is placed in the bottom part of a light water pool which has a diameter of 6 m and a height of 14 m. This pool is placed at the center of a 60 m diameter cylindrical building. The reactor is mainly used for

fundamental research, employing 13 horizontal and 4 inclined beam tubes which extract neutrons. Hot and cold neutrons are produced by graphite and liquid deuterium volumes set up in the heavy water tank and linked to beam tubes. Several beam tubes extend through the building's heavy concrete walls. A cross section and a top view of the heavy water tank are shown Figures 2.3 and 2.4 respectively.

Figure [2.2]: Picture of the reactor taken above the light water pool

Five safety rods (SR) surround the core to shutdown the reactor at any time. The safety rods are tubes made of AIC alloy (Ag-In-Cd) filled with heavy water. Each safety rod has a specific angle and position around the core. When in the inserted position their bottoms are 40 cm below the reactor median plane. When they are moved along their axes to the withdrawn position, their bottoms are 120 cm higher, at 80 cm above the reactor median plane, with the same angle. The safety rods are illustrated in Figure 2.4.

The RHF fuel element is made of 280 curved plates welded to two concentric aluminum tubes. The internal and external diameters of the element are 26.08 cm and 41.36 cm, respectively. The fuel is manufactured by CERCA ("Compagnie pour l'Etude et la Réalisation de Combustibles Atomiques", AREVA group). Each fuel plate is bent into an involute shape with a radius of 13.681 ± 0.005 cm. The advantage of the involute shape is to maintain a constant distance between each plate, optimizing the thermal- hydraulic cooling of the compact core. The specified uncertainties of the distance between two fuel plates, 1.8 mm, are ± 0.3 mm locally and ± 0.25 mm in average for the outer dimensions, according to the Safety Analysis Report [Ref. 3]. The fuel plate and element dimensions are shown in Figures 2.5 and 2.6, respectively.

Each fuel plate has a total height of 90.3 ± 0.02 cm. However the height of the meat (fissile part of the plates made of dispersed UAl_x) is 81.3 ± 0.02 cm. The meat is located in the center of the plate between two borated zones, at the upper and lower extremities, as shown in Figure 2.5. The borated zones act as a reactivity reserve for the end of cycles and to moderate the peak of flux on the edges of the plate. Each plate is composed of a 0.51 ± 0.08 mm thick meat and of an AlFeNi cladding thickness of 0.38 ± 0.08 mm on both sides of the plate. The overall fuel plate thickness is 1.27 ± 0.035 mm. The UAlx powder is enriched at 93% in ^{235}U for a total of 30.6 g of ^{235}U per plate.

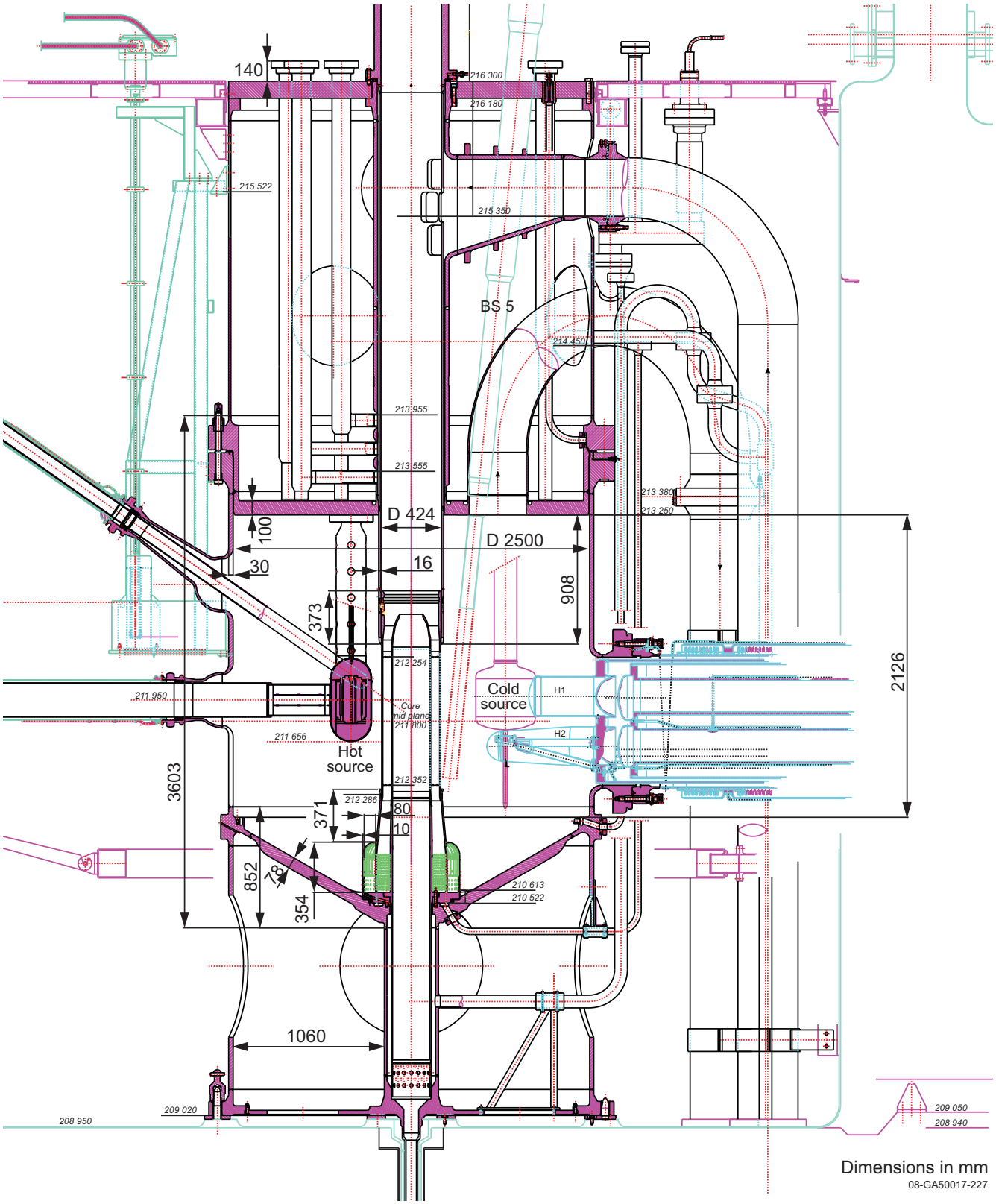

Figure [2.3]: Cross section of the reactor [Ref. 9]

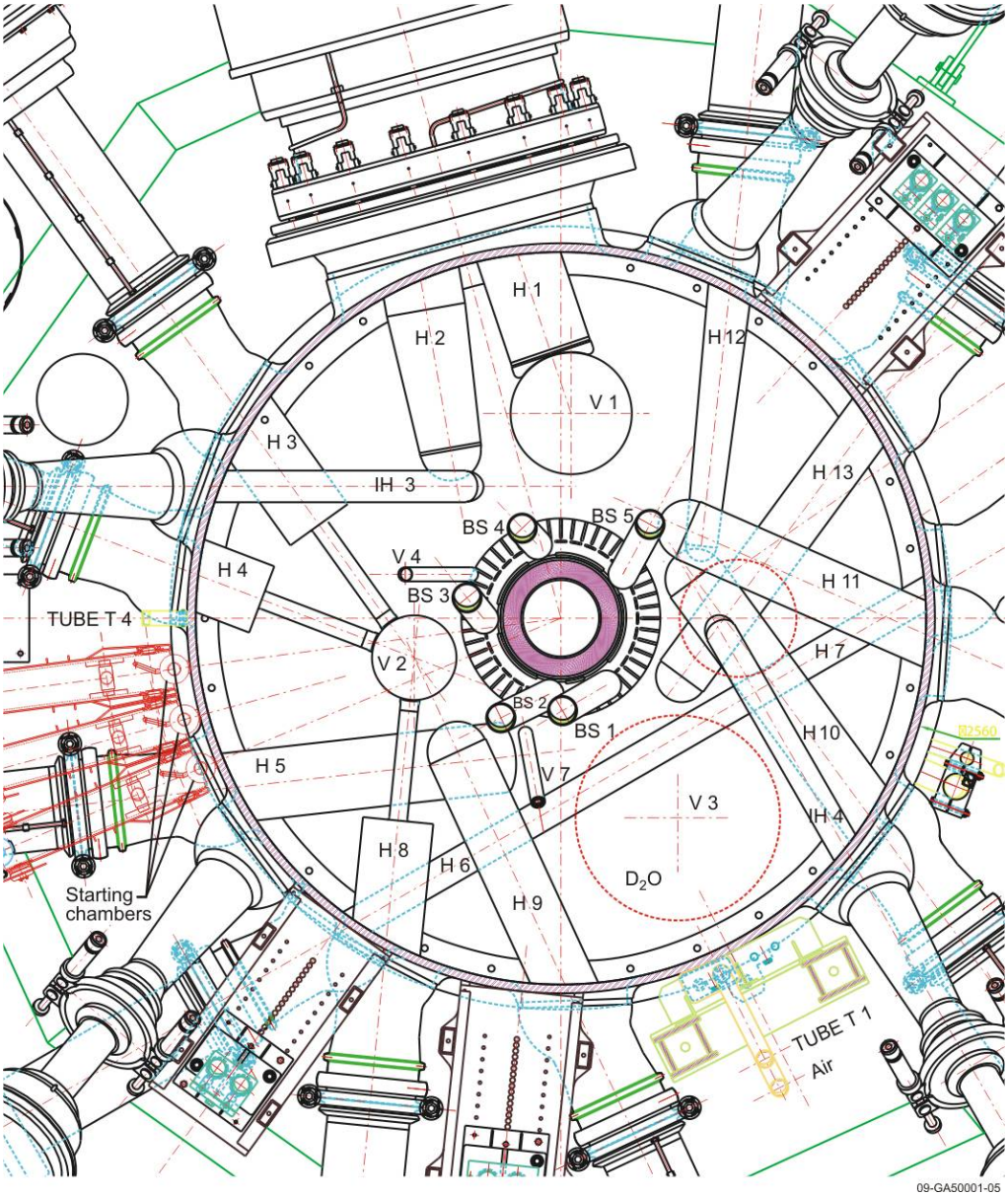

Figure [2.4]: Top view of the reactor. The fuel element is represented in pink. The five safety rods which surround the core are indicated as BS1, 2, 3, 4, 5. [Ref. 9]

RHF is controlled by an absorbing cylindrical control rod inserted in the fuel element inner cylinder. This control rod is composed of two pairs of concentric tubes, each made of an outer Ni tube and an inner Al tube. The RHF control rod mechanisms are set up below the fuel element. Indeed, for technical reasons (easier fuel exchange), the starting position of the control rod was chosen to be fully inserted into the fuel element. At the end of a cycle the whole control rod is withdrawn from the fuel element and below it.

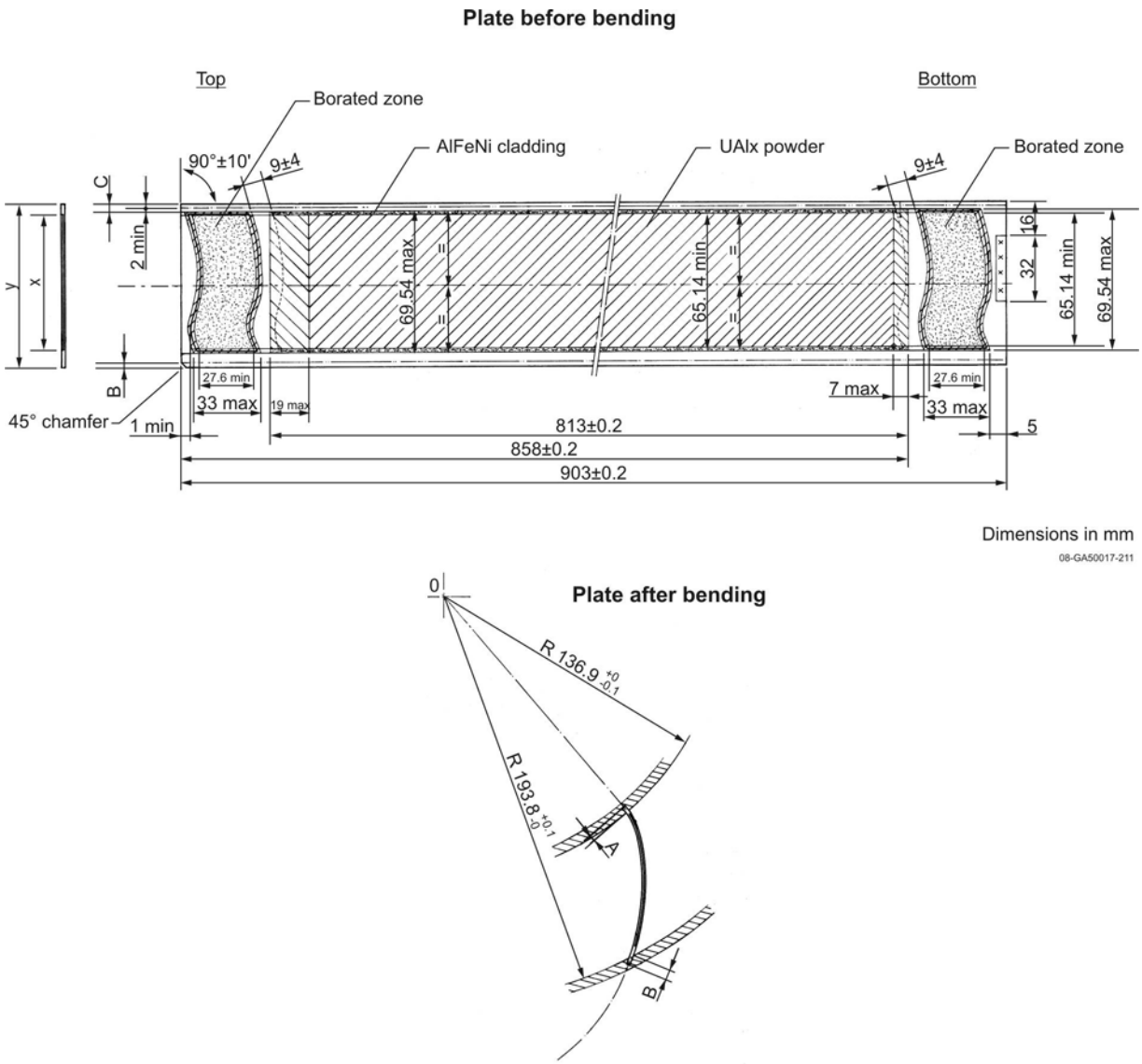

Figure [2.5]: RHF HEU fuel plate dimensions before and after bending [Ref. 10]

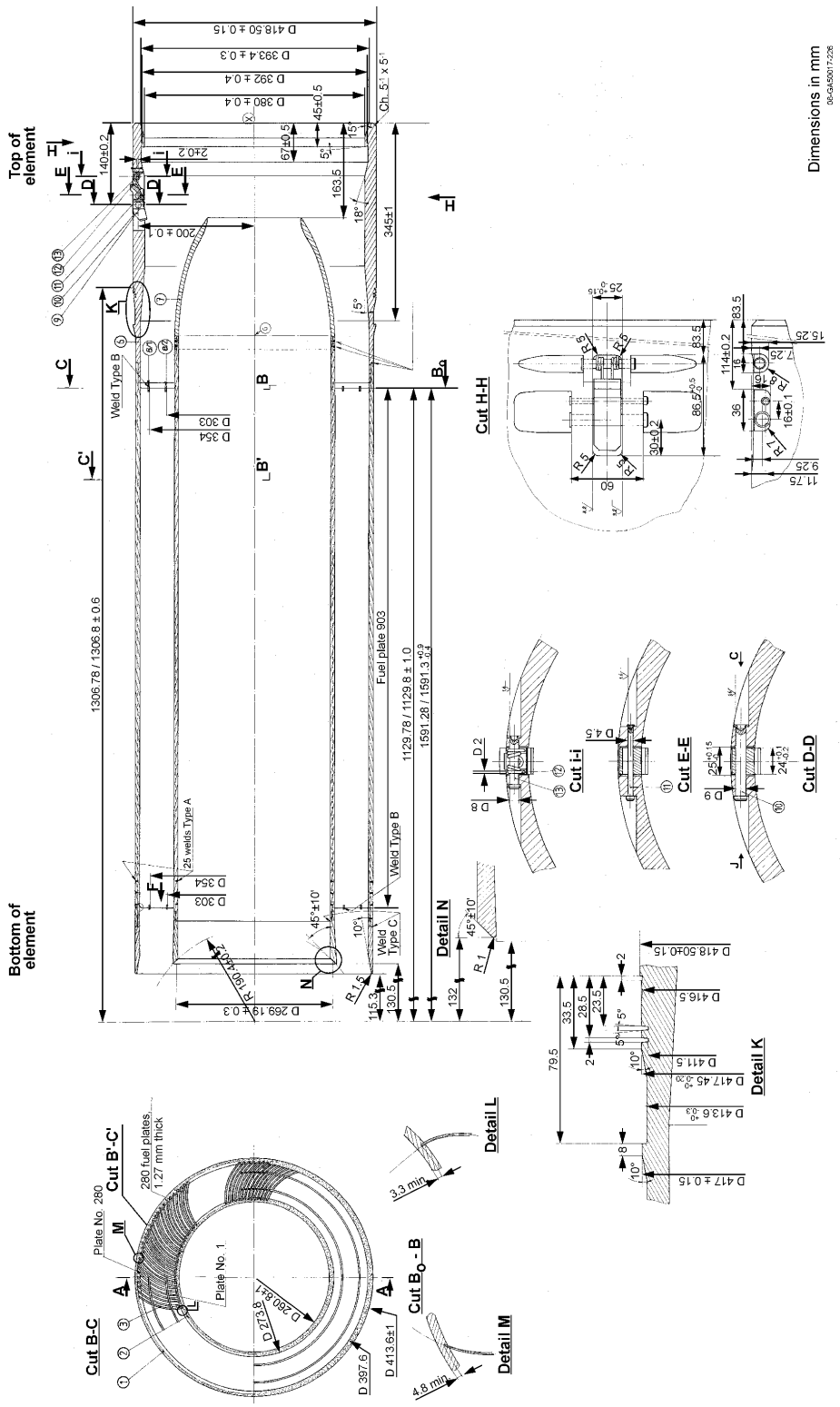

Figure [2.6]: RHF fuel element dimensions [Ref. 10]

III LEU Fuel & Manufacturing Assumptions

The current HEU fuel is a UAl_x powder dispersed in an aluminum matrix. The new LEU UMo fuel proposed is also based on a dispersed technology, a UMo powder mixed in an aluminum matrix. The initiative LEONIDAS (Low Enriched Optimized fuel Nuclear Irradiation group between DOE And European Structure) is in charge of dispersion UMo development and qualification in Europe. The LEONIDAS initiative includes the French laboratory CEA, the French company AREVA, the European laboratory ILL and the Belgian laboratory SCK-CEN. It is scheduled to qualify the ILL plates in the SCK-CEN reactor BR2. Prior experiments have shown that dispersion UMo fuel can suffer a problem of swelling under irradiation [Ref. 2]. Fortunately, addition of Silicon to the aluminum matrix appears effective as a means of controlling fuel-matrix interaction layer growth, which is the root cause of the swelling observed historically. In our calculations we have considered an addition of 3 wt% of silicon in the aluminum matrix and 7 wt% of Molybdenum in the UMo powder. The fuel is enriched up to 19.95% ^{235}U and the UMo powder density is set to 8.3 g/cm^3. The characteristics of the fuel considered are presented in Table 3.1.

Table [3.1]: Isotopic description of the LEU UMo fuel as used in the calculations

isotopes	Density (g/cm^3)	Atomic Density (at/barn.cm)
^{10}B	$2.13x10^{-06}$	$1.28x10^{-07}$
^{11}B	$9.44x10^{-06}$	$5.17x10^{-07}$
^{12}C	$1.35x10^{-03}$	$6.78x10^{-05}$
^{27}Al	$1.44x10^{+00}$	$3.21x10^{-02}$
^{28}Si	$4.09x10^{-02}$	$8.79x10^{-04}$
^{29}Si	$2.15x10^{-03}$	$4.46x10^{-05}$
^{30}Si	$1.47x10^{-03}$	$2.94x10^{-05}$
^{54}Fe	$5.46x10^{-05}$	$6.08x10^{-07}$
^{56}Fe	$8.88x10^{-04}$	$9.55x10^{-06}$
^{57}Fe	$2.09x10^{-05}$	$2.21x10^{-07}$
^{58}Fe	$2.83x10^{-06}$	$2.94x10^{-08}$
^{92}Mo	$8.27x10^{-02}$	$5.42x10^{-04}$
^{94}Mo	$5.27x10^{-02}$	$3.38x10^{-04}$
^{95}Mo	$9.16x10^{-02}$	$5.81x10^{-04}$
^{96}Mo	$9.70x10^{-02}$	$6.09x10^{-04}$
^{97}Mo	$5.61x10^{-02}$	$3.48x10^{-04}$
^{98}Mo	$1.43x10^{-01}$	$8.80x10^{-04}$
^{100}Mo	$5.84x10^{-02}$	$3.51x10^{-04}$
^{234}U	$2.01x10^{-02}$	$5.16x10^{-05}$
^{235}U	$1.52x10^{+00}$	$3.91x10^{-03}$
^{236}U	$3.55x10^{-02}$	$9.06x10^{-05}$
^{238}U	$6.14x10^{+00}$	$1.55x10^{-02}$

Because the UMo fuel is still under qualification, it is difficult to predict the manufacturing uncertainties and performance limitations. In consequence, a series of assumptions had to be made to perform the calculations.

1) Thermal-Hydraulic uncertainties

To control the thermal-hydraulic (TH) behavior of the reactor, the ILL staff measures the 4 following parameters continuously: thermal power, coolant flow, pressure and temperature. Each of them is measured with certain uncertainties to be taken into account in the calculations of thermal margins. The TH uncertainties are given below.

- Thermal power: ± 5%
- Coolant flow in the core: ± 3.5%
- Coolant pressure: ± 2%
- Inlet coolant temperature: ± 1 ^{0}C

These uncertainties have not been included in the in the TH CFD calculations presented in Section 5, which have been performed for nominal RHF conditions. Their effect will be evaluated in future TH analyses. The effect of the power uncertainty has been treated in the calculation of margin to boiling, as defined by the SAR [Ref. 3].

2) Mass tolerance

We have considered the same current mass tolerance given by the fuel manufacturer AREVA CERCA. CERCA specifies a mass of ^{235}U of 30.6 g ± 0.35 (± 1%) per plate but the uncertainty increases to ± 5% in a strip of 3mm of width and to ± 13% in a circle of 3 mm of diameter. As the SAR did, the evaluation of power distribution will be increased by 5% in the entire hot channel except in the hot spot where the power will be increased by 13% [Ref. 3]. These uncertainties are taken into account in the neutronics analyses results, but have not been included in the current CFD analyses.

3) Hot channel and hot spot definition

To evaluate the TH margins, the SAR defines a hot channel as a strip between radii 19.0 cm and 19.5 cm from the center of the core (which corresponds to the outer fuel edge of the plate). Analyses show that the power density is the strongest in this region. Because the power distribution implemented in the TH model comes from the neutronic analyses, we have defined the same hot channel definition in the neutronic model. Axial meshing of the power distribution of the hot stripe was set after consultations with the ILL staff. We have chosen to divide the hot channel axially in mesh of height 0.5 cm. Thus, the typical size of an individual mesh is ~0.5*0.5 = 0.25 cm^2. The studies have shown that this size is able to model the strong gradient of power observed in the hot channel. However, for the HEU core studies, the neutronic evaluation prediction of the maximum heat flux and maximum fission density will be made in a mesh of ~0.3*0.3 = 0.09 cm^2. This area corresponds to the mass tolerance surface of control, which is the smallest surface of control given in the current SAR. Nevertheless,

we will see in subsequent discussion that this limiting mesh definition may be insufficient to model the peaking of the envisaged LEU core (see section 4.4.3.1).

4) Maximum fission density

In the literature, the swelling of a plate is given in function of the fission density. As far as we know, UMo plates with 2.1 wt% of silicon can resist to swelling for a fission density close to 4.10^{21} fission/cm^3 [Ref. 2]. This value will be considered as our maximum allowed value.

5) Maximum heat flux

The qualification of the UMo dispersed fuel will be performed in the Belgian reactor BR2. The maximum heat flux value obtained during the irradiation will be the limit value of qualification. At this date, this limit is not known and so, we will assume the current maximum limit of operation used in BR2 which is 470 W/cm².

6) Other uncertainties

We have considered that the current meat, cladding and coolant channel thickness can still be used for the LEU fuel. Nevertheless, all these dimensions are given with a certain tolerance. These tolerances are not taken into account in our current calculations.

IV Neutronic Analyses

4.1 Description of Neutronics Codes, Model and Methodologies

The purpose of the neutronic study is to show the feasibility of a conversion to an LEU fuel. To reach this goal we have divided the work in three main steps.

1) Build a model of the current core and benchmark it against experience and/or other codes

2) Evaluate the impact of the conversion on the main neutronic parameters by direct replacement of the fuel meat without any other modifications.

3) As a consequence of results obtained in step 2, propose a new element design and re-evaluate the main neutronic parameters.

Basic Neutronic Codes Description

Historically, RHF neutronic studies have been carried out by the French laboratory CEA SERMA, using the codes APPOLO2 (transport and depletion) and TRIPOLI4 (Monte Carlo). They have used the library APPOLIB for APPOLO2 and JEFF3.1 for TRIPOLI4. SERMA has carried out several studies on the current HEU configuration of the RHF and evaluated many parameters [Ref. 4]. The current model results are compared to SERMA results as often as possible.

Recently, ILL has started to perform studies in parallel with SERMA. The ILL experts and tools are concentrated in the Projects and Calculations Laboratory (Bureau de Projets et Calculs in French, BPC). They mainly use the codes MCNPX 2.6 (Monte Carlo) and VESTA 2.00g (depletion) [Ref. 5],[Ref. 6]. The ILL team utilizes ENDF/B7 cross-sections with a customized heavy water thermal neutron scattering kernel, S(α,β).

The ANL Global Threat Reduction Initiative team carried out parallel studies in support of the ILL BPC, using MCNP5 1.51 (Monte Carlo) and REBUS-MCNP (depletion) with the libraries ENDF/B6 and/or ENDF/B7 [Ref. 7],[Ref. 8]. Depletion calculations at ANL were performed in REBUS-MCNP with a newly developed, explicit list of 90 fission products.

RHF Model Description

The RHF MCNP model was developed by the ILL Projects and Calculations Laboratory (BPC). It has been benchmarked with several measurements carried out by the ILL and validated in the International Handbook of Evaluated Reactor Physics Benchmark Experiments (IRPhEP), published by the Nuclear Energy Agency (NEA) in 2009 [Ref. 9].

In this model, all in-pile elements have been taken into account, i.e. all beam tubes, safety rods, cold and hot neutron sources, etc. Nevertheless, some simplifications have been made, as listed below, but a small reactivity impact is expected for each of them.

- The involute shape of the fuel plate is modeled as portions of cylinders. MCNP cell definition needs to define a negative and positive sense for a surface which is not possible with an explicit involute shape. The center of the cylinders is at a constant distance of 14cm from the fuel element axis, with radii of 8.53 and 8.568 cm for the inner cladding (thickness 0.038 cm, 0.015 inches), 8.568 and 8.619 cm for the meat (thickness 0.051 cm, 0.020 inches) and 8.619 and 8.657 cm for the outer cladding (thickness 0.038 cm, 0.015 inches). The meat volume in the MCNP model is 28.003 cm^3 instead of the actual 27.920 cm^3. Thus, the MCNP plate model volume is $\Delta V = 0.3\%$ higher than actual, which is judged good enough to validate the MCNP geometry dimensions.

- All the modeled grids, i.e. the anti turbulence grid linking the fuel element to the heavy water tank and the light water pool intermediary platform, are homogenized in the radial direction. From the point of view of the ILL BPC team, no significant impact on k-effective is expected by this bias.

- The mean value of 3 cm is used for the borated zone height (the manufacturing tolerance is high). But the k-effective is more sensitive to the poison mass than to the poison height.

- The starting and piloting fission chambers are not modeled because they are situated in the light water pool.

- The exiting heavy water pipe in the light water pool over the heavy water tank is not modeled.

- The fuel element aluminum pointed shape is not modeled. Since it is a thin aluminum wall, far away from the meat, above the borated zones, an insignificant impact is expected.

- The density of the liquid deuterium contained in the two cold sources has been set to 0.16 g/cm^3. No void percentage has been considered.

As stated previously, this model has been benchmarked and validated for a fresh core by the NEA. Nevertheless, some depletion calculations have shown that the fuel plate definition in this model is not able to correctly treat the strong burnup gradient existing in the fuel plates [Ref. 9]. In the model described in the IRPhEP, each active zone in a plate is described by one MCNP cell. So, 280 cells are used to describe the 280 active zones. The same process has been used to model the upper and lower poison zone.

To treat the burnup gradient in a plate with the MCNP model, it is necessary to divide each active zone into more than one cell. Considering the dimensions and the strong gradient of fission in a plate, it has been decided to divide the active zone in 3 radial parts and 15 axial parts. Thus, 45 burnup zones are used to describe the meat in each plate. Considering the strong symmetry in the RHF core and in order to define a reasonable number of cells in MCNP, the same depleting material has been applied in each equivalent geometric zone of each of the 280 individual plates. By a similar process,

each poison region has been divided in three axial zones, with the same depleting material applied to equivalent geometric cells in the 280 individual plates.

This modified model has given better results for the depletion calculations than the original model [Ref. 10]. It should be noted that no studies have been carried out to evaluate how many divisions are required to model the gradient of fission without spatial truncation. The number of burnup zones could probably be reduced. Nevertheless, in order to stay as consistent as possible with the ILL BPC studies, the modified MCNP model using 45 burnup zones has been chosen as a base for the neutronic calculations at ANL. Some screenshots of the MCNP model are given Figures 4.2, 4.3 and 4.4.

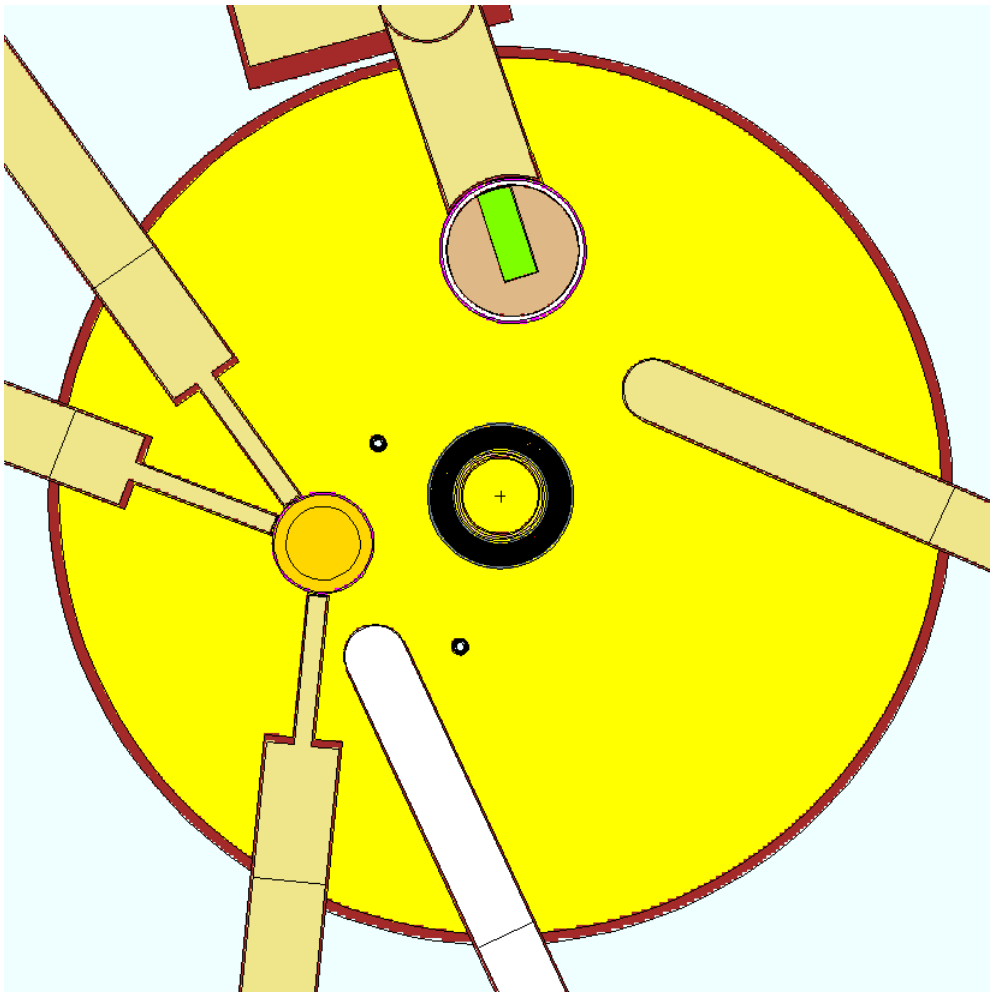

Figure [4.2]: Top view of the MCNP RHF heavy water tank model. The black ring in the center of the picture represents the fuel element. Several beam tubes are also visible.

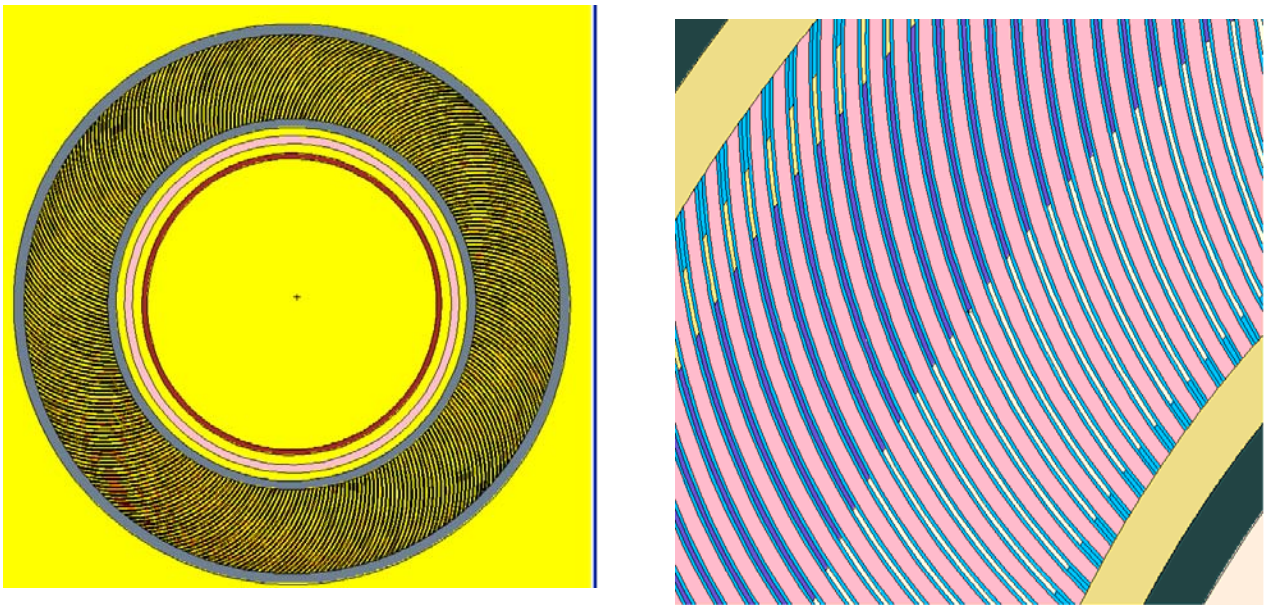

Figure [4.3]: Two top views of the modeled fuel element. The left picture illustrates the entire fuel element of 280 plates. The right picture shows a zoom of fuel plate details, with different meat zone colors to show the three different radial cell divisions for the three distinct radial depleting materials at each axial level.

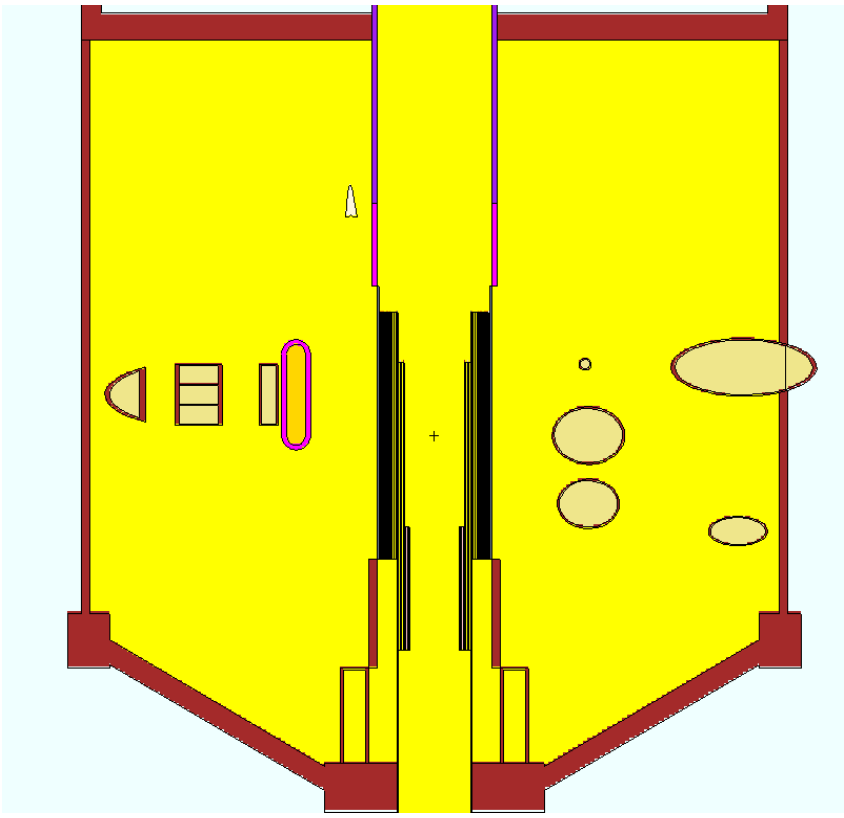

Figure [4.4]: Cross section of the modeled heavy water tank. The fuel element is represented in black in the centre of the picture.

4.2 Computational Model Credibility – HEU core

The goal of this section is to demonstrate the validity of the RHF model and the calculation scheme applied through comparison of HEU core predicted values to experimental data, results of other codes and/or the SAR.

4.2.1 k-effective of a Fresh Core with Critical Control Rod

k-effective was modeled for the reactor with a fresh HEU fuel element and the control rod (CR) set at the first measured critical position. The CR position was furnished by the ILL team from operational history. Because the material definition used to model the CR corresponds to a fresh one (i.e., no prior irradiation of rods), we have had to choose a critical position in the cycle history which corresponds to this configuration: fresh fuel + fresh control rod. Among the information provided by the ILL team, we selected cycle 143. For this cycle, the first critical position was 22.94 cm withdrawn. Under these conditions, we found k-effective = 0.99660 ± 44 pcm (where a perfect criticality prediction would have k-effective = 1.00000). Table 4.1 compares the k-effective obtained by other codes/models for the same configuration. Among the errors of the model, ILL has expressed concern that the heavy water S(α,β) are not estimated as well as other MCNP library data [Ref. 13]. To highlight this point, it is interesting to note the result obtained by the ILL team with another set of S(α,β) but exactly the same model [Ref. 9]. The different S(α,β) library leads to improvement of nearly 200 pcm for this particular k-effective calculation. The CEA k-effective is very close to critical, but unfortunately too much information is missing to determine which factor (temperature, model, library) dominates the difference [Ref. 4].

Table [4.1]: k-effective predictions by different codes/models for a fresh HEU core with the fresh control rod at measured critical position

Author	CODE	LIBRARY	Tmp (K)	S(α,β)	Tmp S(α,β) (K)	keff ± σ (pcm)
CEA[a]	TRIPOLI4	JEF3.1.1	?	?	?	1.00022 ± 20
ILL[b]	MCNPX2.6	ENDF/B7	300	ILL	293	0.99831 ± 36
ANL	MCNP5	ENDF/B7	300	ENDF/B7	300	0.99660 ± 44

4.2.2 Control Rod Worth

The control rod worth has been measured by the ILL team by the kinetic method at a low power. The control rod irradiation history associated with the measured value reported in the SAR was not precisely defined. The calculated reactivity was determined by the reactivity difference of k-effective for two configurations: control rod fully inserted and full withdrawn. The result obtained by the ANL calculation and the other data sources is given in the Table 4.2. The three studies have similar results very close to

[a] See [Ref 4]
[b] See [Ref 9]

the measured one. The ANL value is the closest with a difference of 48 pcm. Assuming the measured control rod was fresh, we can conclude that this element is correctly modeled.

Table [4.2]: Control rod worth predicted by different sources

	SAR (measured)	**SAR (calculated)**	**ANL** Worth ± σ (pcm)	**CEA**[c]
Control rod worth (pcm)	17000	17300	17048 ± 32	17353

4.2.3 Safety Rod Worths

We have evaluated the safety rod (SR) worths individually and for four of them fully inserted. Both methods have been benchmarked against experimental data. Indeed, the evaluation was based on critical experiments of June 24th 2006 and March 19th 2008 [Ref. 9]. These two experiments are briefly described below.

The experiment of June 24th 2006

Nine subcritical approaches took place on June 24, 2006. At the beginning of each approach, the control rod was set in the initial position, (*i.e.* fully inserted). Recall that the control rod must be lowered in order to increase reactivity. The studied safety rod or rods are in the 'operating' (*i.e.,* inserted) position while the other ones are in the withdrawn position. The subcritical approaches were performed with a reactor set at standard operating conditions in the beginning of cycle. These conditions are the following: a ^{235}U standard load of 8.568 kg and a ^{10}B standard load of 5.8 g in the fuel element; heavy water tank filled by pure heavy water (99.9% mol) at 4 bar; hot neutron source not heated by radiation; cold neutron sources filled by 25 K liquid deuterium; safety rods in the withdrawn position (unless specified) and a control rod in the 'zero' position (fully inserted to begin approach to critical).

All these in-pile elements have a significant influence on the reactor reactivity (4650 pcm according to the Safety Analysis Report), especially the hot and cold neutron sources that are made of graphite and liquid deuterium, respectively. The 9 configurations studied are described in Table 4.3. The control rod position given in this table is the distance from the top of the control rod to its starting position, i.e. 9.03 cm above the meat top. For Configurations 1 to 8, the subcritical approach was followed by achievement of reactor criticality and power stabilization at ~50 kW. For the last case, criticality was not achieved due to insufficient excess reactivity to overcome the worth of the inserted safety rods.

[c]See [Ref 4]

Table [4.3]: Configuration studied during the June 24th 2006 experiment with 99.9% heavy water in fuel zone

Case Number	Configuration	Measured Critical Control Rod Position (cm withdrawn)
1	All safety rods (SR) up	22.94 ± 0.2
2	SR1 inserted	52.06 ± 0.2
3	SR2 inserted	48.20 ± 0.2
4	SR3 inserted	48.88 ± 0.2
5	SR4 inserted	49.93 ± 0.2
6	SR5 inserted	45.73 ± 0.2
7	SR1 + SR2 inserted	67.95 ± 0.2
8	SR1 + SR5 inserted	87.05 ± 0.2
9	SR1 + SR4 inserted	No criticality

The experiment of March 19th 2008

Five subcritical approaches were carried out with a light water / heavy water mixture set up between the fuel plates, on March 19th 2008. One of the accident scenarios considered in the RHF SAR is the introduction of light water between the fuel plates. The March 19th 2008 experimental configuration simulated a rupture of the heavy water inlet pipe within the light water pool which surrounds the heavy water reflector tank. Once the fall in primary pressure due to a rupture is detected and the safety rods drop (i.e., insert) in 650 ms. However, the primary coolant pumps have a high inertia which could send a mixture of light water and heavy water into the core (the composition of which would vary with the size of rupture). The mixture would reach the RHF core in 1000 ms.

The accident configuration taken into consideration for reactor safety is the configuration where the core is filled with light water and four of the five safety rods drop. The March 19th 2008 experimental configuration set conditions close to those of the accident involving the introduction of light water. A measurement of the critical control rod position was made for each of the different "stuck safety rod" scenarios.

The critical experiment reproducing the accident situation required some modifications of the RHF fuel element. In this experimental configuration, the heavy water between the fuel plates was replaced by a mixture of 60 atomic% of light water and 40 atomic% of heavy water. The mixture was sealed by two plugs of AG3NE aluminum. A series of subcritical approaches was carried out in order to measure the critical CR position of the reactor in five configurations. The five configurations and the corresponding critical control rod position are described in the Table 4.4.

Table [4.4]: Configuration studied during the March 19th 2008 experiment with 60% light water & 40% heavy water in fuel zone

Case Number	Configuration	Measured Critical Control Rod Position (cm withdrawn)
10	SR1 withdrawn	48.2 ± 0.2
11	SR2 withdrawn	55.0 ± 0.2
12	SR3 withdrawn	49.8 ± 0.2
13	SR4 withdrawn	48.1 ± 0.2
14	SR5 withdrawn	48.4 ± 0.2

Simulations of the Safety Rod Worth Experiments

Table 4.5 presents the results obtained for the first experiment. Case 1 is a reference case and corresponds to the configuration describes in the section 4.2.1 (e.g. all safety rods fully withdrawn). For the cases 2 to 7, the k-effective obtained by the three studies is always higher than the reference k-effective, indicating that the safety rod worth is underestimated in each case. Table 4.6 lists the deviation from critical for each case. The ANL model has a -252 pcm Root Mean Square (RMS) deviation from critical. We suspect a problem of source convergence which prevents the neutron flux to be correctly simulated.

Table 4.7 presents the results obtained for the second experiment. Similar to the cases with 99.9% heavy water, the worth of four SRs fully inserted is underestimated consistently for the three sets of predictions. Table 4.8 lists the deviation from critical for each case. The ANL model has a 564 pcm RMS deviation from critical. The RMS deviation is much larger for the cases with mixed coolant than the cases with 99.9% heavy water coolant.

Table [4.5]: k-effective for the different cases of the March 19th 2006 experiment with 99.9% heavy water in fuel zone

Case Number	CEA	ILL	ANL
	keff ± σ (pcm)	keff ± σ (pcm)	keff ± σ (pcm)
1 D_2O	1.00022 ± 20	0.99831 ± 36	0.99660 ± 44
2 D_2O	1.00631 ± 20	1.00370 ± 36	0.99844 ± 41
3 D_2O	1.00423 ± 20	1.00218 ± 36	0.99717 ± 47
4 D_2O	1.00402 ± 20	1.00176 ± 36	0.99751 ± 49
5 D_2O	1.00644 ± 20	1.00363 ± 36	0.99848 ± 47
6 D_2O	1.00514 ± 20	1.00256 ± 36	0.99827 ± 47
7 D_2O	1.00557 ± 20	1.00125 ± 36	0.99729 ± 40
8 D_2O	-	*0.99976 ± 36*	*0.99689 ± 42*

Table [4.6]: Deviation from Critical for the different cases of the March 19th 2006 experiment with 99.9% heavy water in fuel zone

Case Number	CEA (k-1)/k in pcm	ILL (k-1)/k in pcm	ANL (k-1)/k in pcm
1 D_2O	22	-169	-341
2 D_2O	627	369	-156
3 D_2O	421	218	-284
4 D_2O	400	176	-250
5 D_2O	640	362	-152
6 D_2O	511	255	-173
7 D_2O	554	125	-272
8 D_2O	-	-24	-312
RMS D_2O	**494** ± 200	**238** ± 189	**-252** ± 69

Table [4.7]: k-effective for the different cases of the June 24th 2008 experiment with 60% light water & 40% heavy water in fuel zone

Case Number	CEA	ILL	ANL
	keff ± σ (pcm)	keff ± σ (pcm)	keff ± σ (pcm)
10 60% H_2O	1.00778 ± 20	1.00691 ± 47	1.00550 ± 38
11 60% H_2O	1.00803 ± 28	1.00716 ± 47	1.00573 ± 38
12 60% H_2O	1.00991 ± 20	1.00819 ± 51	1.00639 ± 38
13 60% H_2O	1.00699 ± 22	1.00674 ± 48	1.00520 ± 38
14 60% H_2O	1.00920 ± 22	1.00721 ± 49	1.00548 ± 38

Table [4.8]: Deviation from Critical for the different cases of the June 24th 2008 experiment with 60% light water & 40% heavy water in fuel zone

Case Number	CEA (k-1)/k in pcm	ILL (k-1)/k in pcm	ANL (k-1)/k in pcm
10 60% H_2O	772	686	547
11 60% H_2O	797	711	570
12 60% H_2O	981	812	635
13 60% H_2O	694	669	517
14 60% H_2O	912	716	545
RMS 60% H_2O	**837** ± 103	**721** ± 50	**564** ± 40

Variations in the deviations from critical for the different experiments are not well understood, but the apparent model biases are reasonable. Figure 4.5 illustrates the trends of deviation from critical vs. the number of safety rods inserted. We suspect a problem of neutron source convergence since the deviation from critical increases with the number of safety rods inserted -- and thus with the degree of asymmetry. The ANL model has the most consistent bias. We believe the models are adequate since the reactivity results are conservative.

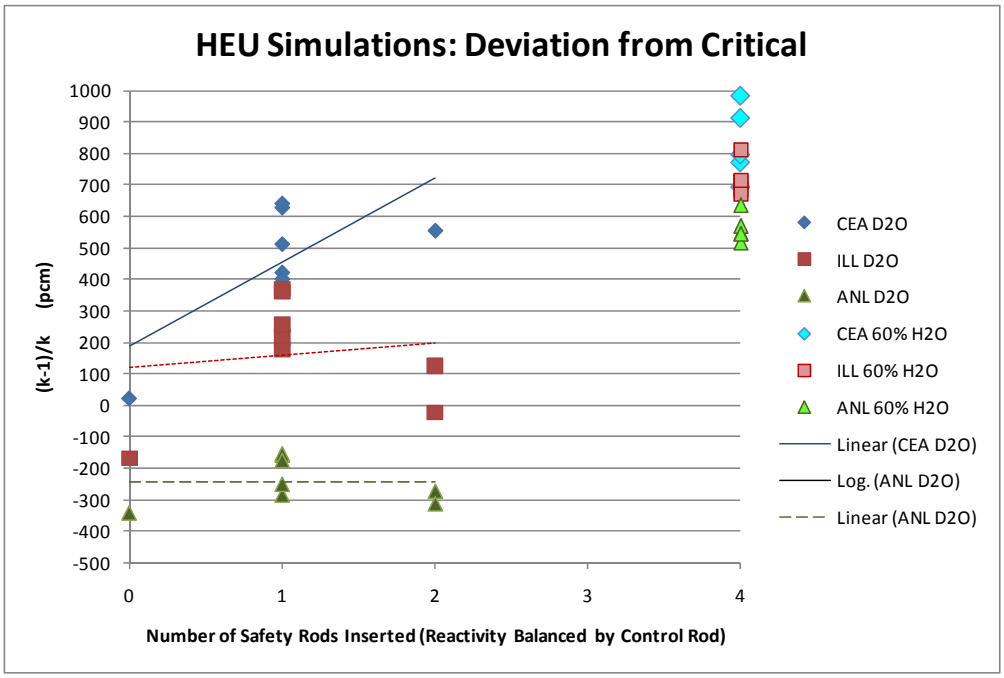

Figure [4.5]: Deviation from Critical for the various fresh HEU core control rod and safety rod states modeled

4.2.4 Heat Flux, Heat Generation and Fission Density

The Heat flux, heat generation and fission density have been calculated by MCNP F6np and F7 tallies which give the fission energy deposition over a cell. We used the F6np tally to evaluate the total energy deposited in the fuel (photons + neutrons) and the F7 to evaluate the entire nuclear power created in the reactor. We were also able to evaluate local values and power distribution in all the plates. Unfortunately, no experimental data are available, so the results have been benchmarked against the SAR data. The final results take into account the same conservative factor as the SAR: due to the ^{235}U mass tolerance (30.6 g ± 0.35 g per plate), the heat flux and heat generation were increased by 5% in the entire hot channel except for the hottest point (hot spot) where the heat flux and heat generation were increased by 13%.

We first evaluated the heat flux, heat generation and fission density for the configuration described in the paragraph 4.2.1 (fresh HEU fuel, fresh control rod sets at 22.94 cm withdrawn). This configuration is the most conservative under normal conditions. Nevertheless, in the SAR calculations, it is stated that fresh fuel was modeled, but no description of control rod position was given. This is an important point because the fission power is strongly pushed into the uncontrolled region above the top of the control rod. In consequence, the control rod position impacts the local values. For the purpose of comparison to the SAR, the fission density has been evaluated in the hot spot and considered as constant during the exposure. The time of exposure has been fixed at 45 days. Table 4.9 presents the results of our calculations compared to the available data given in the SAR.

Table [4.9]: Summary of heat flux, heat generation and fission density

	SAR	**ANL**
Plate - Average heat flux (W/cm²)	174	175 ± 2 [d]
Hot channel - Average heat flux (W/cm²)	364	341 ± 3 [d,e]
Hot spot - heat flux (W/cm²)	460[f,g]	437 ± 3 [d,g]
Total power in the meat (MW)	52.57	53.9 ± 0.6 [d]
maximum fission density (fission/cm^3)	2.10^{21}	2.1×10^{21} [g]
Total nuclear power in the reactor (MW)	57	57 ± 0.6 [h]

The average heat flux in the plate, average heat flux in the hot channel and the maximum heat flux in the hot spot are all consistent with the values reported in the SAR. The total power created in the plates is very close to the value given by the SAR. A difference of 2.5% is observed. The maximum fission density is also consistent. All the calculated values are consistent or coherent with the available data, validating our methodology to determine heat flux, heat generation and fission density for the entire reactor and locally as well.

Figure 4.6 shows the typical heat flux distribution in the hot channel obtained by simulation by the tally F6np which gives the "real" power deposited on the plate. The distribution has been determined in the entire plate, assuming the same mesh definition used for the hot channel. From there, it is easy to apply a normalization in order to obtain the heat generation distribution to implement in the thermal-hydraulic model.

[d] Obtained from MCNP tally F6np
[e] Including a conservative factor of 5%
[f] This value is not given directly in the SAR but is the result of SAR data interpolation made by the ILL staff
[g] Including a conservative factor of 13%
[h] Obtained from MCNP tally F7

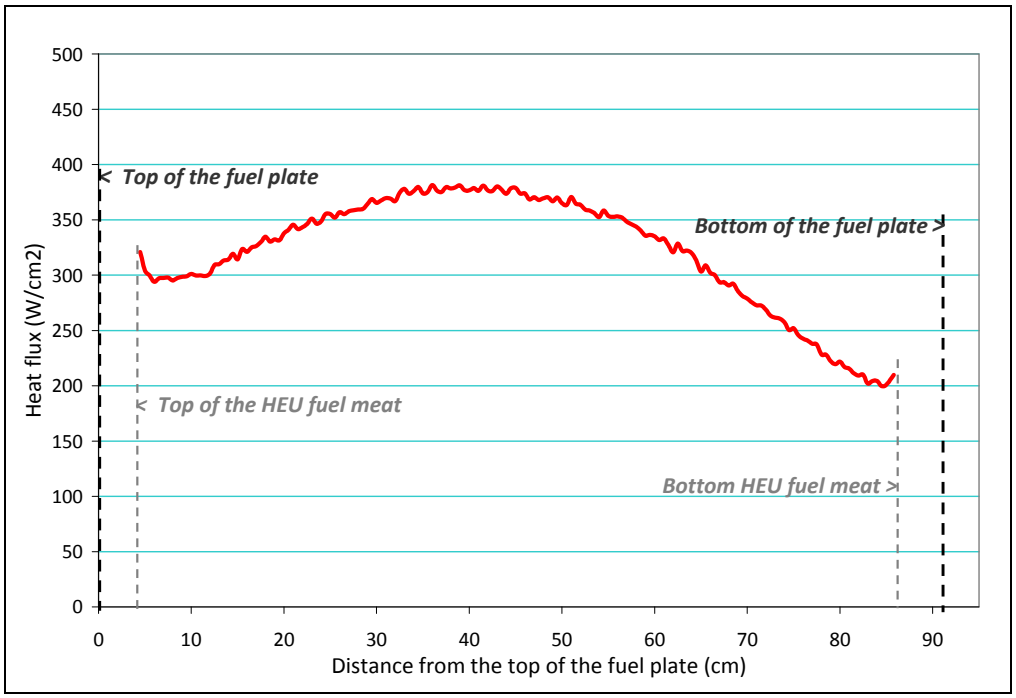

Figure [4.6]: Heat flux distribution in the hot channel obtained with MCNP tally F6np HEU core at 57 MW nuclear

4.2.5 Cycle Length

At the beginning of a new cycle, the control rod (CR) is fully inserted. The CR is then withdrawn until the first critical position is reached. The cycle starts at this time. Then the CR continues to be withdrawn to compensate the drop of reactivity as fission products build up and the fuel is depleted. The cycle is finished when the lowest CR position is reached (i.e., when the CR is fully withdrawn). During a cycle, the power and critical control rod position are continuously tracked by the ILL staff, so this information can be implemented as a benchmark of a depletion model. The cycle simulated is divided in several time steps and for each of them the real control position is set. Models and codes are validated if k-effective near 1.0 is calculated for each steady state step (plus or minus the uncertainties). Cycle 143 was chosen to benchmark the calculations with an HEU core because the control rod was new (i.e., no prior irradiation) and the history of power is well known.

Figure 4.7 shows the Cycle 143 k-effective evolution obtained by the ANL calculations with the REBUS-MCNP code. The black line represents the reference k-effective (obtained at the first steady state calculation). The green curve represents the k-effective evolution predicted by REBUS-MCNP. The plot indicates that most of the predicted points are close to the reference value. In consequence we can conclude that REBUS-MCNP and the depletion model are able to correctly evaluate the cycle length.

For an LEU fuel proposal no critical CR position is known. Thus it was necessary to implement another method in the codes to automatically determine the control rod position. At this date, only the code VESTA, used by the ILL staff, has been upgraded for

this purpose. Users set a target value for k-effective (in our case, the target value is one) and the code will move the control rod position until the target value is found (within an uncertainty). Under these conditions, the cycle length is not determined by the k-effective value, but by the CR position. The cycle length is defined by the period of time between the moment where the CR has reached the first critical position and the moment where the CR has reached full withdrawal. Cycle 143 was again chosen to benchmark the calculations with an HEU core because the control rod was new (i.e., no prior irradiation) and the history of power is well known.

Figure 4.8 shows the critical CR position as a function of time obtained by the ILL staff applying the VESTA code with the automatic criticality search. The black line represents the fully withdrawn position of the control rod. The blue and red curves represent the measured critical CR position during the cycle 143 and the CR position obtained by simulation, respectively. The cycle is over when the CR has reached the minimal position. On the graph, this situation happens when the red line crosses the black line. The control rod position obtained by simulation stays very close to the real one from the beginning to the end of cycle. In consequence, the model and code are able to evaluate correctly the CR motion and should be able to determine the cycle length with an LEU fuel.

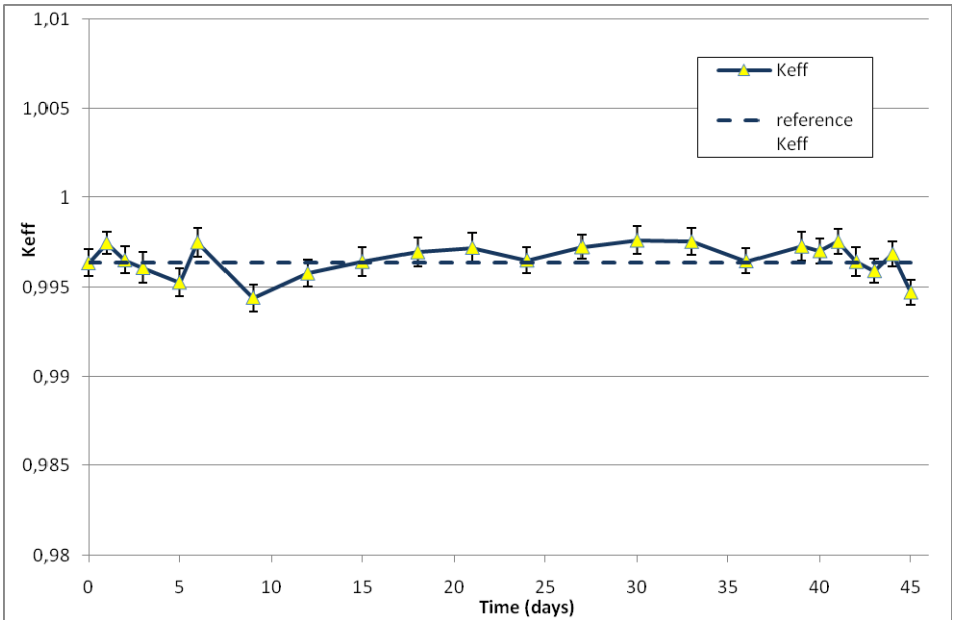

Figure [4.7]: k-effective evolution obtained by REBUS-MCNP for an HEU core at a nuclear power of 57 MW (cycle 143)

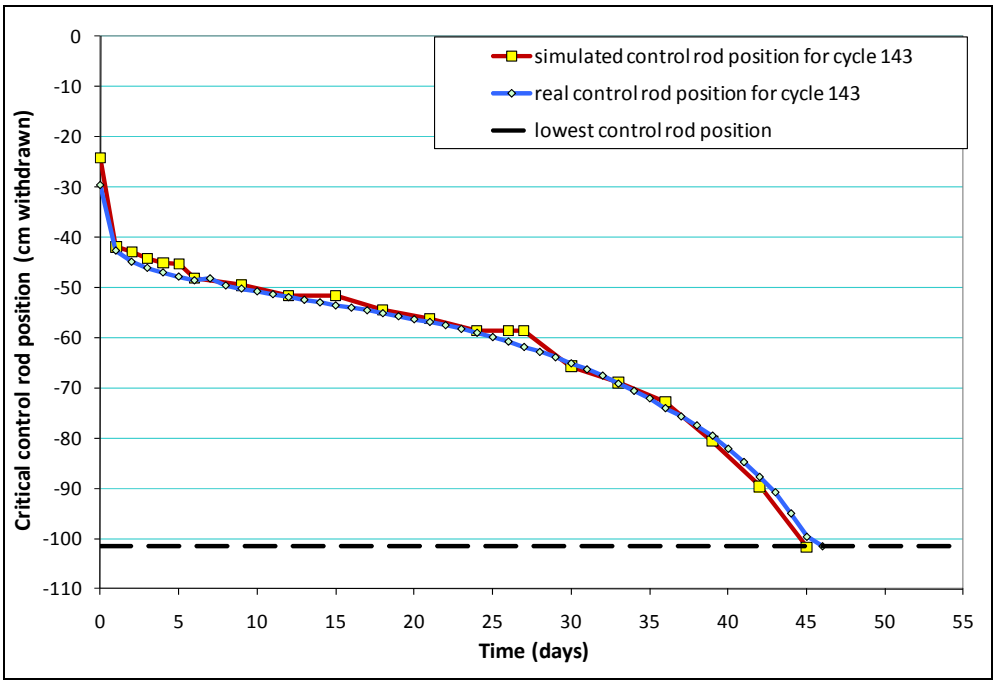

Figure [4.8]: Control rod motion evolution obtained by VESTA and the automatic critical search for an HEU core at 57 MW (cycle 143)

4.2.6 Kinetic Parameters

At this date, only the Beff has been evaluated by the ANL team. To obtain this parameter, we have used the "classic" MCNP methodology which consists of evaluating the k-effective with and without the delayed neutrons. This methodology has been benchmarked against experience in many other configurations with good results [Ref. 11]. Because this evaluation is strongly linked to the library used during the calculation, we have performed this study with more than one library. To evaluate the Beff with an LEU configuration we will take the library which gives the most conservative result for the HEU. Table 4.10 compares our results to those obtained by other sources. The results do not take into account the photo fissions. As we can see, the four values are close. The maximum discrepancy occurs between the ANL result using ENDF/B6 and the SAR and is equal to 28 pcm, which is close to the uncertainty value. Because the result obtained with ENDF/B7 is more conservative, we will use this library for the Beff evaluation for an LEU core.

Table [4.10] Summary of HEU Beff values obtained by different studies

	ANL		**CEA**	**SAR**
Library	ENDF/B6	ENDF/B7	APPOLIB	-
Beff (pcm)	705	685	693	677
Uncertainties (pcm) at 1 σ	27	28	?	-

4.2.7 Summary of ANL Code and Model Performance

The goal of section 4.2 was to validate model and codes. A series of key parameters have been evaluated and have shown that our calculation scheme gives consistent or conservative results:

- The k-effective for fresh HEU fuel and a fresh control rod at critical height and normal configuration is close to the criticality.
- Control rod and safety rod worths have been evaluated with consistent results.
- The global and the local distributions of power obtained by calculation are consistent with the data given in the SAR.
- Our ability to predict the CR position during depletion (and thus the cycle length) has been demonstrated.
- The Beff value obtained is close to the other evaluations.

Currently, there is no experimental data available about the UMo behaviour or composition after irradiation, so we cannot benchmark our LEU simulation against experiment. However, the biggest change that we have to make in the model comes from the fuel description. Between the HEU and the LEU fuel, the main changes are the fissile material proportions and the addition of Molybdenum and Silicon. Because we do not foresee any reasons for these changes to impact the simulation methods and because the results obtained with an HEU core are judged adequate, we can evaluate the LEU neutronics with confidence.

4.3 Evaluation of LEU Direct Replacement Core Performance

In this second part of the neutronic analyses, we present the study of the simplest case that we can imagine for converting the RHF: switching from the HEU fuel meat to the UMo LEU fuel meat without any other modifications. This solution could be the least expensive and the fastest to realize. However, the fuel manufacturer AREVA CERCA cannot guarantee the possibility of manufacturing plates with LEU UMo fuel with borated zones. Indeed, the strong difference of hardness between both materials could be a problem during the fabrication process. Consequently, we have considered cases both with and without boron. The key aspects cycle length and neutron flux have been simulated. These points are enough to highlight the difference between the use of HEU and LEU fuel.

4.3.1 Cycle Length

Figure 4.9 shows the predicted control rod (CR) motion as a function of time for the two LEU designs (with and without boron) at 57 MW.

The simulation was carried out by the code VESTA using the automatic critical search (see section 4.2.4). In order to save time, the depletion calculations have been carried out with a non-divided model (one MCNP cell for each plate). Nevertheless, we expect a slight overestimation of the cycle length for a non-divided model. The cycle is complete when the top of the control rod has reached the minimal position (represented by the black line on the graph).

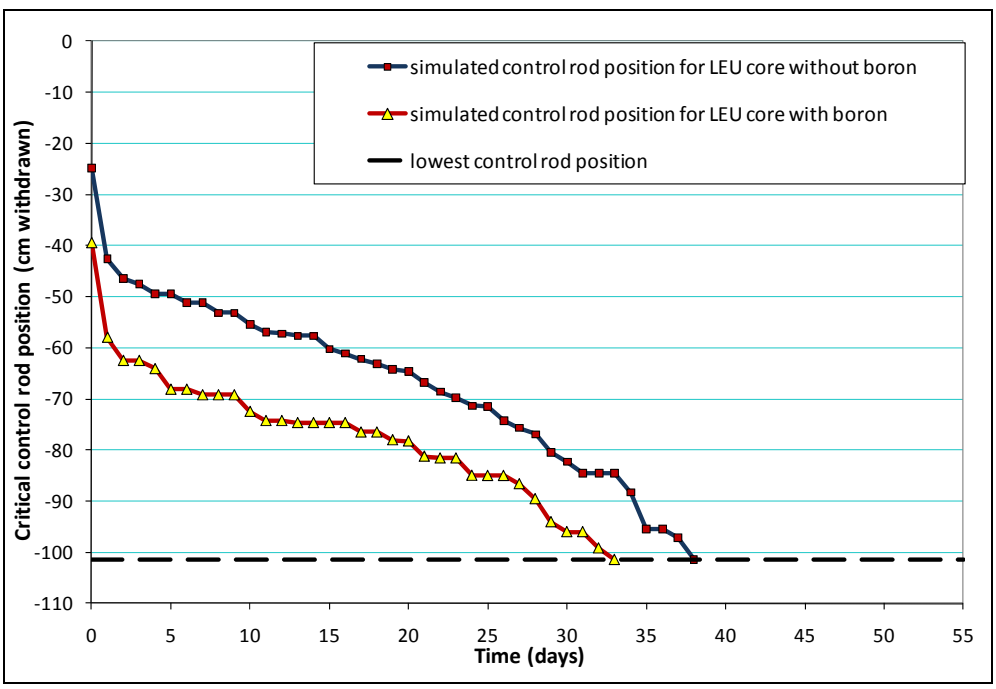

Figure [4.9]: Comparison of cycle length obtained for several LEU configurations - Nuclear power set at 57 MW. Model non-divided. Obtained by VESTA and the critical search

Cycle lengths are estimated to be 33 days (± 1 day at 1 sigma) for the LEU configuration with boron and 39 days (± 1 day at 1 sigma) for the LEU configuration without boron.

Recall that the key purpose of the boron is to reduce the intensity of the peak of power during the first days of the cycle. Nevertheless, the poison must be sufficiently burned at the end of cycle. Indeed the boron supplies an amount of antireactivity which has to be compensated by the CR and if too much boron is still present at the end of cycle, the CR will reach the minimum position too fast, reducing the cycle length.

This is exactly what we observed with the configuration LEU with boron. The cycle length with boron is less than the cycle length without boron. The analysis of the ^{10}B composition at the end of cycle has shown that 32% of the initial boron is still present in the bottom poison zone at the end of cycle. Nevertheless, we can already conclude that, even with an optimized amount of poison, the cycle length could not be longer than 39 days, which would represent a drop of 14.3% relative to an HEU core operating at the same 57 MW nuclear power (58.3 MW thermal power).

4.3.2 Neutron Flux

The impact on neutron flux has been evaluated by the ILL staff with a neutron mapping obtained by the code MCNPX and by the ANL staff with an analytic method presented below.

The relation between power and flux is given by: $$\frac{P}{Q} = \tau_f = \Sigma_f \Phi$$

With: P Thermal power density in the core (W/cm^3)

Σ_f Macroscopic cross-section of fission (cm-1)

Q Energy created by fission (J)

Φ Neutron flux (n/cm²/s)

τ_f Fission rate (fission/s)

As a first approximation, we can consider Q as independent of the kind of fuel used, thus equal for both HEU and LEU configurations.

So, we can write: $$\Sigma_{f,LEU}\Phi_{LEU} = \Sigma_{f,HEU}\Phi_{HEU}$$

And because: $$\Sigma = n\sigma = \frac{\rho N_{avo}}{M}\sigma$$

With:

n Atomic density (at/barn.cm)

σ Microscopic cross-section (barn)

ρ Density (g/cm^3)

N_{avo} Avogadro number (Atom/mol)

M: Molar mass (g/mol)

We can write:
$$\frac{\rho_{LEU}\sigma_{f,LEU}}{M_{LEU}}\Phi_{LEU} = \frac{\rho_{HEU}\sigma_{f,HEU}}{M_{HEU}}\Phi_{HEU}$$

And finally we obtain:
$$\Phi_{LEU} = \frac{\rho_{HEU}\sigma_{f,HEU} \times M_{LEU}}{\rho_{LEU}\sigma_{f,LEU} \times M_{HEU}}\Phi_{HEU}$$

We can try to estimate the variation of flux for a fresh core with the previous equation. The densities, molar masses and HEU neutron flux are known. Figure 4.10 shows neutron spectra for the LEU and HEU configurations. Some differences exist between both spectra mainly due to the difference of ^{235}U quantity. Thus the microscopic cross-section of fission is not the same in both fuels. We have evaluated these cross sections for a fresh core using the MCNPX code. We have considered the ^{235}U as the only fissile material.

Using the following values (where HEU values are for 57 MW nuclear):

$$\rho_{^{235}U,HEU} = 1.1 g/cc$$
$$\rho_{^{235}U,LEU} = 1.52 g/cc$$
$$\sigma_{f,HEU} = 74 barn$$
$$\sigma_{f,LEU} = 58 barn$$
$$\Phi_{HEU} = 1.5x10^{15} n/cm^2/s$$

We can expect an LEU neutron flux of: $\Phi_{LEU} = 1.398x10^{15} n/cm^2/s$

This value represents a drop of 6.8% of neutron flux in comparison to an HEU core operating at the same thermal power. Applying the code MCNPX, the ILL staff has realized a mapping of the thermal neutron flux in the median plane of the reactor. Figures 4.11 and 4.12 show the mapping for HEU and LEU configurations, respectively [Ref. 10]. The blue ring at the centre of the pictures represents the core, which is surrounded by thermal neutrons in the reflector (in red on the pictures). Though the mapping resolution is not sufficient to allow accurate evaluation of the numeric difference between HEU and LEU fuels; we can see clearly a drop of the thermal neutron density for the core loaded with UMo.

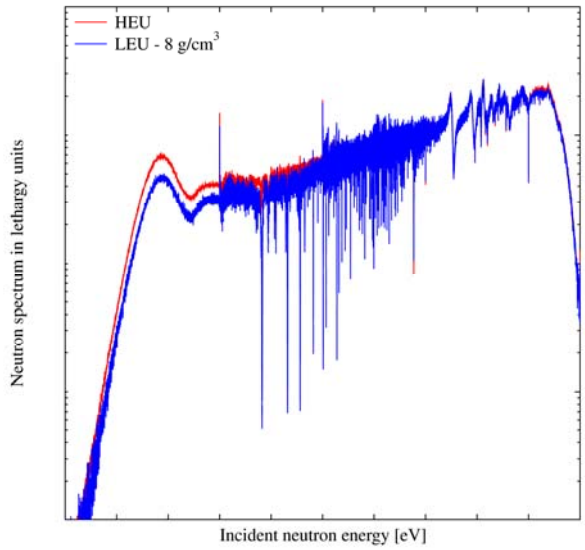

Figure [4.10]: Neutron spectrum for fresh HEU and LEU Direct Replacement Configuration

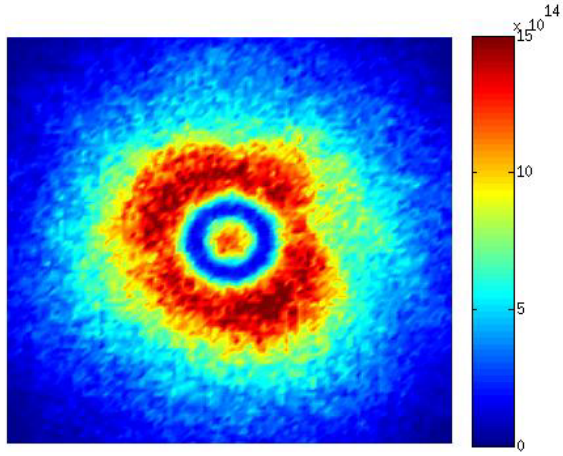

Figure [4.11]: Thermal neutron mapping in the median plane of the HEU core

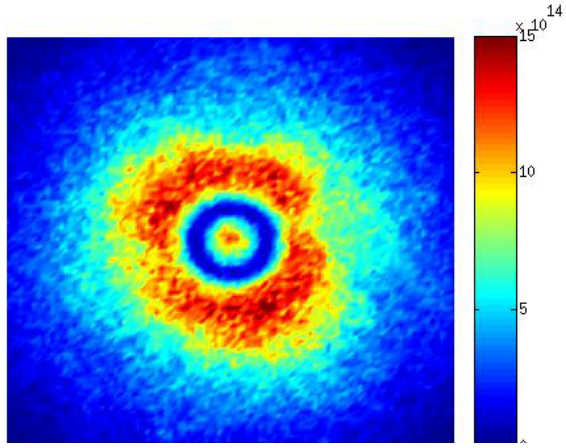

Figure [4.12]: Thermal neutron mapping in the median plane of LEU Direct Replacement Configuration

4.3.3 Conclusions of LEU Direct Replacement Core Evaluation

We have studied the direct replacement of HEU fuel meat with LEU U-Mo fuel. We have evaluated the cycle length and the thermal neutron flux. The simulations have shown that the cycle length is strongly impacted by the change of fuel. Indeed, with an optimized amount of boron, the cycle length cannot exceed 39 days -- a drop of 14% with respect to HEU core at 57 MW (nuclear). In addition, the thermal neutron flux would decrease by roughly 7%.

Under these conditions, ILL has judged that the reactor performances are too negatively impacted to seriously envisage the conversion. Thus, ILL and ANL staff have developed alternative LEU fuel element designs. The summary of the research and the associated first results are presented on the next section.

4.4 New LEU Plate Design

4.4.1 Ways to Optimize the Conversion

This section summarizes the first calculations carried out to optimize the conversion of the RHF. The LEU fuel qualification by the LEONIDAS group is already based upon a given dispersion fuel composition. Accordingly, the only way to perform conversion is to modify the plate geometry. The modifications have to be as minor as possible. Therefore we have decided to make no modification on the external plate dimensions or the thickness of the meat. With these options, the core of the RHF does not need to be modified. The only modifications are within the plates.

Results presented in section 4.3.1 have shown that a core loaded with the UMo fuel penalizes both cycle length and neutron flux. In addition, the fabrication of LEU plates with boron is not guaranteed. Consequently, we have chosen to consider the presence of boron within the plates as impossible and tried to find other solutions.

4.4.2 The 'Extended Meat' Configuration

It is obvious that the cycle length depends of the amount of fuel. Because we envisage a plate design without boron, we have studied a solution where the fuel length is extended to replace the boron zones. The fuel volume has been extended 4 cm on the top and at the bottom. This new configuration is called 'Extended Meat' and is shown in Figure 4.13.

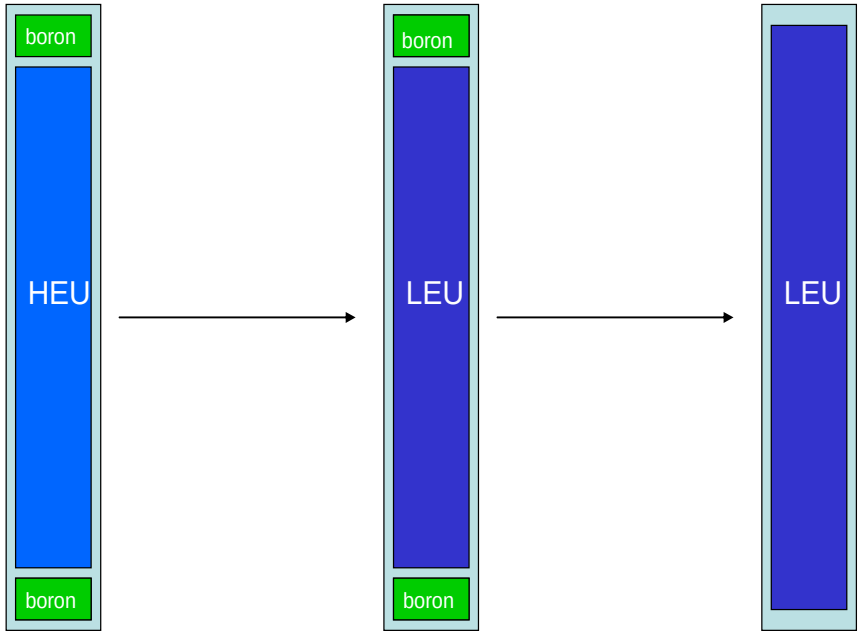

Figure [4.13]: Scheme of plates. Respectively HEU plate, LEU plate as studied in section 4.3 and "Extended Meat" LEU plates.

The increase of fuel in Extended Meat configuration is nearly 9%. In order to evaluate the impact of these changes, a first series of depletion calculations have been carried out with a non divided model (one MCNP cell for each plate, since this model is faster than the divided model). Figure 4.14 shows the control rod motion (blue curve) obtained for this configuration using the VESTA code with the automatic critical search. As shown, the extended meat configuration is promising: the control rod reaches the lowest position (represented by the black line) at day 51. On the graph, this situation occurs when the blue curve crosses the black line. This result demonstrates the positive impact of the fuel extension. Indeed the cycle length is increased from 39 to 51 days. Nevertheless, recall that non divided models were used during the calculations, so a slight overestimation is expected.

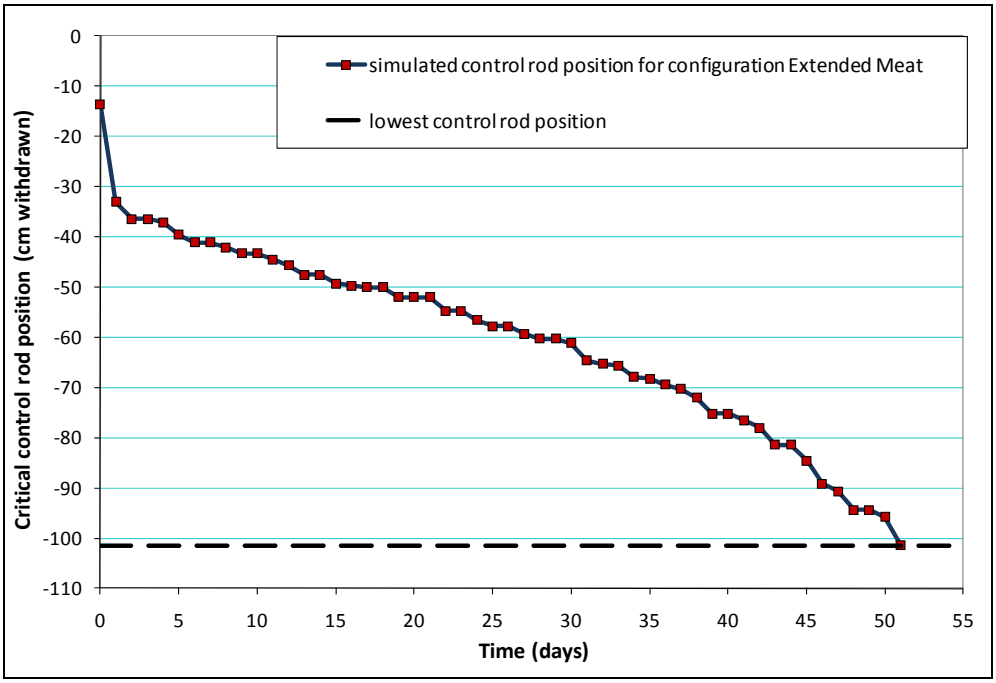

Figure [4.14]: Cycle length for extended meat LEU configuration. Nuclear power set at 57 MW. Model non-divided. Obtained by the VESTA code with the critical search

Of course, the "Extended Meat" configuration is not designed to manage the peak of power on the extreme parts of the plate since the boron was removed. To understand the impact, we have evaluated the heat flux distribution in the hot channel for a fresh critical core. Results are presented in Figure 4.15. In order to make a comparison, the heat flux distribution obtained for a normal HEU configuration is also plotted. For both cases, the CR was set at the initial critical position. The boron effect is clear: without poison on the extreme part of the plate, two peaks appear on the top and at the bottom. The two peaks do not have the same amplitude due to the CR position (inserted from the bottom of the core). The initial critical position of the CR is close to 25 cm below the top of the fuel meat. The maximum heat flux obtained for the Extended Meat LEU configuration is close to 554 W/cm², without conservative factors (predicted by MCNP F6np tally with mesh of 0.5x0.5 cm^2), which is much higher than the presumed fuel

qualification limit of 470 W/cm². The extended meat configuration could solve the problem of cycle length, but amelioration is needed to reduce the intensity of the peak of power on the top edge of the plate.

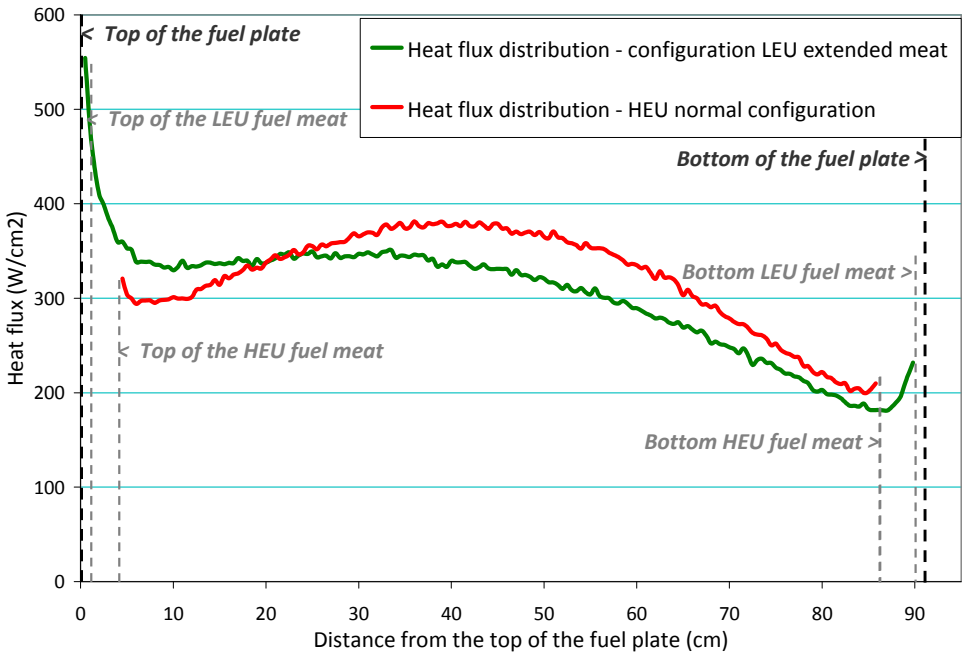

Figure [4.15]: Heat flux in the hot strip for both HEU and the LEU extended meat configuration. Nuclear power set at 57 MW

At this date, two main solutions have been proposed. The first arose from the observation that the 'hot spot effect' could be spread across the plate. Indeed, if we remove a small amount of fuel on the top of the plate we can create the geometric conditions for the appearance of several hot spots. Thus, we can spread the intensity of the peak of power through all the hot spots and thus decrease the maximum intensity. This configuration is called 'bevelled edge'.

Preliminary studies of the bevelled edge configuration have predicted a maximum heat flux value close to 450 W/cm², which is considerably better than for the extended meat configuration. However, the cycle length advantage of the extended meat configuration would be reduced due to the reduction of total fuel mass for the bevelled meat. In addition, this solution would be difficult to manufacture. For each cut made on the plate, several new tolerances are introduced. Consequently, the number of manufacturing control steps would increase considerably. Although this solution may be studied further, the second option, described in the next sections, is preferred.

4.4.3 The Relocated Poison Configuration

As explained before, the drop of cycle length observed with the LEU fuel can be solved by a fuel extension along the plate. Because of the difference of hardness between the boron and the LEU fuel, we do not believe it will be possible to maintain boron zones

in the plates. Unfortunately, the peak of power becomes problematic when the poison is removed, so ILL and ANL staff have worked together to define a new site to relocate the poison in the fuel element.

The poison acts like a 'filter' where neutrons are captured and so, the position of this filter defines its efficiency: the closer it is situated to the top of the plate, the better it will control the top edge peak. The current poison position is by far the most efficient. Upon consideration of the fuel element geometry and manufacture (particularly the welds), several different configurations were been proposed. Among these solutions, only the one which has been judged the least difficult to manufacture has been studied.

We propose a configuration with the poison in an annular shape, a belt, affixed to the outer radius of the fuel element. The position of this belt has not been decided. The most efficient is obviously to place the belt at the same height as the top of the plate, where the heat flux is problematic. However, a weld point is made at that location to fix the plates to the outer tube, so we have studied the possibility of fixing the belt just above the top of the plates. CERCA has warned that the outer tube manufacturing process is complex, so the poison belt placement process could be technically difficult. Above the outer tube, there is a "head" (i.e., an end fitting). This head is not subject to the same technical constraints, so its manufacturing process is less complex. CERCA has indicated a preference to fix the belt along the head. Unfortunately, the distance between the belt and the top of the plates becomes important and the belt efficiency decreases. As we will show in the following sections, this decrease can be solved, within a certain range, by an augmentation of the poison density.

4.4.3.1 Determination of the Maximum Heat Flux & Maximum Fission Density

As stated in section 2, the maximum heat flux value considered in this study is the maximum operating value of BR2, which is 470 W/cm². Nevertheless, MCNP requires the definition of a surface where the heat flux evaluation can be made. As far as we know, BR2 staff uses a surface of 4.35x0.375 cm². But the BR2 heat flux peak is not near an axial edge of a plate. In the RHF, studies show a strong axial and radial gradient of power. In consequence, when we evaluate the heat flux with MCNP, we observe that the smaller the surface of control, the higher the maximum heat flux. Because the heat flux cannot exceed a fixed value, the characteristics of the poison belt (position, nature of poison, poison density, dimensions) have to be adapted as a function of the maximum heat flux obtained by MCNP, which depends of the size of the surface of control.

To solve this problem, two different approaches have been explored. First, the surface of control was set as the smallest one described in the current SAR, which corresponds to the mass tolerance: The ^{235}U mass can exceed the nominal average by 13% within a circle of 3 mm of diameter. Selecting a circle of 3mm of diameter as the surface of control has the advantage of being based on a physical value. Unfortunately, this solution has the disadvantage that it may not predict the maximum value. So, a progressive reduction of the surface area was employed to determine the asymptotic heat flux as the surface tends to zero. This second approach has the disadvantage that it may be too conservative by ignoring conduction and local coolant condition. As we will see in the next section, the recommended designs of the two control-surface approaches are different.

Assuming a maximum heat flux value of 470 W/cm² and considering the strongly conservative hypothesis that this flux stays constant during the cycle (i.e., the peak does not burn out as expected in actual application), we can apply the following normalization to obtain the maximum fission density:

$$Fd = \frac{2q''}{1.602.10^{-19} eQ_r} \quad t$$

With:

Fd	Fission density (Fission/cm^3)
q''	Heat flux (W/cm²)
e	Meat thickness (cm)
Qr	Energy per fission (eV/fission)
t	Time of exposure (s)

Considering a constant heat flux of 470 W/cm², a meat thickness of 0.051cm and a time of exposure of 51 days, we obtain a conservative maximum fission density of 2.56×10^{21} fission/cm^3 which is well below the maximum allowed value of 4.1×10^{21} fission/cm^3.

4.4.3.2 Nature and Density of Poison

At this date, three main kinds of poisons have been considered: boron, gadolinium and cadmium. Currently the poison used in the RHF is a powder of boron mixed in an aluminum matrix. The density of ^{10}B in this powder is close to 6×10^{-3} at/barn.cm which represents 2.4% of the natural boron density. Nevertheless we have assumed the possibility to increase this density through 24% of the natural density. We have assumed the natural isotopic composition for the description of the gadolinium and cadmium. Both materials have been studied in the form of a foil.

4.4.3.3 Dimensions of the Poison Belt

The dimensions (height and thickness) of the poison belt must be realistic in terms of both manufacturing and efficiency of peak control. For the poison in a powder form, a study has been carried out to evaluate the sensitivity of the height and the thickness of the belt. The poison used was boron as used in the current HEU fuel. The bottom of the belt was fixed at 1cm above the top of the fuel plates. We have arbitrarily fixed the minimum thickness as the one used in the current plates which is 0.051 cm. The maximum of thickness considered has been set to double the minimum value, 0.102 cm. The minimal height has been arbitrarily chosen as the current height of the current boron zone, 3 cm. Taking into account the dimensions of the top of the fuel element, the maximum height has been set at 5cm. The methodology was divided in two steps. First, the height of the poison belt was fixed to determine the heat flux evolution as the thickness was changed. Second, the thickness of the poison belt was fixed to evaluate the heat flux evolution as the height was changed.

Figure 4.16 shows the evolution of the maximal heat flux as a function of the thickness of the poison belt. The height was fixed at 4 cm. A strong drop is observed as

the thickness increases. Nevertheless, the effect saturates when the thickness is more than approximately twice the current thickness.

Figure 4.17 shows the evolution of the maximal heat flux as a function of the height of the poison belt. The thickness was fixed at 0.094 cm. A strong drop is observed as the height increases. Then, the effect saturates when the height is greater than 4 cm.

In the rest of our calculations, dimensions of the poison belt were fixed for all configurations. The thickness has been set to 0.094 cm and the height to 4.42 cm. These dimensions are in the range of 'saturation' described previously. A cladding border has been implemented to surround the poison belt in order to be as realistic as possible. The thickness of the cladding is the same of the current plate, which is 0.038 cm.

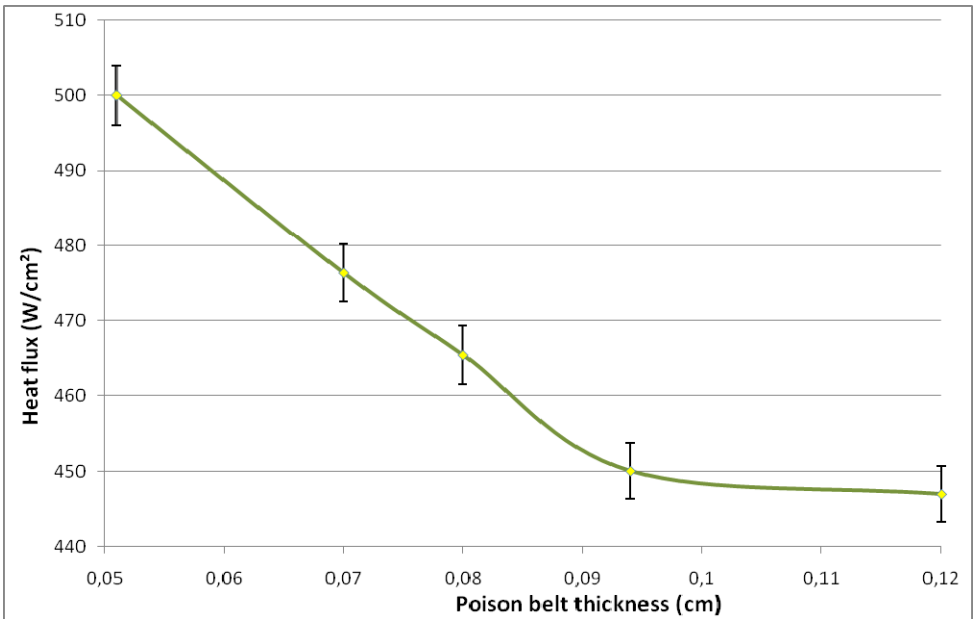

Figure [4.16]: Maximum heat flux as a function of the thickness of the poison belt. The height was fixed at 4 cm. Control area set at 0.5x0.5 cm^2

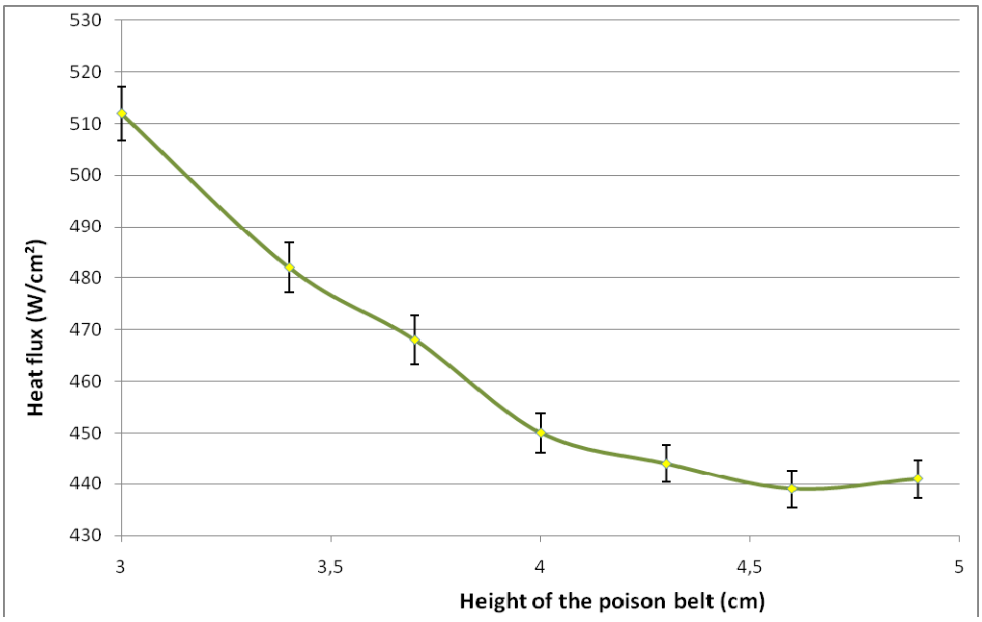

Figure [4.17]: Maximum heat flux as a function of the height of the poison belt. The thickness was fixed at 0.094 cm. Control area set at 0.5x0.5 cm^2

4.4.3.4 Cadmium and Gadolinium Foil

The study of the cadmium and gadolinium foil as possible alternative poisons has been carried out in a range of 4-5.5 cm above the top of the plates. For the cadmium and gadolinium foil, a height of 4.42 cm has been selected. The density has been set to 99.95% of purity. The thickness has been set in a range of 0.094 cm to 0.2 cm.

Indeed, the optimal position of the foil is determined by the poison cross section and by the efficiency. Gadolinium and Cadmium capture cross sections are considerably stronger than boron, so for a similar position, both elements are burned faster than the boron. The peak of power stays problematic during at least 35-40 days and so, the poison has to act during at least this period which is impossible if the cadmium or gadolinium belt is too close to the top of the plates. The minimal distance has been evaluated to be 4cm above the top of the plates. On the other hand, studies indicated that the efficiency of these foils is not sufficient when they are positioned 5.5 cm above the top of the plates. Using a surface of control of ~0.3x0.3 cm^2, studies show that a foil thickness of 0.094 cm is enough to satisfy the qualification limit for any position chosen in the stated range.

Unfortunately, when the asymptotic control-surface method is applied, studies show that the maximum heat flux is always above the limit regardless of the thickness and position of a Gadolinium of Cadmium foil.

4.4.3.5 Optimal Boron Powder Poison Belt

This section compiles the results obtained regarding the maximum heat flux as a function of all the parameters described above: position of the belt, density of poison and size of surface of control.

As stated previously, the most efficient position is not the easiest one to manufacture, so we have studied how the maximum heat flux is impacted as the distance from the top of the plates to the belt increases and for different boron density. Subsequently, it was possible to evaluate the minimum boron density required to remain under the qualification limit as a function of the belt position. This study has been carried out with both a surface of control of ~0.3x0.3 cm² and with the asymptotic method.

Results are shown in Figure 4.18 and 4.19. As can be seen, results strongly differ for both methods.

Considering a surface of control of 0.3x0.3 cm², the maximum allowed density is reached when the distance between the top of the plates and the bottom of the belt is approximately 5.5 cm. The distance between the top of the plates and the outer border of the outer tube is close to 4.3 cm and so, assuming the maximum allowed boron density, the belt could be fixed along the head of the fuel element.

Figure [4.18]: Evolution of the minimum boron density required to satisfy the limit of qualification as a function of the distance from the top of the plates to the bottom of the belt. The heat flux has been evaluated in a surface of control of ~0.3x0.3 cm²

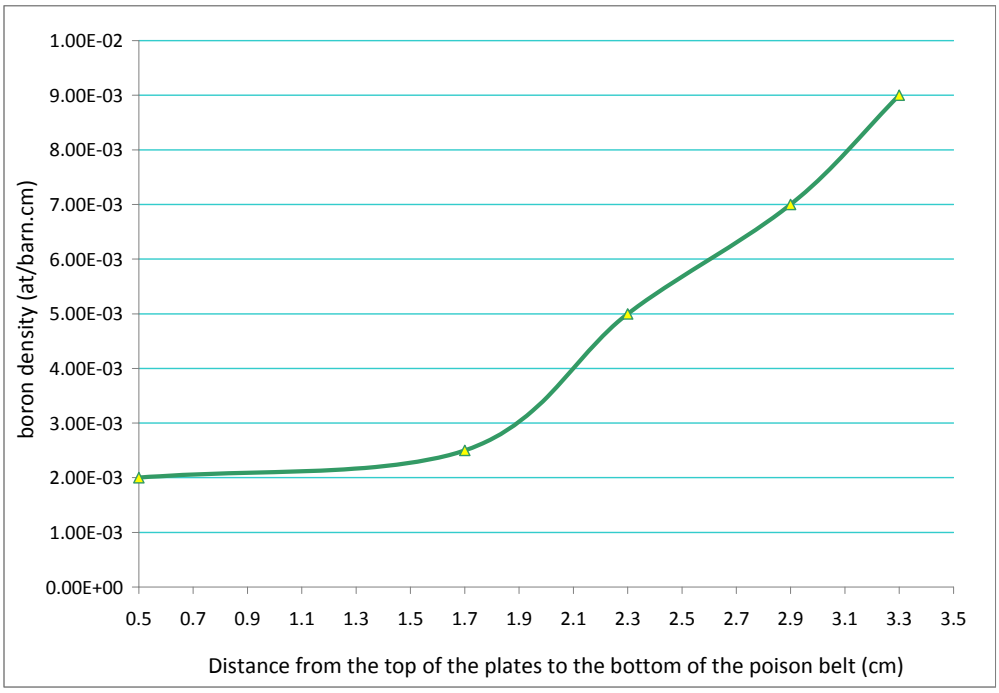

Figure [4.19]: Evolution of the minimum boron density required to satisfy the limit of qualification as a function of the distance from the top of the plates to the bottom of the belt. The heat flux has been evaluated with the asymptotic method.

For the case of the asymptotic meshing method, the maximum allowed boron density is reached when the distance between the top of the plates and the bottom of the belt is close to 2.5 cm. This result indicates that either the belt should be set along the outer tube or that modification of the current system of fixation between the outer tube and the head of the fuel element might be required. Recall that the current border between the outer tube and the head occur 4.3 cm above the top of the plates.

In addition to the complexity of the fuel element manufacturing, there is a concern about the poison density. The boron cross section (n,α) is strong, so the production of ^{4}He is not negligible. We do not know the mechanical impact on the poison belt if the production rate of ^{4}He is higher than for the HEU fuel plate boron zones.

Considering all the results obtained about the position, nature and density of the poisoned belt and taking into account the uncertainties, we can formulate the following conclusions:

- The belt should be placed as close as possible to the top of the plates in order to increase the efficiency and to decrease the minimum required boron density.
- Because the question of the surface of control remains unresolved, the asymptotic method should be preferred.

Considering these points, we recommend the use of a boron belt along the outer tube positioned 0.5 cm above the top of the fuel plates, with a ^{10}B density of $2.3x10^{-3}$ at/barn.cm. A distance of 0.5 cm seems reasonable to avoid changes to the plate welding process. Though Figure 4.19 indicates that a density of $2x10^{-3}$ at/barn.cm is enough for the proposed position, we have increased the poison density 15% to cover the manufacturing uncertainties.

This configuration has been used as the reference LEU design for the thermal-hydraulic studies.

4.4.3.6 Cycle Length

A first depletion calculation has been carried out for the LEU Relocated Poison configuration, using the divided model (45 cells to describe the fuel meat) and the VESTA automatic critical search. Then, a second depletion has been performed with REBUS-MCNP applying the Control Rod (CR) positions found by VESTA.

The VESTA calculation predicted the cycle length per full CR withdrawal. The REBUS-MCNP calculation has been used to check that the k-effective stays stable during all the cycle. Though the belt poison modeled in these calculations was set at 9 cm above the top of the plates with a density of $3.5x10^{-3}$ at/barn.cm (thus not representative of the proposed design), we expect the cycle length to have been evaluated correctly.

Recall that the nature, position or even the density of the poison does not impact the cycle length if it is burned sufficiently. For the presented configurations, we have checked that the amount of poison at the end of cycle is completely negligible, The recommended design has a lower boron density in a poison belt positioned closer to the top of the fuel plates, so the local neutron flux will be higher and the recommended poison belt will be burned even faster than in the depletion calculations performed thus far. In consequence the cycle length given in this paragraph should not be impacted by the recommended design.

The selected LEU design will be explicitly evaluated in subsequent analyses. The time-consuming depletions could not be repeated for each candidate as the design process progressed.

Figure 4.20 shows the CR motion predicted by VESTA with the automatic critical search. The cycle is over when the CR has reached the minimal position (on the graph, this situation occurs when the green line crosses the black line). Thus, the cycle length is estimated to be 47.5 days (± 1 day at 1 sigma). In comparison of the typical cycle length obtained with an HEU core at the same power (57 MW) that represents an increase of 2.5 days.

Figure 4.21 illustrates the k-effective versus time obtained by REBUS-MCNP using the CR position obtained by VESTA. The k-effective obtained at t = 0 (first calculation, no depletion) is a k-effective of reference. As we can see, during all the cycle the k-effective stays stable around the reference k-effective, thus confirming the result obtained by VESTA.

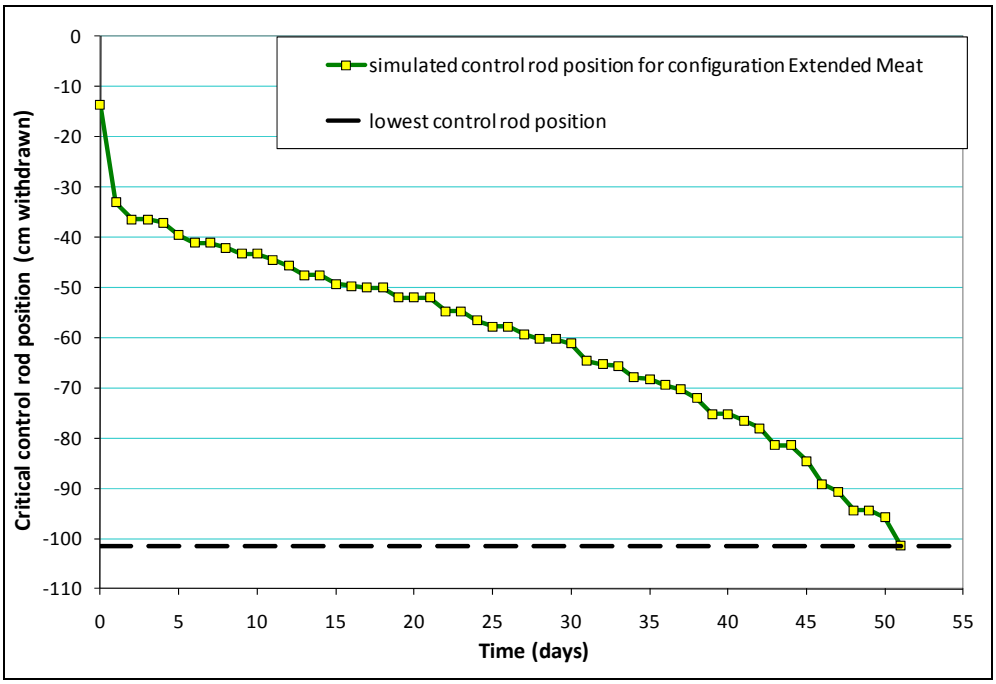

Figure [4.20]: Control rod motion evolution obtained by VESTA with the automatic critical search. LEU Relocated Poison Configuration at 57 MW, divided model

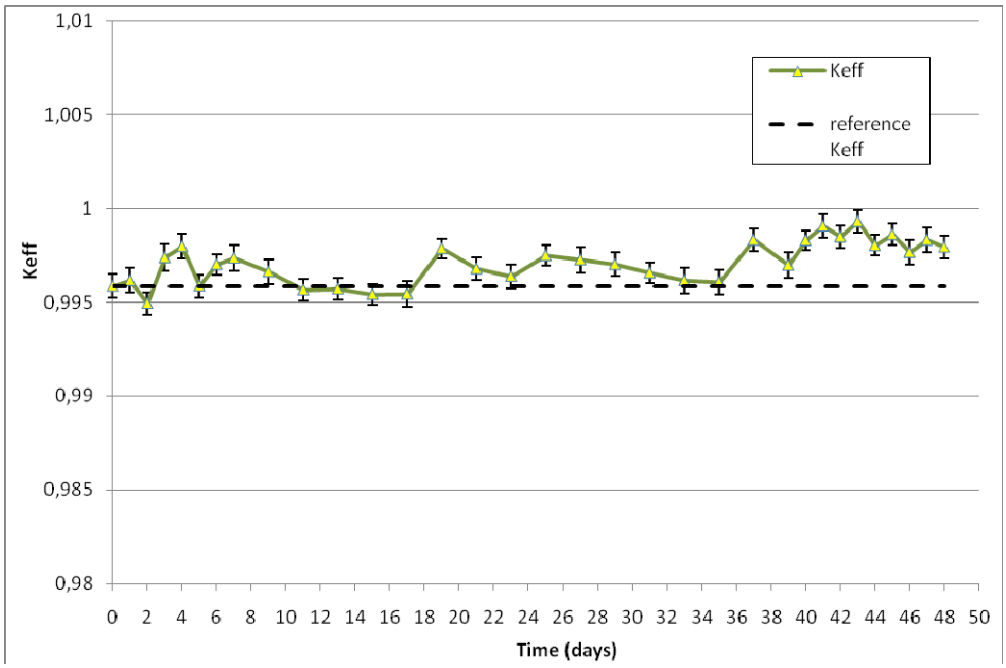

Figure [4.21]: k-effective evolution obtained by REBUS-MCNP using the VESTA control rod positions. LEU Relocated Poison Configuration at 57 MW, divided model.

4.4.3.7 Safety and Control Rod Worths for LEU Relocated Poison Configuration

We have seen in section 4.3.2 that a slight change occurs in the core neutron spectrum between an HEU and an LEU configuration, so we have evaluated the possible consequence on the safety rods (SR) and control rod efficiency.

We have evaluated the worth of one, two, three, four and five SR fully inserted. To make a comparison, we have carried out this study for an HEU core and for the recommended LEU Relocated Poison configuration. Because the control rod can introduce a bias, we have considered two cases: with and without control rod.

Results are presented in Figures 4.22 and 4.23 for the cases with and without control rod, respectively. Both graphs show the same trend: with an LEU core, the safety rod efficiencies drop by approximately 5.5%.

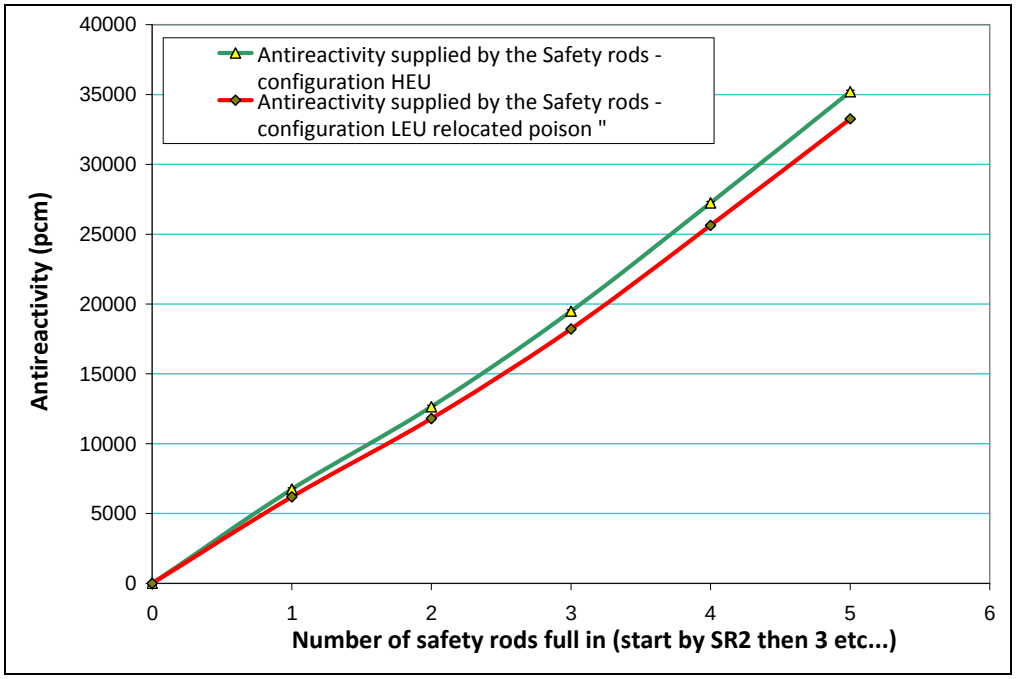

Figure [4.22]: Safety rod worths for HEU and for LEU Relocated Poison Configuration where the control rod is fully inserted

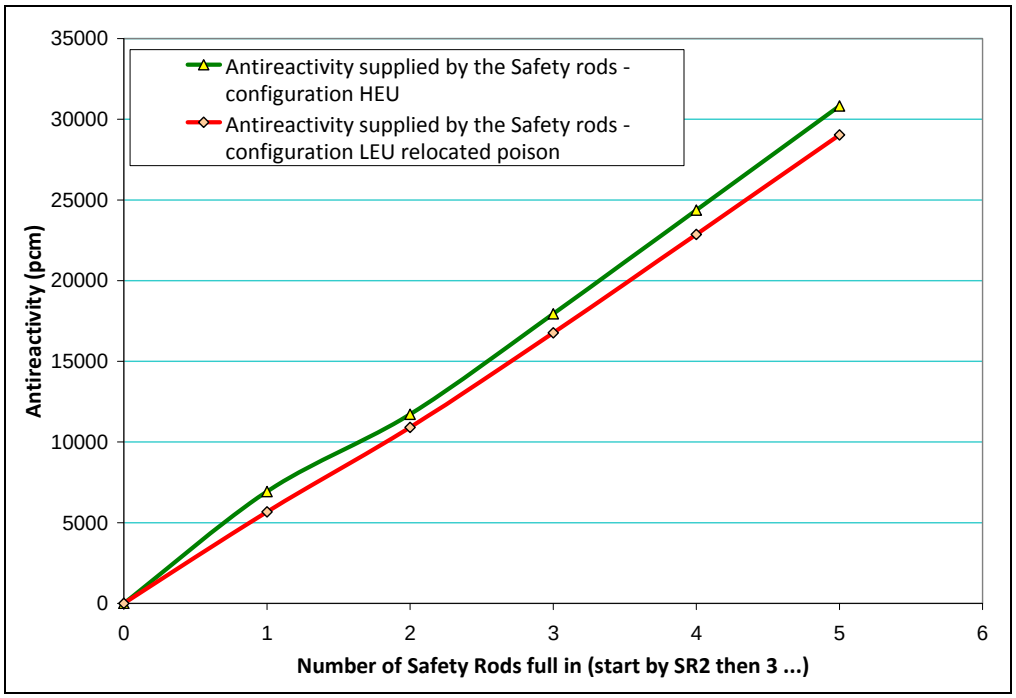

Figure [4.23]: Safety rod worths for HEU and for LEU Relocated Poison Configuration where the control rod is fully withdrawn

Applying the same methodology discussed in section 4.2.2, the control rod (CR) worth for the LEU Relocated Poison configuration was evaluated. A worth of 15,289 pcm (± 52 pcm at 1 sigma) was calculated, in comparison to 17,048 pcm calculated for the HEU core. That represents a decrease of nearly 10%. Two reasons can explain this result. First, the hardening of the spectrum in the central column (where the CR is located) will reduce the CR capture rate. Second, the LEU core studied has a meat extension of 4 cm on the top and at the bottom along the same axis as the control rod motion, so the distance between the top of the fuel and the top of the fully inserted control rod would be decreased by 4 cm. This would prevent the CR from capturing neutrons as efficiently as an HEU configuration.

In order to determine whether these decreases in rod worths have a significant importance, we have evaluated the safety margin in the ILL accident reference scenario.

Accident Scenario

As described in section 4.2.3, one of the accidental scenarios considered in the RHF SAR is the introduction of light water between the fuel plates. This situation could occur if there is a rupture in the heavy water inlet pipe within the light water pool that surrounds the heavy water reflector tank. Once the fall in primary pressure due to a rupture is detected and the safety rods drop (i.e., insert) in 650 ms. However, the primary coolant pumps have a high inertia which could send a mixture of light water and heavy water into the core (the composition of which would vary with the size of rupture). The mixture would reach the RHF core in 1000 ms.

This accident configuration was simulated by MCNP. Light water was modeled above the fuel element and between the fuel plates. The fuel element was fresh and the control rod set at the first critical position (22.94 cm withdrawn). In addition, the accident scenario considered four of the five safety rods fully inserted and the last "stuck" fully withdrawn. Thus, we have studied five cases. For each, a different SR is set in the withdrawn position. The k-effective obtained for each case is compiled in the Table 4.11. As can be seen, the highest k-effective is obtained when SR 5 is stuck. In this configuration, the k-effective is 0.99058 (± 40 pcm at 1 sigma). Recall that the result is conservative due to the underestimation of the safety rod worths. This results show that, even under this accident configuration, the reactor maintains shutdown margin for the recommended LEU Relocated Poison configuration.

Table [4.11]: k-effective obtained for 5 accident configurations

CONFIGURATION	k-effective ± σ (pcm)
SR 1 withdrawn	0.98780 ± 44
SR 2 withdrawn	0.97095 ± 36
SR 3 withdrawn	0.98751 ± 48
SR 4 withdrawn	0.98870 ± 37
SR 5 withdrawn	**0.99058 ± 40**

4.4.3.8 Beff

The Beff has been evaluated by the “classic” MCNP methodology which consists of evaluating the k-effective with and without the delayed neutrons. Per section 4.2.6, we have used the library which has given the most conservative result for an HEU core: the ENDF/B7 library. We calculated a value of 657 pcm (± 28 pcm at 1 sigma) for the LEU Relocated Poison configuration in comparison to 685 pcm (± 28 pcm at 1 sigma) with the HEU core. These two values are close (indeed within statistics) but have been evaluated for the fresh core. Due to the non-negligible production of plutonium in the LEU fuel, we evaluated the change of Beff with burnup. At the end of the cycle a Beff of 658 pcm (± 31 pcm at 1 sigma) was predicted for the LEU Relocated Poison Configuration. Thus, the presence of plutonium in the depleted core did not significantly impact Beff.

4.4.3.9 Brightness in the Beam Tubes

The brightness in the beam tubes has been evaluated by the ILL staff [Ref. 12]. ANL has only evaluated the brightness in the horizontal and vertical cold source. Figures 4.24 and 4.25 show the brightness predicted in a neutron energy range of 10^{-9} to 10^{-6} MeV. The figures clearly show a drop of brightness with the LEU configuration. We have evaluated the loss at 10-12% in comparison of an HEU core at the same power of 57 MW nuclear. ILL results converge to the same conclusion for all beam tubes. Recall, however, that the HEU fuel is currently operated at 52 MW nuclear.

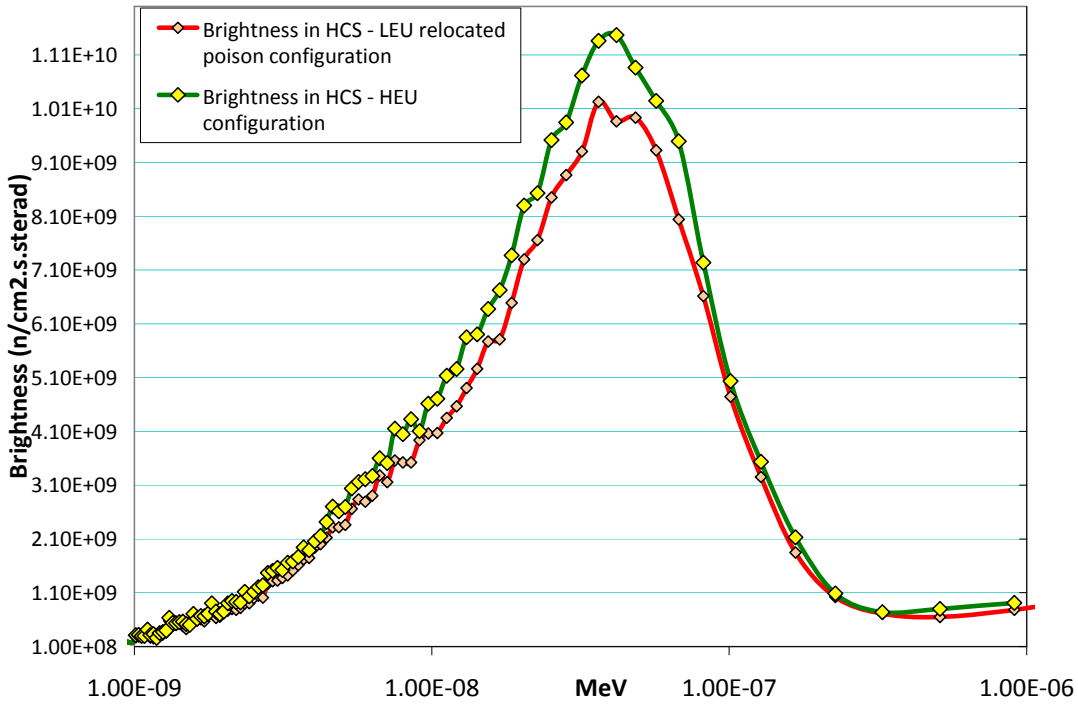

Figure [4.24]: Brightness in the Horizontal Cold Source (HCS) evaluated for HEU and LEU Relocated Poison Configuration at t=0 - nuclear power of 57 MW

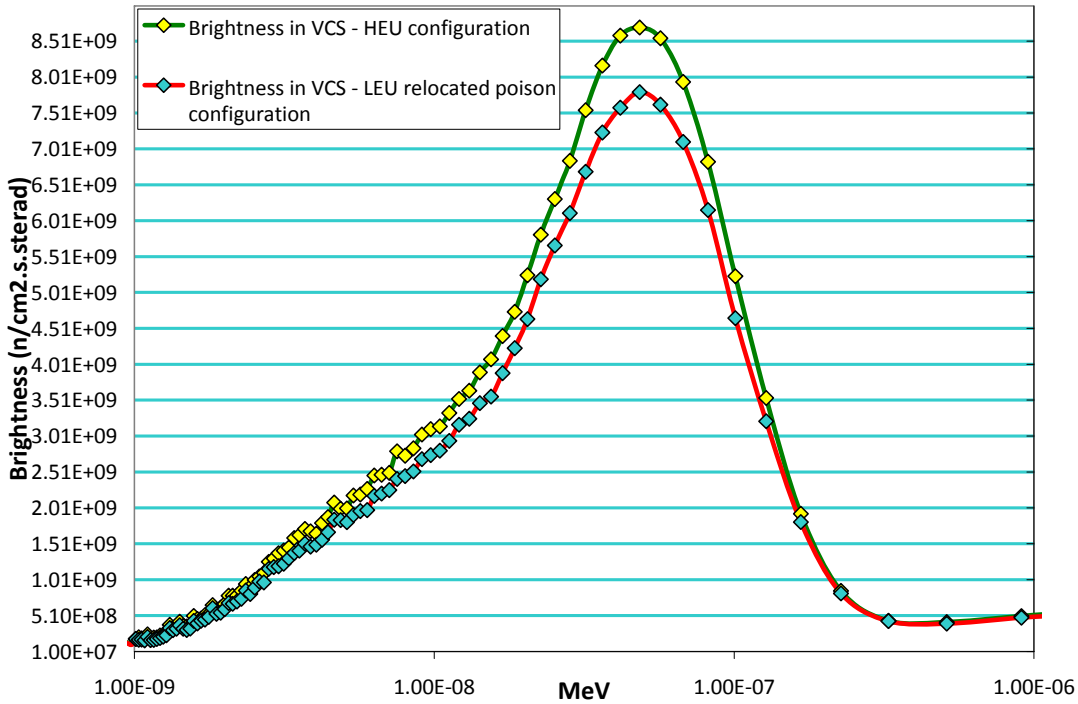

Figure [4.25]: Brightness in the Horizontal Cold Source (VCS) evaluated for HEU and LEU Relocated Poison Configuration at t = 0 - nuclear power of 57 MW

4.5 Summary of Neutronic Analyses

The goal of the neutronic analyses was to determine the impact of RHF conversion to LEU dispersion UMo fuel.

Credibility of the computational models was demonstrated. An extensive series of HEU core benchmarks has shown that codes and models are able to predict correctly or conservatively all parameters needed (cycle length, safety and control rod worth, power distributions, Beff).

Using the credible models, we have studied the performance of a core loaded with LEU UMo. Cycle length and neutron flux appear to be too strongly degraded for the simplest case of direct replacement of the HEU fuel meat with LEU UMo fuel meat.

Thus, a long investigation was performed in order to design an alternative LEU fuel element. Based on a reasonable set of manufacturing assumptions, a promising configuration has been found called the LEU Relocated Poison configuration. In this configuration, the amount of fuel meat has been increased by roughly 9% without any modifications on the external plate's dimensions by removing the boron zones from the plates. In order to manage the peaking factor, it is proposed that a belt of boron poison be fixed along the outer radius of the fuel element.

Key performance metrics were evaluated for the recommended LEU. Table 4.12 compiles the main results that we have calculated compared to an HEU core operating at the same nuclear power.

Table [4.12]: Comparison of performance between an HEU core at 57 MW nuclear and the recommended LEU design at the same power

	LEU 57MW	**HEU 57 MW**	**% Change (LEU-HEU)/HEU**
Cycle length (days)	47.5	45.0	***5.6%***
max. Brightness HCS (n/cm²/s/sterad)x10^{-10}	1.02	1.14	***-11.8%***
max. Brightness VCS (n/cm²/s/sterad)x10^{-10}	0.78	0.87	***-10.3%***

As can be seen, the cycle length is increased by roughly 5.6% but with a drop of brightness close to 10.5%. We have not evaluated the brightness everywhere, but the ILL team did and reached the same conclusion.

Recall that the RHF reactor is currently operated at a power lower than rated power in order to increase cycle length for operational efficiency. Thus, it is important to compare the LEU core performance with the current typical performance of the reactor. The RHF typically operates at 52 MW nuclear, resulting in an increase of cycle length but reduced the neutron flux. Table 4.13 compiles the main results that we have obtained for the recommended LEU Relocated Poison configuration compared to the current HEU core performance.

Table [4.13] Comparison of performance between an HEU core at 52 MW nuclear (current condition of operation) and the recommended LEU design at 57 MW nuclear

	LEU 57MW	**HEU 52 MW** ***(current condition of operation)***	**% Change (LEU-HEU)/HEU**
Cycle length (days)	47.5	49.5	***-4.0%***
max. Brightness in HCS (n/cm²/s/sterad) x 10^{-10}	1.02	1.04	***-1.9%***
max. Brightness in VCS (n/cm²/s/sterad) x 10^{-10}	0.78	0.79	***-1.3%***

In comparison to the current condition of operation, the LEU recommended design can maintain the RHF performance at a high level: 4% of loss of cycle length (2 days) and brightness drop of less than 2%. Thus, the LEU recommended design is a promising solution for the RHF conversion.

V Thermal-Hydraulic Analyses

5.0 Introduction

This chapter presents the Computational Fluid Dynamics (CFD) model developed for the analysis of the impact of conversion to LEU dispersion UMo on the thermal-hydraulic performance and safety margin of the ILL Grenoble High Flux Reactor (RHF) and preliminary results of thermal-hydraulic analyses performed for the RHF HEU and LEU configurations.

5.1 Review of RHF Geometry

The RHF has one fuel element, made of 280 curved plates welded to two concentric aluminum tubes. All of the curved plates are bent into an involute shape. This shape has the advantage of maintaining a constant distance between two plates within the overall cylindrical geometry of the compact core. Figure 5.1 is a diagram of the fuel element. The element is placed in a heavy water tank which is itself surrounded by a light water pool. The heavy water plays the dual role of neutron moderator and coolant. The RHF is controlled by a central rod. The position of the control rod is adjusted during the cycle to maintain criticality. For the current HEU fuel, two borated zones exist in the lower and upper parts of each fuel plate. The borated zones help to reduce power peak intensities at the axial edges of the plates. The HEU fuel is a mix of U-Al_x in an aluminum matrix. The enrichment in ^{235}U is 93%.

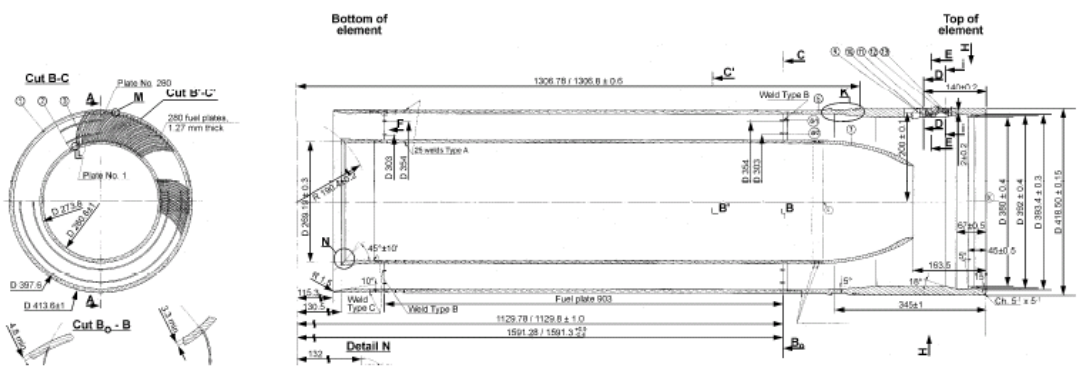

Figure [5.1]: Fuel element overview [Ref. 10]

The dimensions of the HEU fuel plate including the fuel meat, the borated zones and the cladding are illustrated in Figure 5.2.

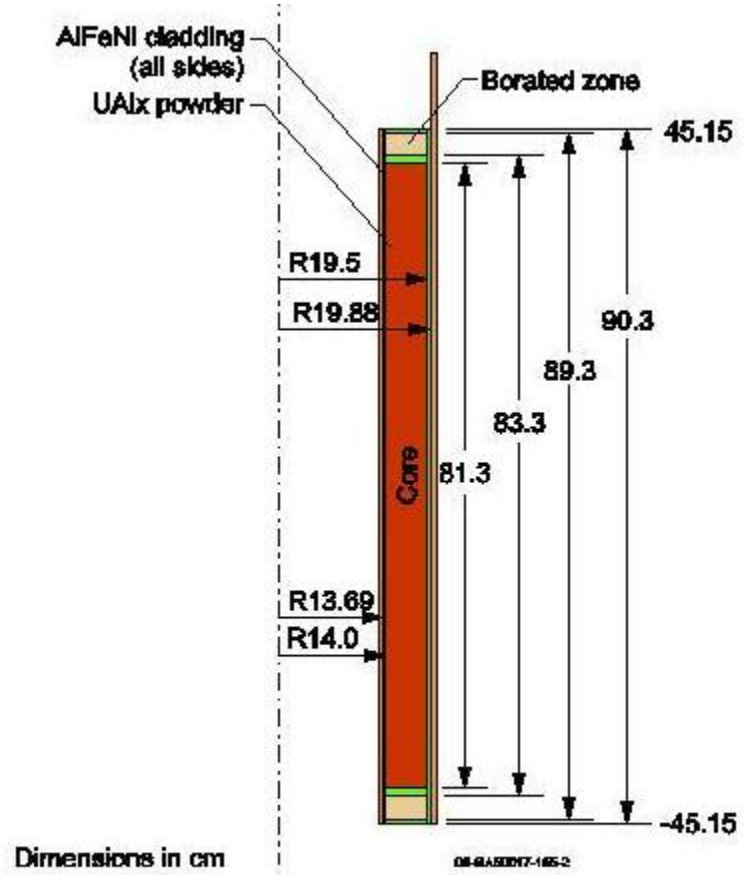

Figure [5.2]: HEU fuel plate dimensions [Ref. 9]

5.2 The CFD Model of the HEU RHF Reactor

The thermal-hydraulic performance of the RHF has been evaluated using the STAR-CD CFD code [Ref. 14]. The STAR-CD model of the RHF describes two coolant channels bound by a full fuel plate, two half-plates and the outer and inner rings, as illustrated in Figure 5.3. The outer surfaces of the two half-plates are designated as cyclic boundaries. The fuel plate is constructed as an arc of a circle, with the radius of the inner cladding surface $R_{cladding}$ = 8.53 cm. This is an approximation of the involute and was selected because the same approximation is used in the neutronic calculations that determine the RHF power generation distribution. The CFD model is script-based and thus the geometry, mesh size and physical parameters can be easily modified for future sensitivity studies.

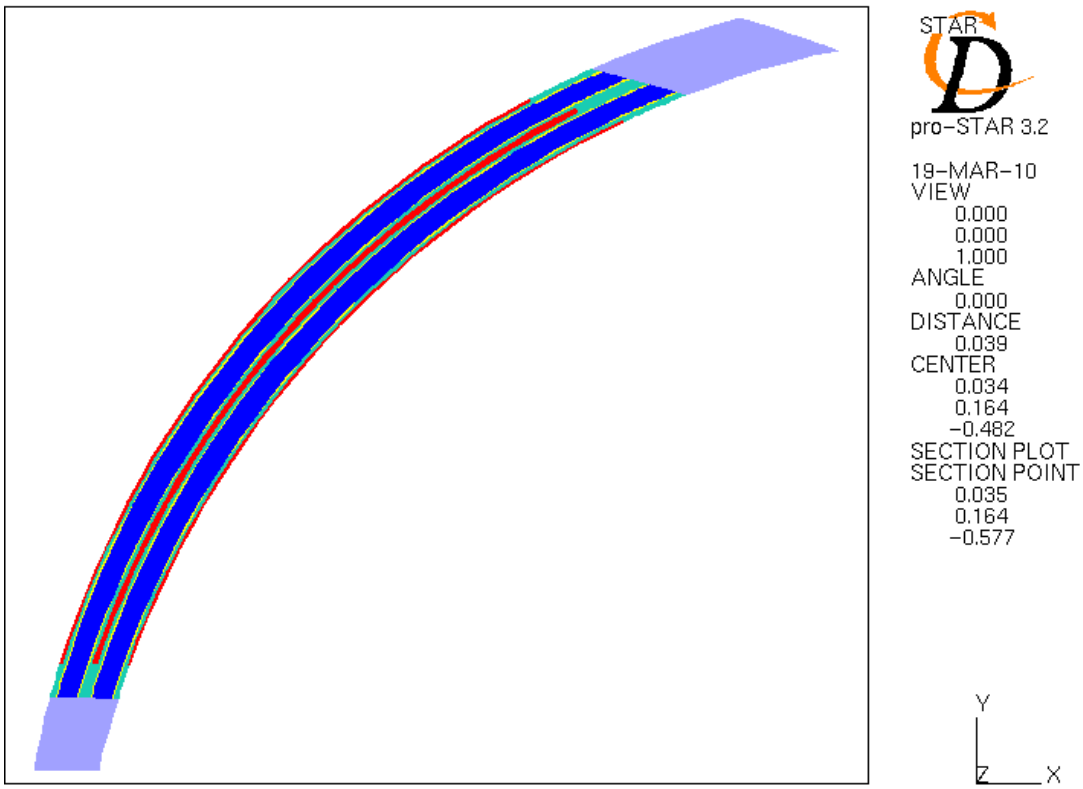

Figure [5.3]: Cross section through the coolant channels and fuel plates modeled, viewed from the +z direction: blue - coolant; red - fuel; green - cladding; yellow - cladding surface cells; light blue - inner and outer rings

The axial structure of the CFD model of the HEU configuration is illustrated in Figure 5.4. The model includes the cladding, borated regions and fuel meat region, with the dimensions shown in Figures 5.1 and 5.2. A short inlet plenum with L = 1 cm was added at the inlet. A longer outlet plenum is used at the outlet, with L = 5 cm. Both plena are needed to ensure convergence of the pressure solution in the presence of parallel coolant channels. The longer outlet plenum is necessary due to the presence of the

expansion at the exit of the inter-plate sub-channels, which can cause numerical problems at the outlet boundary condition if this boundary is too close to the flow expansion.

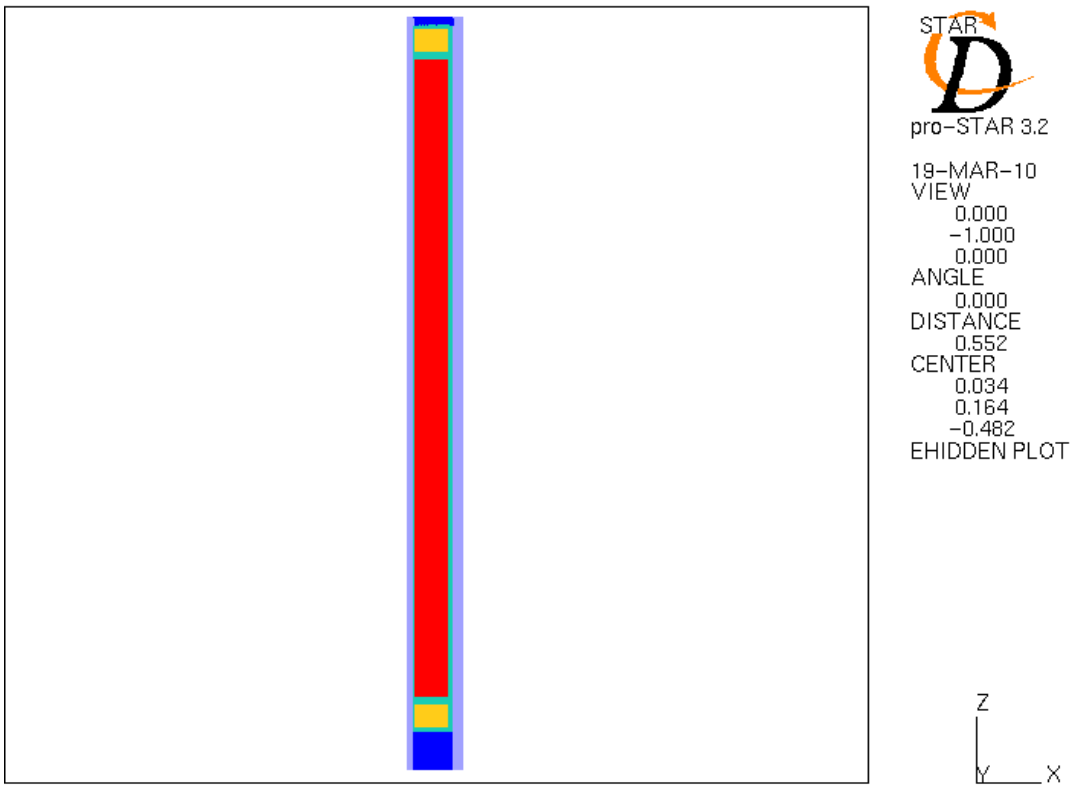

Figure [5.4]: Cross section through the centerline of the HEU fuel plate, viewed from the -y direction illustrating the features of the CFD model: blue - coolant; red - fuel meat; green - cladding; orange - borated regions; light blue - inner and outer rings

5.2.1 The CFD Computational Mesh

The computational mesh used in the CFD analyses is controlled by parameters defined in the script. Thus, changing the mesh size for various regions of the domain is relatively easy, provided that convergence is achieved. The mesh parameters used in the preliminary calculations described in this report are listed below:

- Number of layers in the fuel meat along the curved centerline - 30
- Number of layers in the fuel meat thickness - 4
- Number of layers in the fuel cladding thickness - 3
- Number of layers in the bottom cladding end along the curved centerline, between the lower end of the fuel meat and the upper edge of the lower ring - 8
- Number of layers in the top cladding end along the curved centerline, between the upper end of the fuel meat and the lower edge of the upper ring - 12
- Number of layers in the bottom ring along the curved centerline - 4
- Number of layers in the top ring along the curved centerline - 6
- Number of fluid layers in a coolant channel - 20

- Number of layers in the coolant channel along the curved centerline, facing the fuel meat region - 30
- Number of cells in z direction, top plenum - 10
- Number of cells in z direction, first cladding region - 3
- Number of cells in z direction, top borated region - 6
- Number of cells in z direction, second cladding region - 4
- Number of cells in z direction, fuel meat region - 20
- Number of cells in z direction, third cladding region - 4
- Number of cells in z direction, bottom borated region - 6
- Number of cells in z direction, fourth cladding region - 3
- Number of cells in z direction, bottom plenum - 20

A coarse axial mesh with only 20 axial cells in the fuel meat was used in the initial HEU scoping calculations. To study the sensitivity of the maximum coolant temperature to the computational mesh, calculations were performed with 10 layers and 20 layers in the coolant channel between adjacent fuel plates. The model with 10 layers in the coolant channel contains a total 217,840 cells and the model with 20 layers in the coolant channel contains 317,520 cells. A detail of the computational mesh with 20 layers in the coolant channel is shown in Figure 5.5.

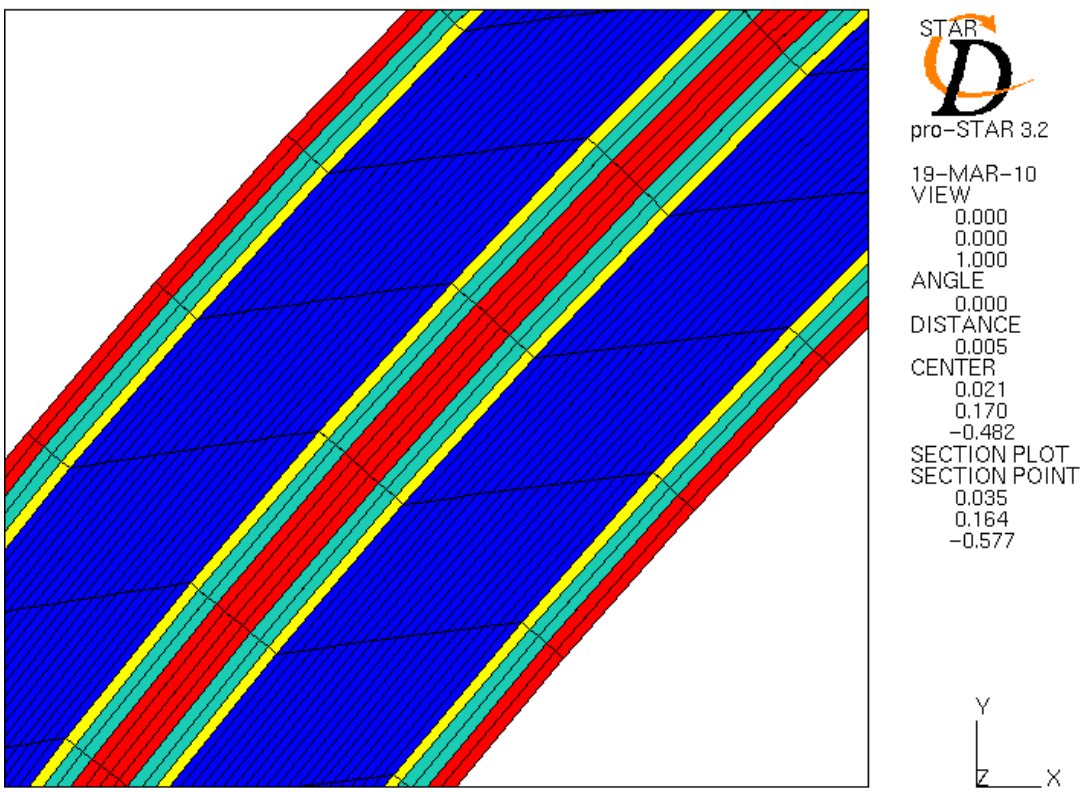

Figure [5.5]: CFD Computational mesh detail: red - fuel meat; green - cladding; yellow - cladding surface cells; blue - coolant

5.2.2 Material Properties

The material properties [Ref. 15] used in the current CFD model are listed below:

Heavy water D2O properties:
- Density – 1105.6 Kg/m3
- Viscosity - 1.0×10^{-3} Kg/(m*s)
- Conductivity - 0.5799 W/(m*K)
- Specific heat - 4242.0 J/(Kg*K)

Aluminum properties:
- Density - 2702.0 Kg/m3
- Conductivity - 237.0 W/(m*K)
- Specific heat - 903.0 J/(Kg*K)

Aluminum properties were used for the cladding and ring regions. The same properties were used in the scoping calculations reported, for the fuel meat and borated regions, which have high aluminum content.

5.2.3 Boundary Conditions

The boundary conditions used in the CFD model are listed below:

Coolant inlet boundary (upper plenum inlet):
- Boundary type: Inlet
- Velocity: -9.894 m/s (corresponding to -17.0 m/s in inter-plate coolant channel)
- Temperature: 30 C

Inlet wall boundary (ring cross sections at the upper plenum inlet):
- Boundary type: Wall
- Temperature: 30 C
- Heat resistance: 4.59×10^{-4} (m^2*K)/W

Coolant outlet boundary (lower plenum outlet):
- Boundary type: outlet
- Outlet pressure: 4 bar (absolute)

Outlet wall boundary (ring cross sections at the lower plenum outlet):
- Boundary type: Wall
- Temperature: adiabatic

Inner ring wall boundary:
- Boundary type: Wall
- Temperature: 30 C
- Heat resistance: 4.59×10^{-4} (m^2*K)/W

Outer ring wall boundary:
Boundary type: Wall
Temperature: 50 C
Heat resistance: 8.76×10^{-4} m^2*K/W

Left and right half-plate boundaries (center-line cross sections):
Boundary type: Cyclic

5.2.4 Power Source

The power source distribution in the fuel meat was provided by separate neutronic calculations for a mesh with 163 cells in the axial direction, 11 cells in the plate "radial" direction (i.e., from inner edge of fuel meat to outer edge of fuel meat) and one cell covering the thickness of the fuel meat. A procedure was developed to remap the neutronic mesh distribution on the CFD fuel meat mesh used in the scoping calculations, with 20 axial cells, 30 cells in the plate "radial" direction and 4 cells across the fuel meat thickness. This procedure ensures that the total power used in the CFD analysis is the same as the total power predicted by the neutronic calculations. The total RHF power produced in the fuel meat is approximately 53 MW for HEU operation at 57 MW nuclear. Within the CFD model, 53 MW was assumed to be generated in the fuel meat. The additional heat deposited in structure and coolant due to photon transport was neglected in these preliminary calculations, following the same approach as ILL [Ref. 15].

5.3 Preliminary CFD Analysis of the HEU RHF Reactor

A preliminary CFD analysis of the HEU RHF reactor was performed using the nominal operating conditions and the thermal-hydraulic results of this analysis were compared with corresponding results obtained in a similar CFD analysis performed by the ILL BPC team with the CFX code [Ref. 15].

5.3.1 Results of Preliminary HEU RHF Analysis

In this section we present the results of CFD HEU calculations performed using the model with 20 coolant cells across the coolant channel. The coolant temperature distribution in the coolant cell layer adjacent to the fuel plate is shown in Figure 5.6. The coolant temperature distribution at the wall surface is shown in Figure 5.7. The temperature distribution for the cladding cells at the outer surface of the cladding, adjacent to the coolant, is shown in Figure 5.8. The following maximum temperatures are observed:

Maximum coolant cell temperature
T(coolant cell, max) = 338.4 K (65.25 C)

Maximum coolant wall temperature
T(coolant, wall surface, max) = 372.87 K (99.72 C)

Maximum cladding surface cell temperature:
T(cladding surface cell, max) = 373.7 K (100.55 C)

The best measure of the coolant maximum temperature is provided by the coolant wall temperature T(coolant, wall surface). This temperature is calculated by the code using the law of the wall and is expected to show little sensitivity to the coolant cell size, as long as the y^+ (the non-dimensional distance from the wall to the first grid point) values remain in a reasonable range, usually 30-50. In this calculation with 20 cells across the coolant channel the y+ values are in the range 27-38 for most of the wall cells in the inter-plate channel. The maximum cladding surface temperature is only 0.8 K higher than the maximum coolant temperature and provides a reliable upper bound. The maximum coolant temperature in the cells adjacent to the cladding is - as expected - substantially lower than the coolant wall temperature. The use of this temperature is not recommended for safety studies, as it would take a very fine mesh near the cladding surface to bring it close to the actual coolant wall temperature.

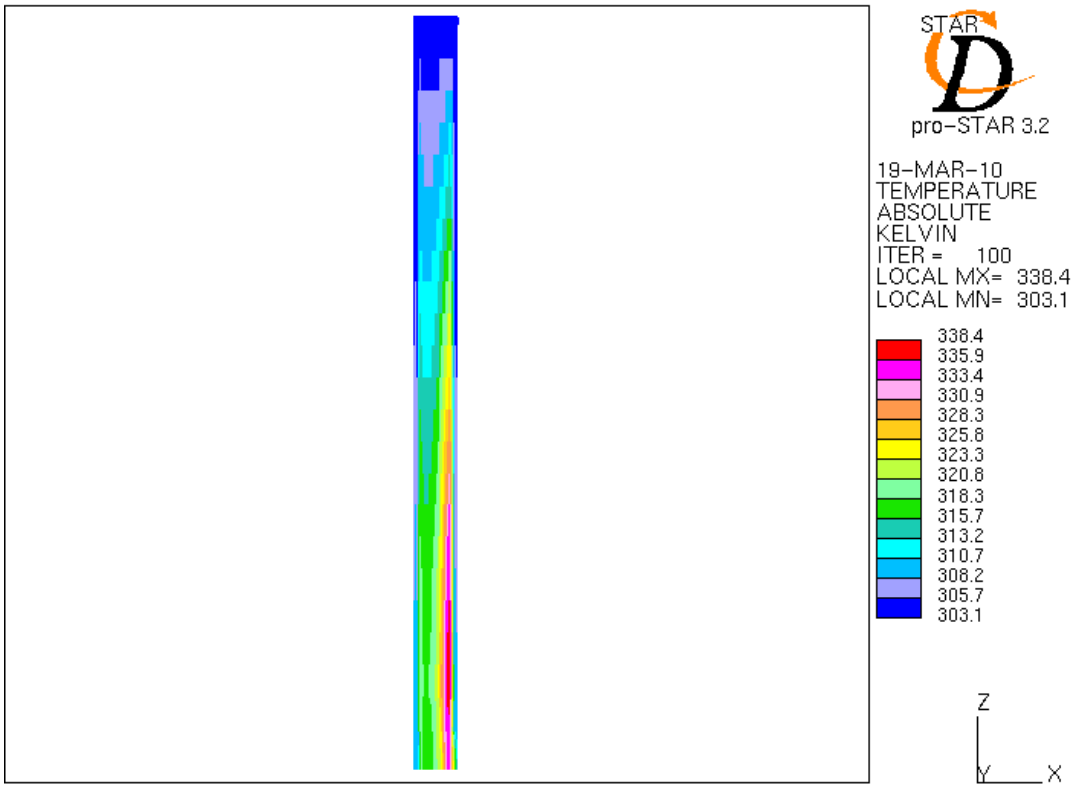

Figure [5.6]: Coolant temperatures [K] at the center of cells adjacent to the fuel plate surface, view from the -y direction. Maximum temperature 338.4 K

A parametric evaluation of a coarser CFD mesh was performed to determine whether the predictions were sensitive to spatial discretization. The maximum temperatures obtained in a calculation using a coarser model, with 10 coolant cells across the coolant channel are presented below:

Maximum coolant cell temperature
T(coolant cell, max) = 337.6 K (65.25 C)

Maximum coolant wall temperature
T(coolant, wall surface, max) = 372.38 K (99.75 C)

Maximum cladding surface cell temperature:
T(cladding surface cell, max) = 373.2 K (100.55 C)

These results show the same pattern as those obtained with the finer mesh, with the coolant wall temperature being close to the cladding surface temperature. Both these

temperatures are only ~0.5 K lower than the values obtained with the finer mesh model, indicating that the sensitivity of these temperatures to the coolant mesh size is limited.

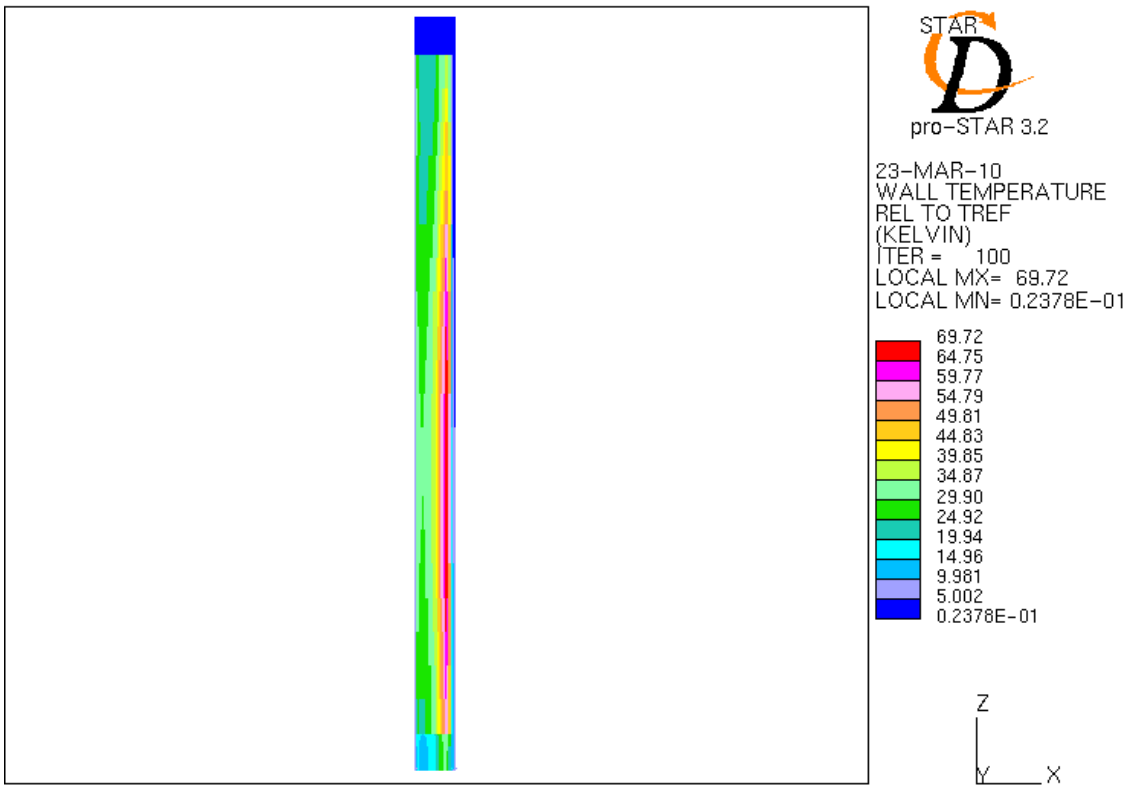

Figure [5.7]: Coolant temperatures [K] at the fuel plate surface, view from the -y direction. Maximum temperature 372.87 K (99.72 C), TREF = 303.15 K

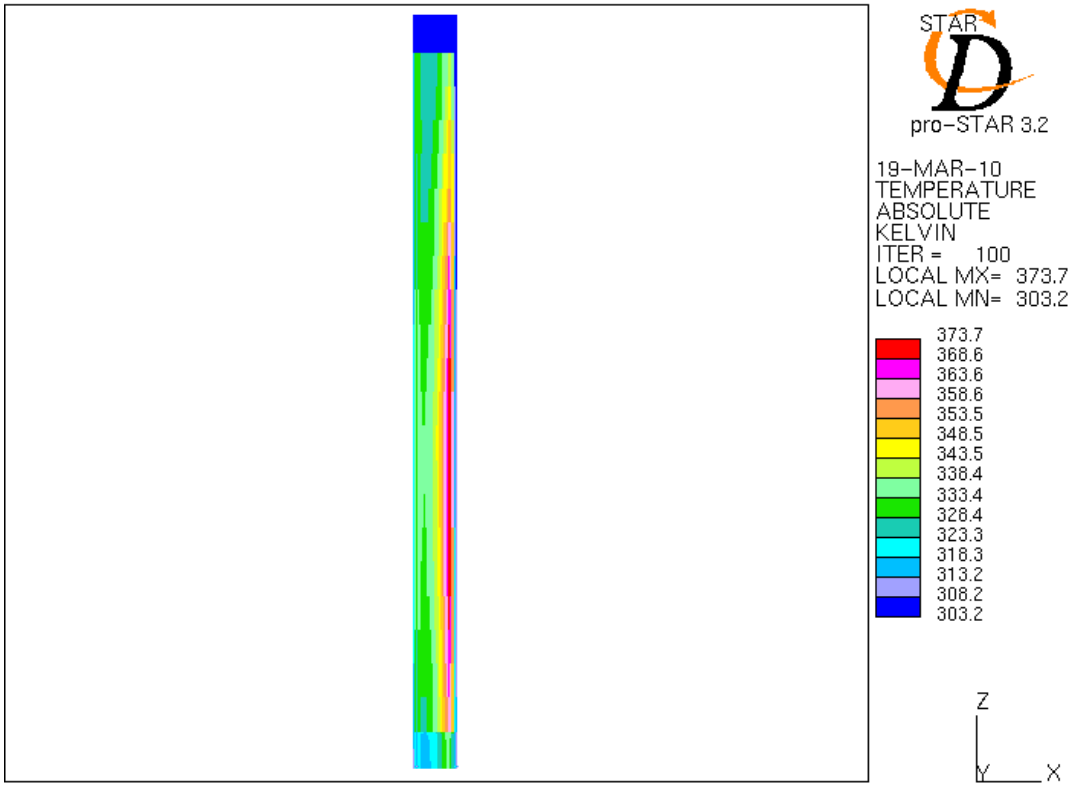

Figure [5.8]: Cladding temperature [K] at the center of cells at plate surface (adjacent to coolant), view from the -y direction. Maximum temperature 373.7.4 K (100.55 C)

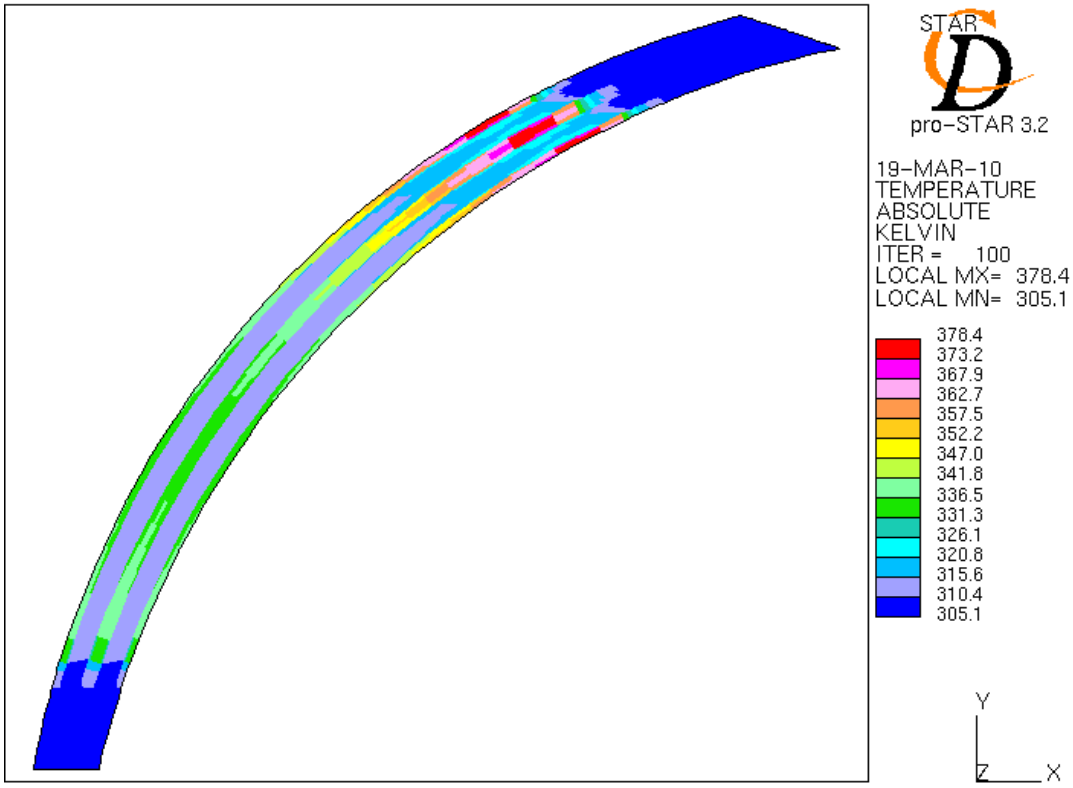

Figure [5.9]: Temperature distribution [K] in a cross section at z = - 0.5 m from inlet, below the plate axial centerline.

A view of the temperature distribution in a cross section through the model at z = - 0.5 m from inlet is shown in Figure 5.9. The maximum temperature T = 378.4 K (105.25 C) occurs in the fuel meat region at the outer edge of the fuel plate, due to the high local power source. A more detailed view of the temperature distribution in the coolant channel can be seen in Figure 5.10. The highest coolant temperature occurs at the same radial location as the highest fuel temperature. The coolant near the outer ring remains relatively cold due to the presence of the low temperature ring material, despite its proximity to the high temperature coolant region.

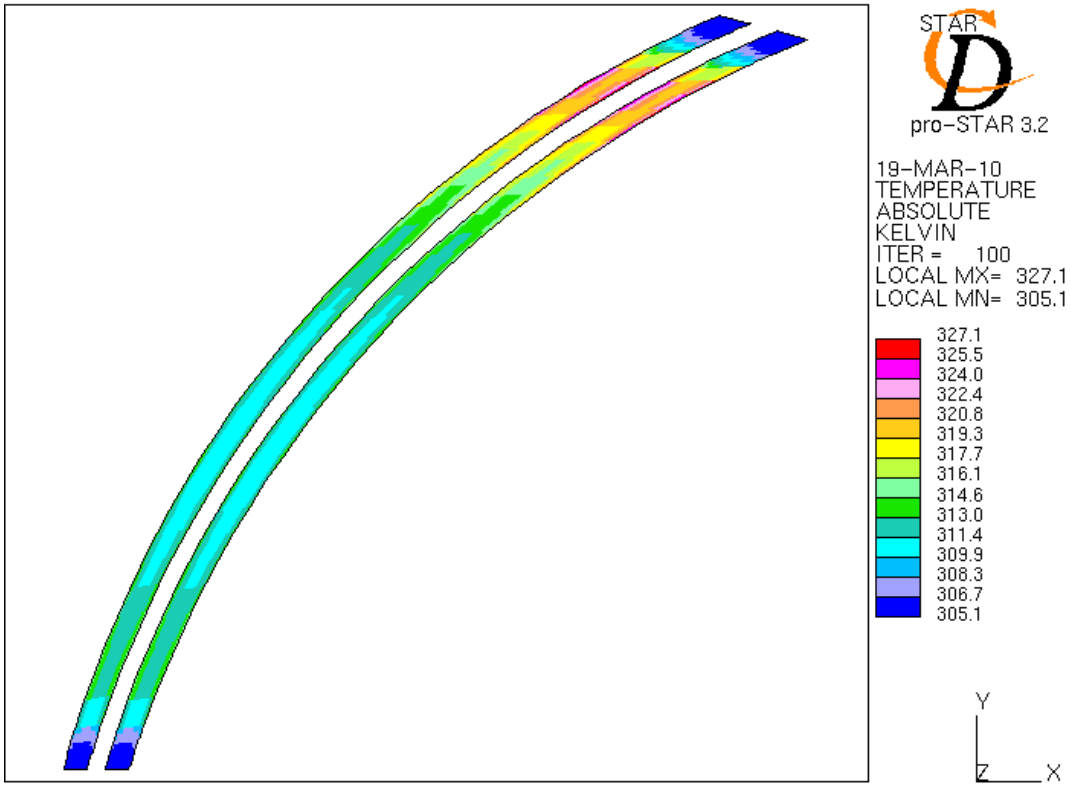

Figure [5.10]: Coolant temperature distribution [K] in a cross section at z = - 0.5 m from inlet, below the plate axial centerline.

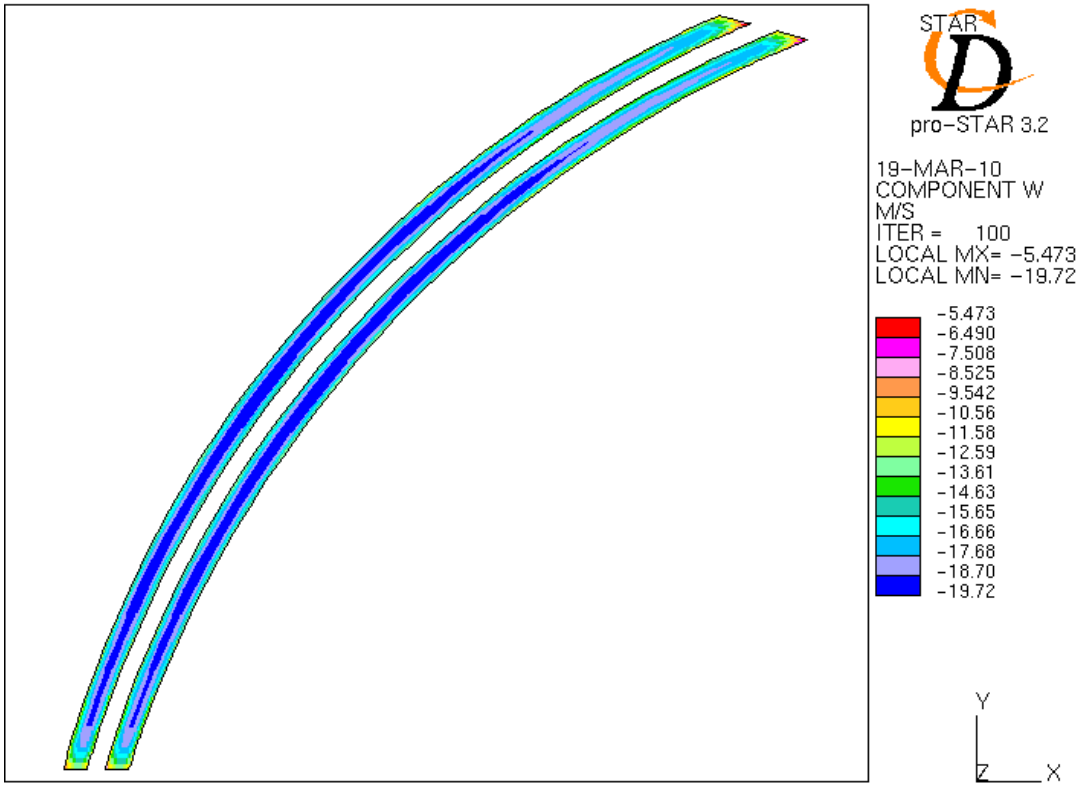

Figure [5.11]: Coolant axial velocity distribution (w component, m/s), cross section at z = - 0.5 m from inlet, below the plate axial centerline.

The distribution of the axial velocity component w in the coolant channels is illustrated in Figure 5.11, for a cross section through the model at z = - 0.5 m from inlet. The maximum velocity (in absolute value) is - 19.72 m/s and occurs at the center of the coolant channel but closer to the inner ring. The lowest absolute value of w is - 5.473 m/s and occurs in the corners formed by the fuel plates and the aluminum rings.

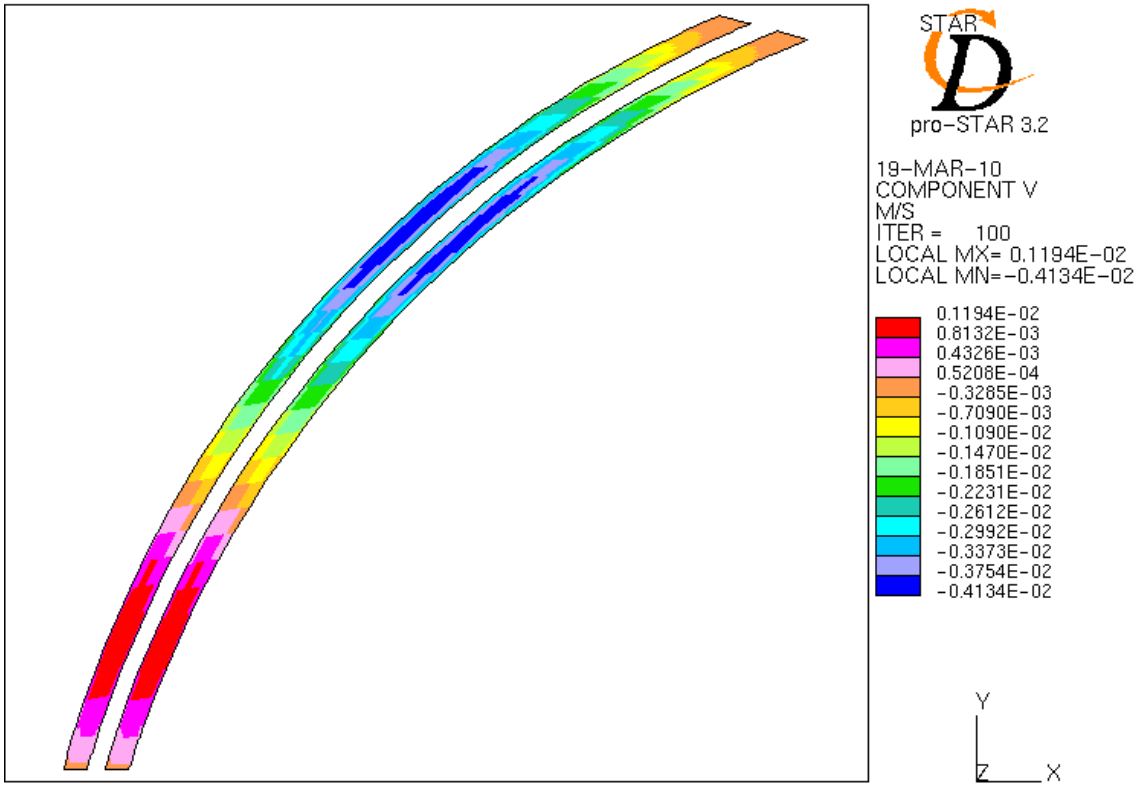

Figure [5.12]: Coolant transverse velocity distribution (v component, m/s), cross section at z = - 0.5 m from inlet, below the plate axial centerline.

The distribution of the velocity component v (along the y axis) in the coolant channels is illustrated in Figure 5.12, for a cross section through the model at z = - 0.5 m from inlet. It shows that the coolant at both ends of the coolant channel tends to move towards the center of the channel along the curved channel centerline with the v component ranging from - 4.1 mm/s in the outer region, to + 1.2 mm/s in the region closer to the inner ring.

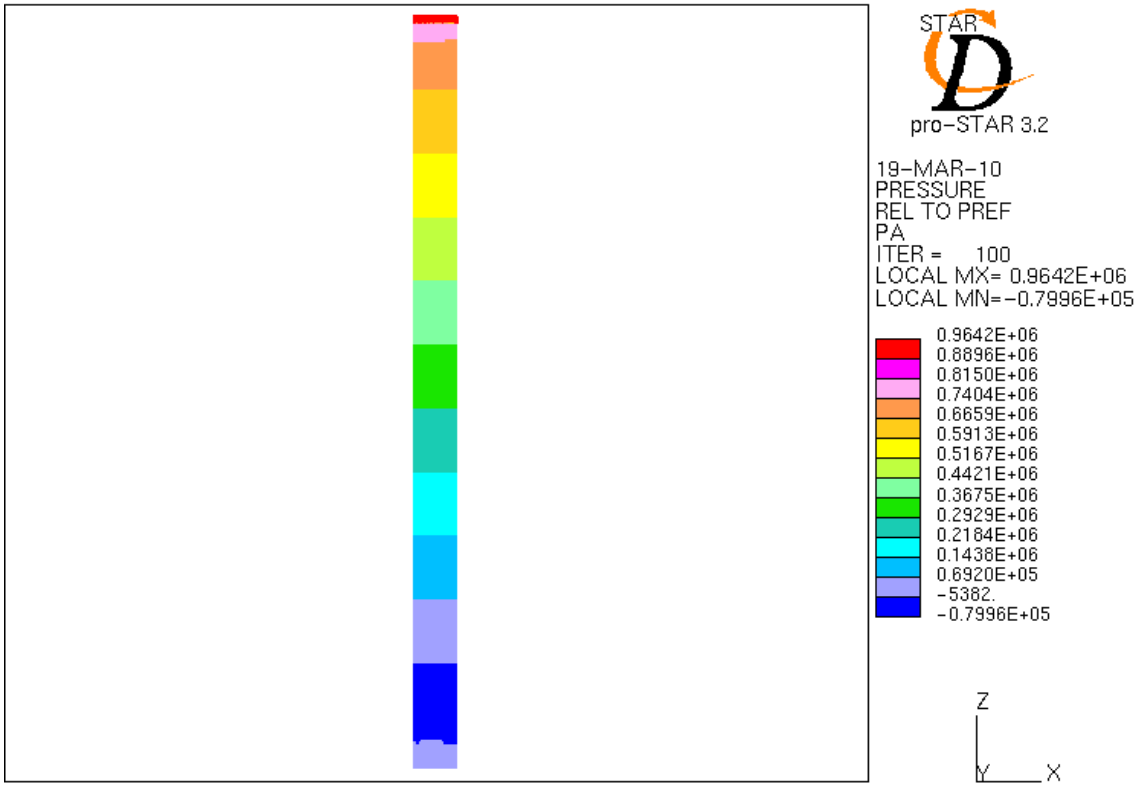

Figure [5.13]: Pressure distribution in the coolant channel [Pa] (relative to PREF = 4.0 bar), view from the -y direction.

The pressure in the coolant channel, relative to the outlet pressure PREF = 4.0 bar is shown in Figure 5.13. The total pressure drop between inlet and outlet is 9.6×10^5 Pa. This pressure drop includes the pressure drops due to contraction at the flow entrance from the inlet plenum into the inter-plate channels and the expansion at the flow exit from the inter-plate channels into the outlet plenum.

5.3.2 Discussion of Preliminary HEU RHF Analysis Results

The maximum coolant temperature, based on the coolant temperature at the surface of the fuel plate, is 99.72 C. This value is lower than the maximum coolant temperature of 104 C obtained in [Ref. 15]. The saturation pressure corresponding to 99.72 C is approximately 1.0 bar. Assuming that the outlet pressure is 4.0 bars [Ref. 15] and noting from Figure 5.13 that the pressure change due to the expansion into the outer plenum is approximately 0.8 bars, we estimate that the lowest pressure in the inter-plate channel is approximately 3.2 bars, corresponding to a saturation temperature of approximately 137 C. Thus there is a margin of approximately 37 C to the saturation limit. The onset of nucleate boiling (ONB) occurs at a temperature higher than the saturation temperature, with the superheat needed for ONB predicted by several empirical models. The margin to saturation and ONB was determined for both the HEU and LEU

fuel in calculations presented in section 5.4 of this report, using the actual channel pressure calculated at the location of the maximum wall surface temperature. The average coolant temperature at the outlet is 47.66 C. This value is lower by 3.04 C than the corresponding temperature of 50.7 C obtained in [Ref. 15]. A comparison of the thermal balance between the current calculations and [Ref. 15] indicates that the lower temperatures in the current calculations are due primarily to the higher coolant channel cross section area. The coolant channel cross section area of the current model is 135.7×10^{-6} m^2, while the corresponding area reported in [Ref. 15] is 115.8×10^{-6} m^2. These modeling differences will be clarified in future detailed safety analyses.

5.4 Preliminary CFD Analysis of the Proposed LEU RHF Reactor

A CFD model of the LEU RHF configuration was developed. Preliminary CFD analyses of the LEU RHF reactor were performed using the nominal operating conditions and the thermal-hydraulic results of this analysis were compared with corresponding results obtained in similar CFD analyses of the HEU RHF reactor.

5.4.1 The CFD LEU Model

The LEU RHF fuel element uses a fuel plate with the same overall dimensions and shape as the HEU RHF fuel element, but the boron regions at the top and bottom of the fuel plate have been removed and the fuel meat region has been extended axially. The boron region is now located outside the region modeled by the CFD model. Its influence on the thermal-hydraulics is taken into account through the power distribution provided to the CFD model by the neutronic calculations. The geometry of the LEU CFD is illustrated in Figure 5.14. The fuel meat region now extends from 5 mm below the top of the plate to 0.5 cm above the bottom of the plate, for a total length of 89.3 cm covering the axial length occupied in the HEU fuel plate by the boron regions, fuel meat and separating cladding regions shown previously in Figure 5.4. All other geometric features of the CFD model remained the same as described above in Section 5.2.

5.4.1.1 The Refined CFD Computational Mesh for the HEU and LEU Models

The computational mesh used for HEU analyses reported in this section remains the same as described in Section 5.2.1, with the exception of number of axial cells in the fuel meat. The axial mesh in the fuel meat, which in the preliminary calculations described above used a coarser discretization with 20 axial cells, was refined to allow a more accurate representation of the axial power distribution, especially at the upper and lower ends of the fuel region where larger axial power generation gradients are present. The total number of axial cells in the HEU fuel meat has been increased to 56 cells, with 15 cells at the top and 14 cells at the bottom of the fuel meat having a length of 1.0 cm and 26 cells in the middle region having a length of 2.0 cm. An additional cell with the length of 0.3 cm is used at the bottom of the fuel meat region, providing compatibility with the discretization approach used in the neutronic power calculations.

The computational mesh used for LEU analyses remains the same as described in Section 5.2.1, with the exception of the axial mesh structure in the fuel plate. The boron regions have been removed and the axial length of the fuel meat is now 89.3 cm as described above in Section 5.4.1. The axial mesh in the fuel meat was refined in a manner similar to the HEU refinement described above. The total number of axial cells in the LEU fuel meat was increased to 60 cells, with 15 cells at the top and 14 cells at the bottom of the fuel meat having a length of 1.0 cm and 30 cells in the middle region having a length of 2.0 cm. An additional cell with the length of 0.3 cm is used at the bottom of the fuel meat region, providing compatibility with the discretization approach used in the neutronic power calculations.

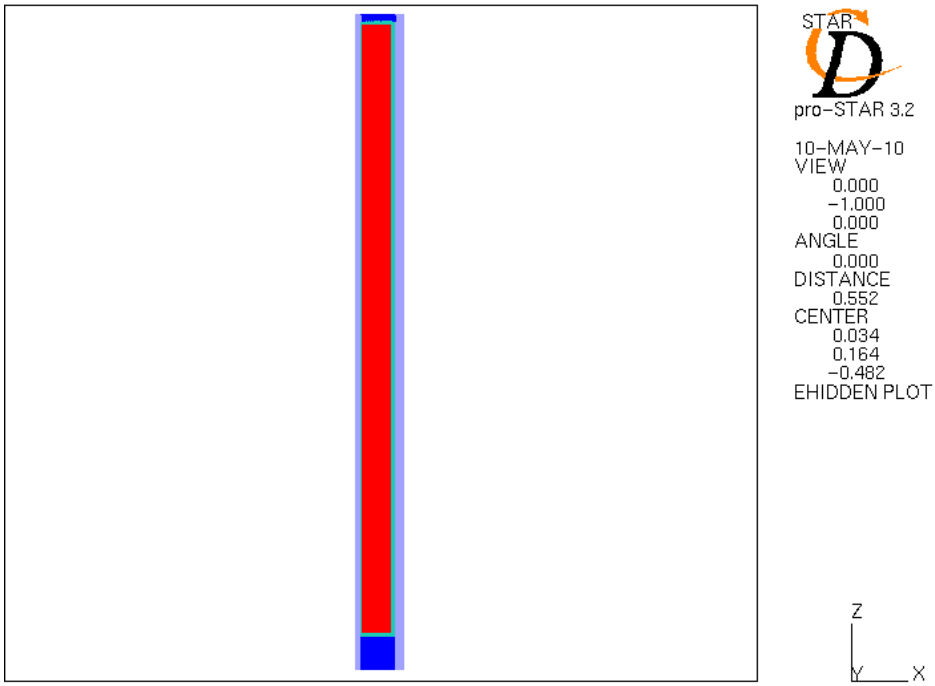

Figure [5.14]: Cross section through the centerline of the LEU fuel plate, viewed from the -y direction illustrating the features of the CFD model: blue - coolant; red - fuel meat; green - cladding; light blue - inner and outer rings

5.4.1.2 Boundary Conditions

For these preliminary analyses of both the LEU and HEU configurations we selected the nominal operating conditions. The boundary conditions remain similar to those described in Section 5.2.3, but small changes have been made, noted below, to provide a more accurate representation of the nominal operating conditions:

Coolant inlet boundary (upper plenum inlet):

Inlet coolant velocity: -10.118 m/s (corresponding to a volumetric flow rate Q = 2372 m^3/hr and to -17.385 m/s inter-plate coolant velocity)

Inlet coolant temperature: 30 C

Coolant outlet boundary (lower plenum outlet):

Boundary type: outlet

Outlet pressure: 4.36 bar (absolute)

5.4.1.3 Power Source

The power source distribution in the LEU fuel meat was provided by separate neutronic calculations for a mesh with 179 cells in the axial direction (178 cells with a length of 0.5 cm and one cell with the length of 0.3 cm), 11 cells in the plate "radial" direction (i.e., from inner edge of fuel meat to outer edge of fuel meat) and one cell covering the thickness of the fuel meat. A procedure was developed to remap the neutronic distribution on the CFD fuel meat mesh described above, with 60 axial cells, 30 cells in the plate "radial" direction and 4 cells across the fuel meat thickness. This procedure ensures that the total power used in the CFD analysis is the same as the total power predicted by the neutronic calculations. Neutronic calculations predict that the total LEU RHF power generated in the LEU fuel meat is 54.39 MW for a core producing 57 MW nuclear. This power was increased in the CFD calculations described in this section to 55.06 MW, in order to account for the additional power generated in the coolant and structures. In the CFD calculations all of the 55.06 MW was assumed to be generated in the fuel meat.

A similar procedure was used for HEU analyses described below. The total power modeled in the refined HEU analysis was 53.6 MW for a core producing 57 MW nuclear, in order to be consistent with the existing SAR. That power breakdown was described in the SAR as 53.0 MW generated in the fuel meat and 0.6 MW generated in the coolant and structures. In the CFD calculations all the 53.6 MW was assumed to be generated in the fuel meat.

The axial power distribution for the LEU Relocated Poison Configuration and HEU fuel plates, at the outermost radial cell, is shown in Figures 5.15 and 5.16, respectively.

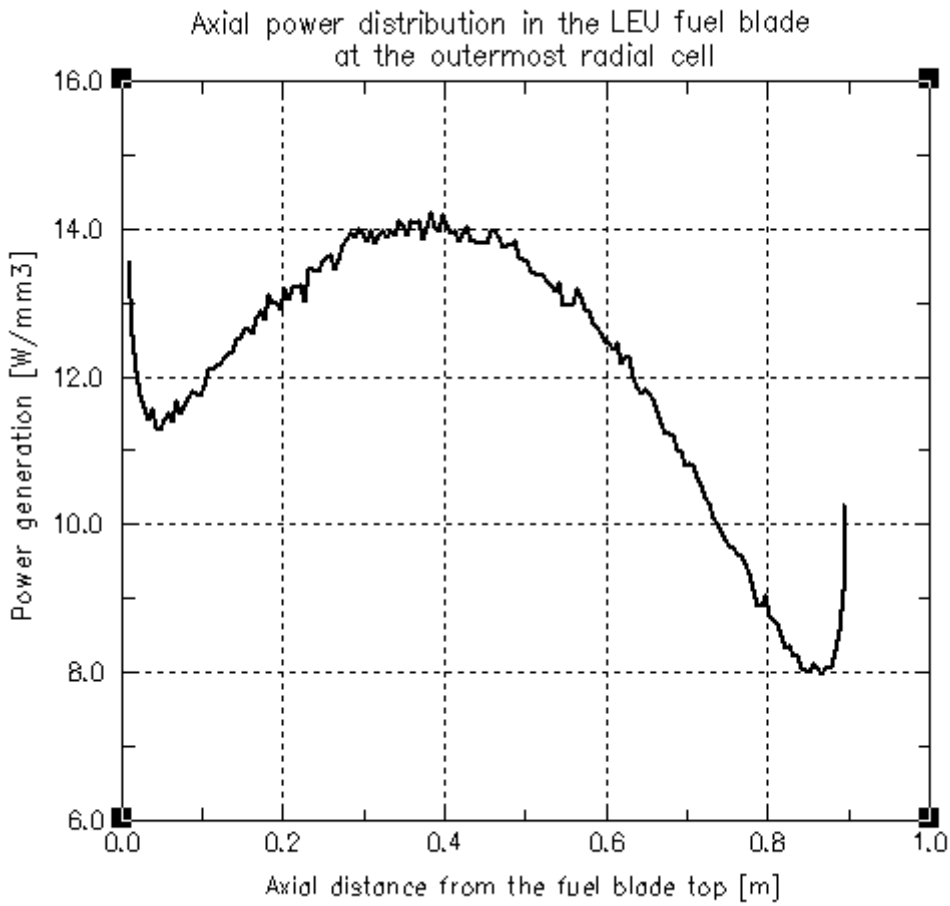

Figure [5.15]: Axial power distribution in the LEU Relocated Poison Configuration fuel meat at the outermost radial cell

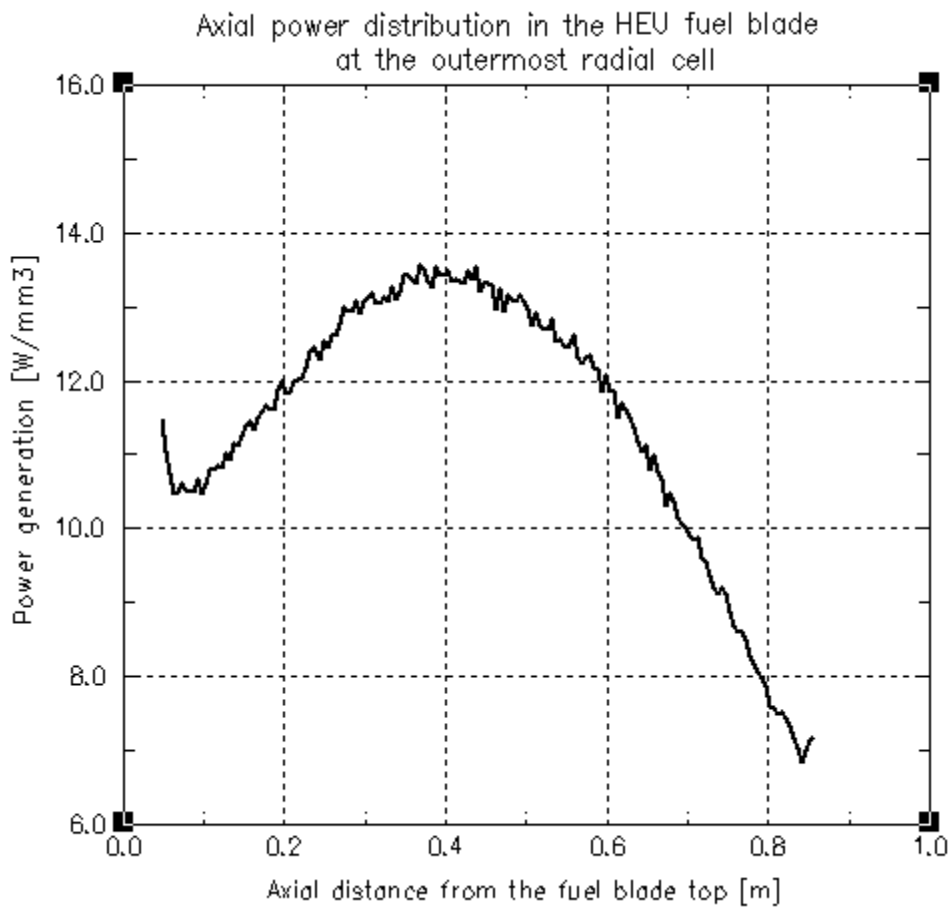

Figure [5.16]: Axial power distribution in the HEU fuel meat at the outermost radial cell

5.4.2 Results of Preliminary LEU RHF Analysis

In this section we present the results of CFD LEU calculations performed with the model described in the preceding sections. These results are compared with corresponding results obtained from the HEU calculations. The HEU analyses were performed with the refined axial discretization described above in Section 5.4.1.1 and using the same nominal conditions as those used in the LEU calculations and described above in Section 5.4.1.2.

5.4.2.1 Coolant and Cladding Temperature Results

The coolant temperature distribution in the coolant cell layer adjacent to the fuel plate is shown in Figure 5.17. The coolant temperature distribution at the wall surface is shown in Figure 5.18. The temperature distribution for the cladding cells at the outer surface of the cladding, adjacent to the coolant, is shown in Figure 5.19. The following maximum temperatures are observed:

Maximum LEU coolant cell temperature:
T(coolant cell, max) = 343.2 K (70.05 C)

Maximum LEU coolant wall temperature:
T(coolant, wall surface, max) = 379.11 K (105.96 C)

Maximum LEU cladding surface cell temperature:
T(cladding surface cell, max) = 380.0 K (106.85 C)

The best measure of the coolant maximum temperature is provided by the coolant wall temperature T(coolant, wall surface). This temperature is calculated by the code using the law of the wall and is expected to show little sensitivity to the coolant cell size, as long as the y^+ (the non-dimensional distance from the wall to the first grid point) values remain in a reasonable range (usually 30-50). In this calculation with 20 cells across the coolant channel the y+ values are in the range 27-38 for most of the wall cells in the inter-plate channel. The maximum cladding surface temperature is only 0.8 K higher than the maximum coolant temperature and provides a reliable upper bound. The maximum coolant temperature in the cells adjacent to the cladding is - as expected - substantially lower than the coolant wall temperature. The use of this temperature is not recommended for safety studies, as it would take a very fine mesh near the cladding surface to bring it close to the actual coolant wall temperature.

The LEU temperatures are compared with the corresponding HEU temperatures in Table 5.1. The HEU temperatures are slightly different from the HEU presented in section 5.3.1 due to the modified nominal conditions used, which are consistent with the nominal conditions used for the LEU analysis. The LEU maximum coolant wall surface temperature is 2.56 C higher than the corresponding HEU temperature.

Table [5.1]: Comparison of LEU and HEU coolant and cladding surface temperatures

	LEU	HEU
T(coolant cell, max) [K]	343.20	339.20
T(coolant, wall surface, max) [K]	379.11	376.55
T(cladding surface cell, max) [K]	380.00	377.50

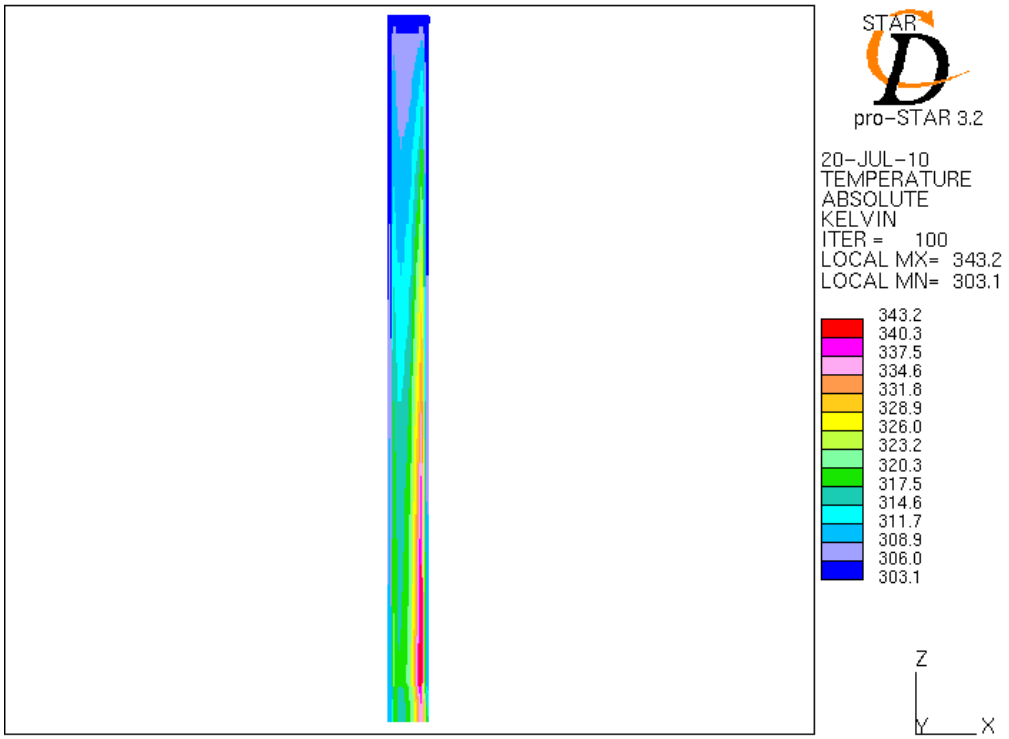

Figure [5.17]: Coolant temperatures [K] at the center of cells adjacent to the LEU fuel plate surface, view from the -y direction. Maximum temperature 343.2 K

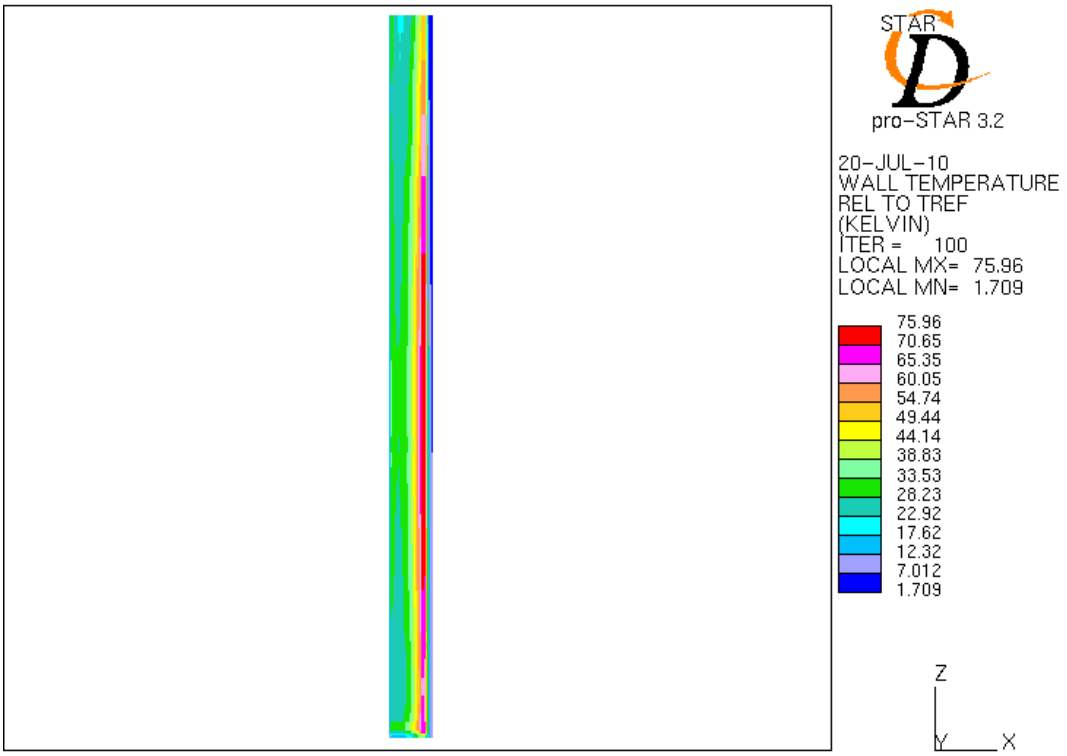

Figure [5.18]: Coolant temperatures [K] at the fuel plate surface, view from the -y direction. Maximum temperature 379.11 K (105.96 C), TREF = 303.15 K

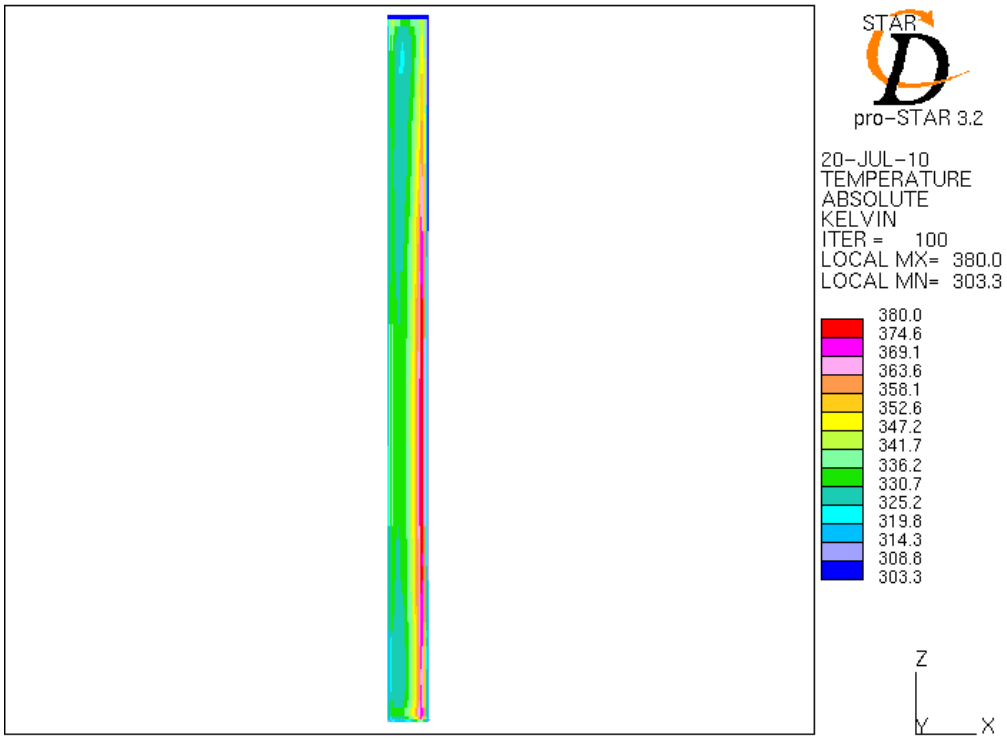

Figure [5.19]: Cladding temperature [K] at the center of cells at plate surface (adjacent to coolant), view from the -y direction. Maximum temperature 380.0 K (106.85 C)

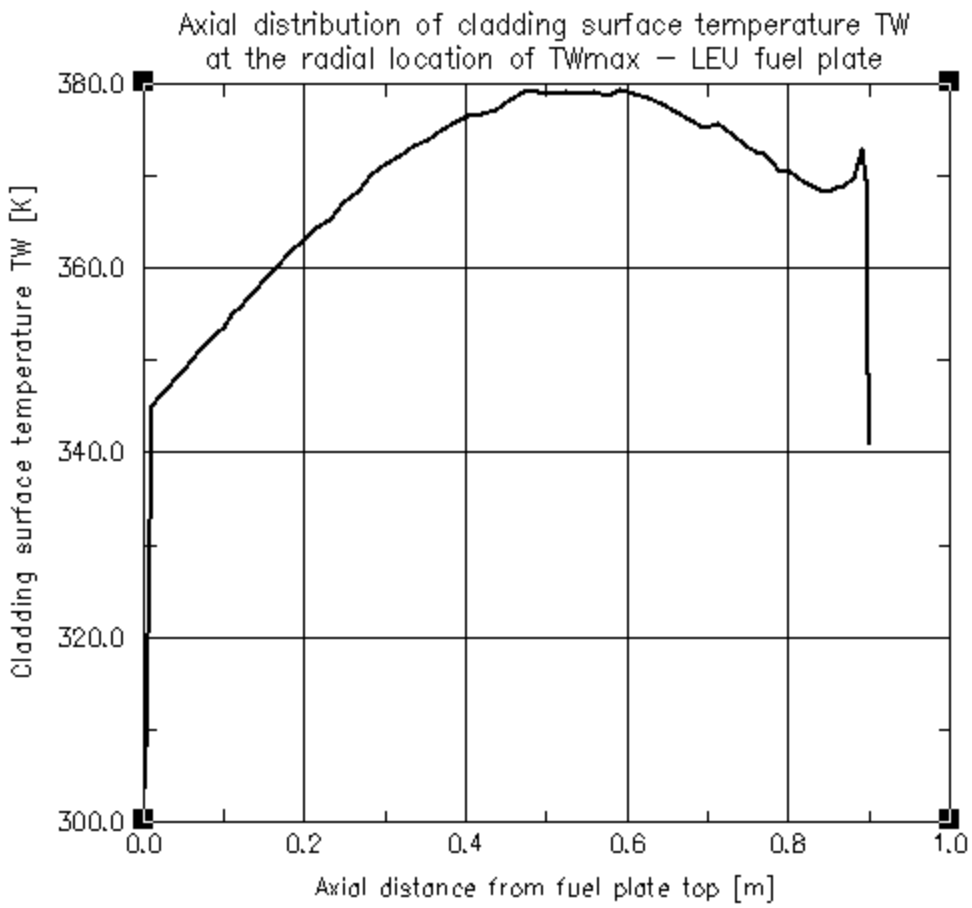

Figure [5.20]: Axial distribution of cladding surface temperature at the radial location of T(wall surface, max) for the LEU fuel plate

The axial variation of the coolant temperature at the cladding surface at the radial location of the maximum temperature is shown for the LEU Relocated Poison Configuration in Figure 5.20 and for the HEU fuel in Figure 5.21. The maximum wall surface temperature occurs for the LEU fuel plate at z = -0.59 m from the top of the plate, at a radial location R = 19.175 cm. For the HEU, the location of the maximum surface temperature is at z = -0.525 m from the top of the plate and at the same radial location. For both LEU and HEU the maximum occurs on the outer side of the curved fuel plate (relative to the center of curvature). However, a similar local maximum temperature occurs on the inner side of the plate, which is only 0.1 C lower.

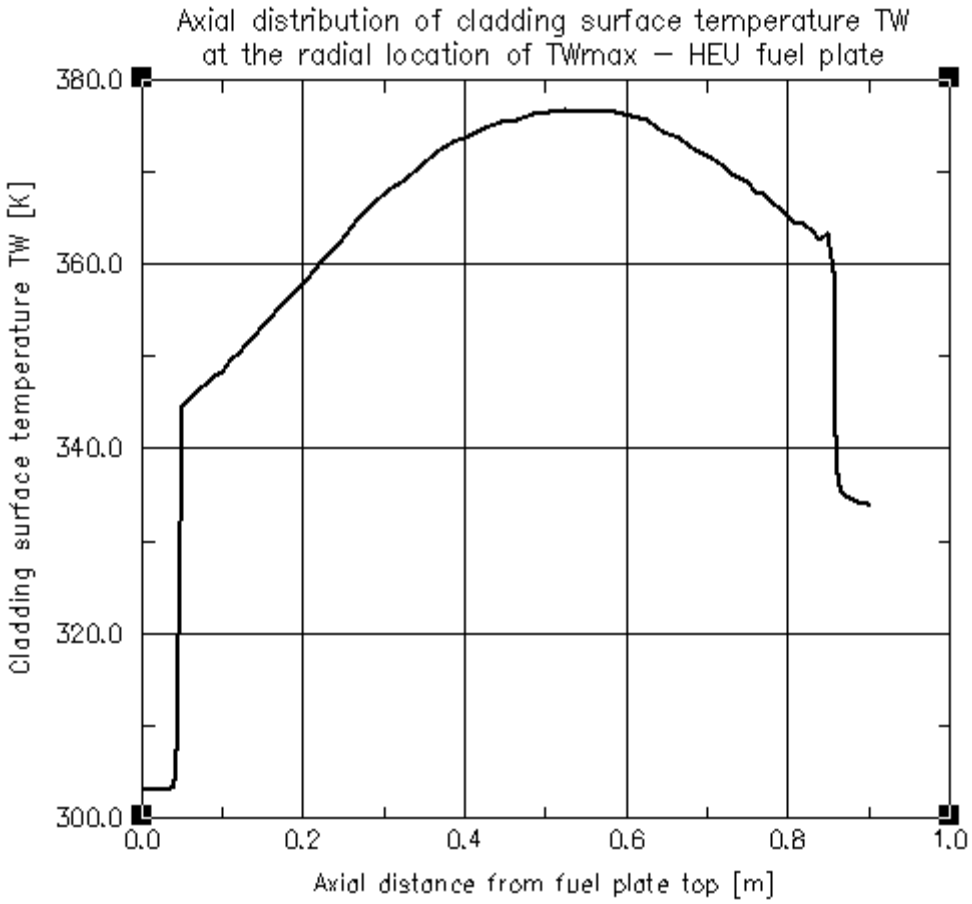

Figure [5.21]: Axial distribution of cladding surface temperature at the radial location of T(wall surface, max) for the HEU fuel plate

5.4.2.2 Predictions of Margin to Boiling

The margin to saturation, onset of nucleate boiling (ONB), and fully developed nucleate boiling (FNB) have also been examined for the LEU fuel configuration and compared with the corresponding margins for the HEU fuel configuration. To determine the minimum margin to saturation DTsat, we conducted a global search over all the coolant cells adjacent to the cladding surface. For each cell the local coolant pressure was used to determine the corresponding D2O saturation temperature Tsat and the margin to saturation was calculated as:

DTsat = Tsat - Tcoolant, wall surface 5.1

A similar procedure was used to determine the minimum DTonb, the margin to ONB, and the minimum DTfnb, the margin to FNB:

DTonb = Tonb - Tcoolant, wall surface 5.2

DTfnb = Tfnb - Tcoolant, wall surface 5.3

where Tonb and Tfnb are the onset of nucleate boiling and full nucleate boiling temperatures and are calculated as:

Tonb = Tsat + DTsuperheat, onb 5.4

Tfnb = Tsat + DTsuperheat, fnb 5.5

The value of DTsuperheat, fnb was calculated using an established nucleate boiling wall superheat correlation, the Jens-Lottes correlation [Ref. 16] which was also used in the French HEU RHF analysis [Ref. 17]. The wall superheat according to the Jens-Lottes correlation, DTsuperheat, jl is calculated as:

$$DT_{superheat,jl} = 0.79 \frac{q''^{0.25}}{\exp(\frac{P}{6.2})} \qquad 5.6$$

where:

q’’ = heat flux [W/m2]
P = pressure [MPa]
DT = superheat temperature difference [C]

The Jens-Lottes correlation has been developed for high pressure boiling heat transfer and its applicability to the RHF conditions and CFD RHF analyses should be further investigated. It was included in the analyses described in this section for comparison with the results obtained by ILL CFX analyses of the RHF reactor [Ref. 17].

The value of DTsuperheat, onb was calculated using the widely used Bergles-Rohsenow correlation [Ref. 18]. The ONB superheat according to the Bergles-Rohsenow correlation, DTsuperheat, br is calculated as:

$$DT_{superheat,br} = 0.556(\frac{q''}{1082P^{1.156}})^{0.463P^{0.0234}} \qquad 5.7$$

where:

q’’ = heat flux [W/m2]
P = pressure [bar]
DT = superheat temperature difference [C]

The Bergles-Rohsenow correlation was obtained for water over the pressure range 1-138 bar, which includes the RHF operating pressure range. Bergles-Rohsenow results are also more conservative than those obtained with the Jens-Lottes correlation and we recommend using this correlation for the evaluation of the RHF reactor margin to ONB. We present below the LEU and HEU results for both correlations. When calculating the local DT superheat with equations 5.6 or 5.7, the local heat flux and coolant pressure was used for each coolant cell adjacent to the cladding surface.

The axial variation of the margins to saturation, FNB, and ONB, at the radial location of the global minimum margin to saturation is shown in Figure 5.22 for the LEU fuel plate. The corresponding curves for the HEU plate are shown in Figure 5.23.

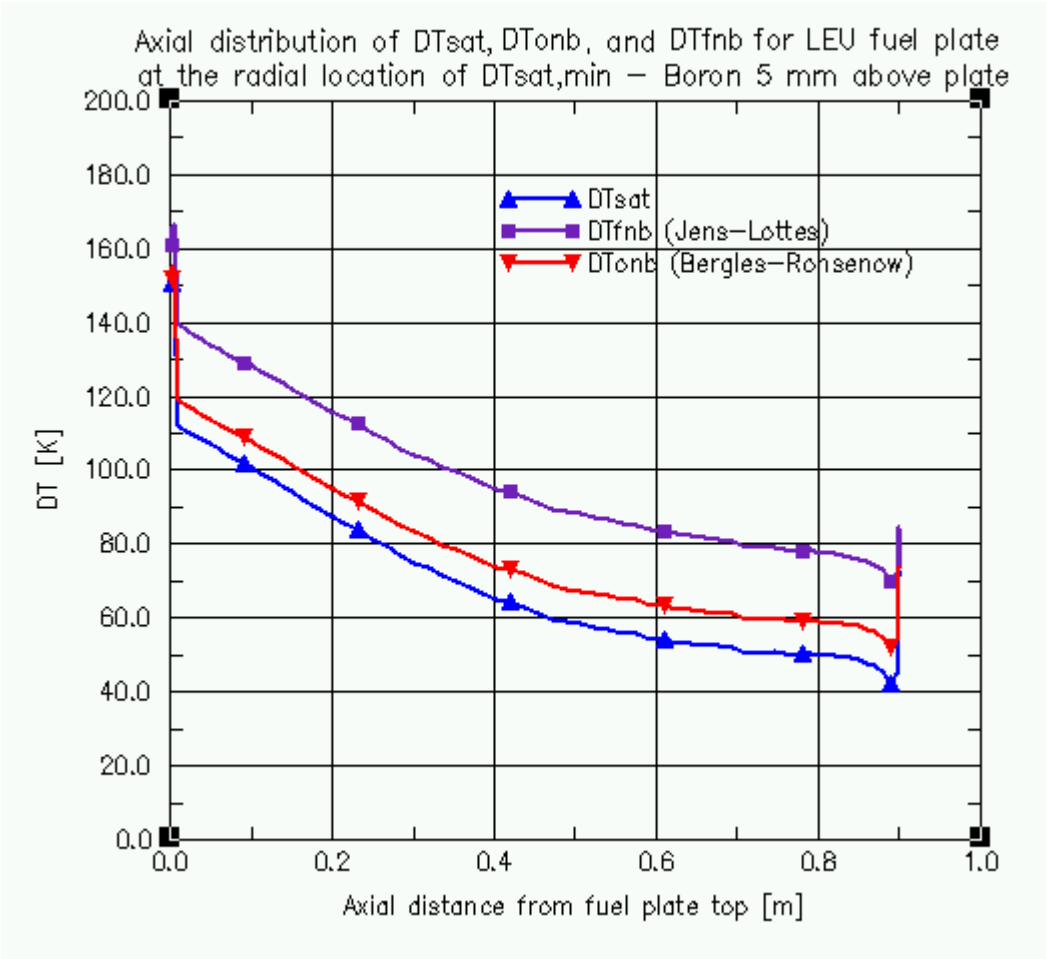

Figure [5.22]: Axial distribution of DTsat, DTonb, and DTfnb for the LEU Relocated Poison Configuration

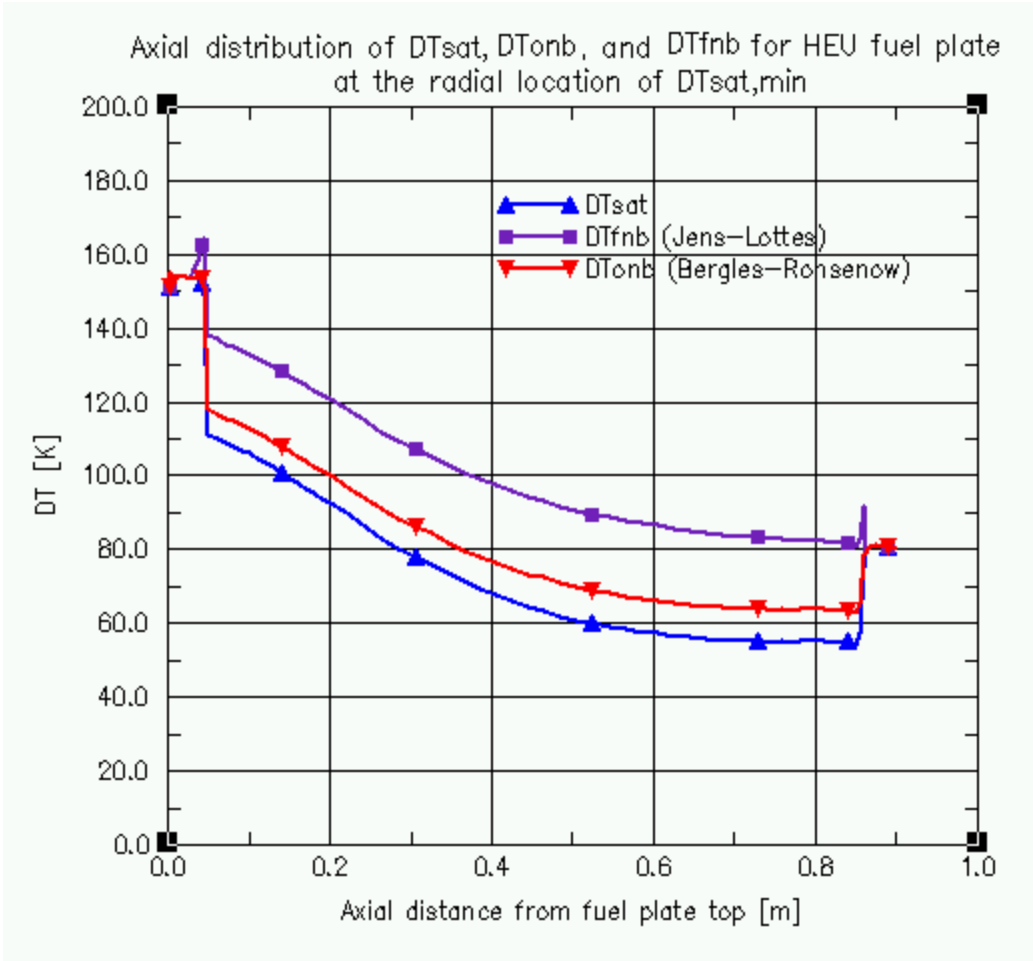

Figure [5.23]: Axial distribution of DTsat, DTonb, and DTfnb for the HEU fuel plate

The minimum margins to saturation, FNB and ONB for the LEU and HEU fuel plates are summarized in Table 5.2. The margins to both ONB and FNB for LEU are lower by approximately 10 K than the same margins for the HEU fuel, when using either the Bergles-Rohsenow correlation or the Jens-Lottes correlation. The minimum value for DTsat and DTonb occurs for the LEU fuel at z = - 0.890 m from the top of the fuel plate (i.e. at the bottom of the fuel meat region), at the radial location R = 191.75 mm. For the HEU fuel plate the minimum margins occur at z = -0.850 m from the top of the fuel plate (i.e. at the bottom of the fuel meat region), at the radial location R = 191.75 mm.

Table [5.2]: Minimum margins to saturation, ONB and FNB for the LEU and HEU nominal cases

	LEU	HEU
DTsat [K]	42.2	54.2
DTonb (Bergles-Rohsenow) [K]	52.0	62.7
DTfnb (Jens-Lottes) [K]	70.3	79.4

The lower margins to saturation, ONB, and FNB for the LEU fuel plate are due in part to the higher neutronic flux at the bottom of the fuel meat as shown in Figure 5.15 and in part to the lower local coolant pressure, since the fuel meat region extends further down and is closer to the expansion at the entrance to the lower plenum than in the case of the HEU fuel plate. However, the LEU fuel plate maintains a substantial margin to ONB, 52.0 K according to the Bergles-Rohsenow correlation.

It is noted that although in the nominal case studied the minimum margin to ONB occurs at the bottom of the fuel meat region, this location depends on the characteristics of the case analyzed. In the nominal case the coolant flow rate is sufficiently high so that the pressure drop dominates the axial power generation decrease towards the bottom of the plate. In a case with a lower flow rate however, the pressure drop is lower and the axial power profile can become dominant, causing the location of the minimum margin to ONB to move up towards the center of the fuel plate where the heat flux is higher.

Following a procedure used in previous RHF safety studies at ILL, we performed a series of LEU and HEU analyses, increasing gradually the power of the reactor in order to determine the power level at which the margin to saturation, ONB, and FNB become zero. The variation of these margins with the RHF core power level for the LEU and the HEU fuel is illustrated in Figures 5.24 and 5.25 respectively.

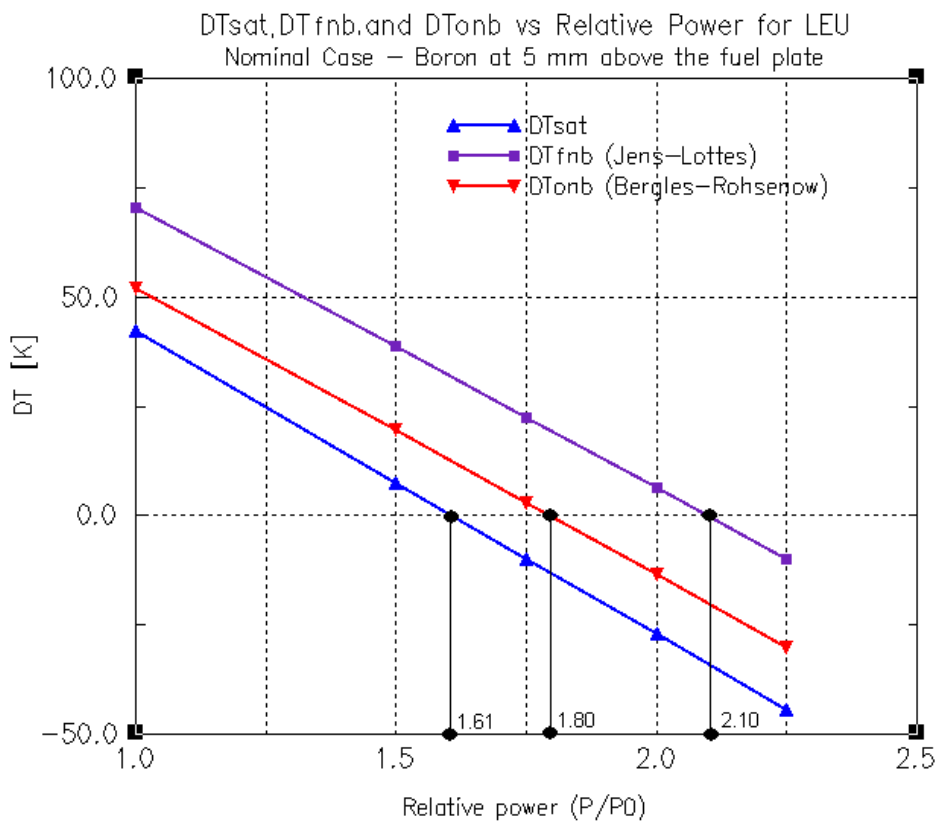

Figure [5.24]: Variation of the margins to saturation, ONB and FNB with relative RHF power for the LEU Relocated Poison Configuration (P0 = 55.06 MW)

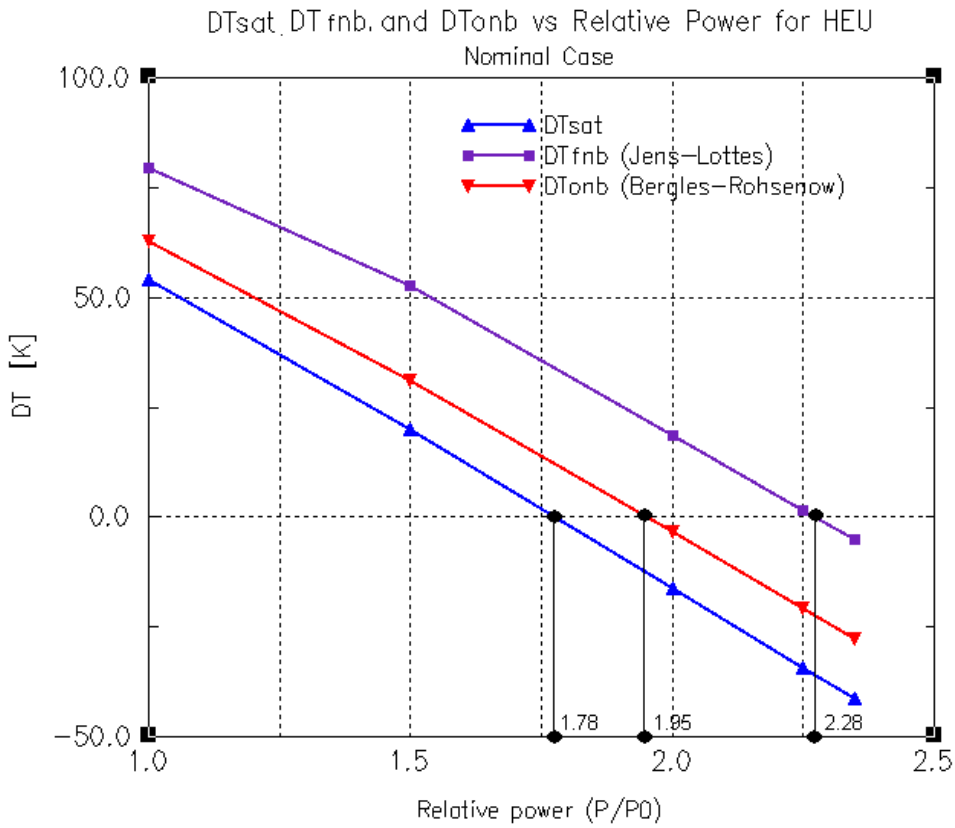

Figure [5.25]: Variation of the margins to saturation, ONB and FNB with relative RHF power for the HEU fuel (P0 = 53.61 MW)

The relative and absolute core power levels at which the saturation, ONB, and FNB margins become zero for the LEU and HEU fuel plates are summarized in Tables 5.3 and 5.4, respectively.

Table [5.3]: Relative RHF core power levels at which the margins to saturation, ONB, and FNB become zero

	LEU	HEU
P (DTsat = 0) / P0	1.61	1.78
P (DTonb, br = 0) / P0	1.80	1.95
P (DTfnb, jl = 0) / P0	2.10	2.28

Table [5.4]: Absolute RHF core power levels at which the margins to saturation, ONB, and FNB become zero

	LEU	HEU
P (DTsat = 0) [MW]	88.65	95.43
P (DTonb, br = 0) [MW]	99.11	104.54
P (DTfnb, jl = 0) [MW]	110.12	122.23

Following the ILL approach as described in the SAR [Ref. 3], we have used the power levels in Table 5.4 to evaluate the margin relative to Vr, the power level at which a scram is initiated. The margin relative to Vr is calculated as:

$$M(V_r) = 100\frac{(0.95P_{boiling} - V_r)}{V_r} \qquad 5.8$$

where:

P(boiling) = power level at which the saturation or ONB margin becomes zero [MW] (the factor 0.95 takes into account the global power uncertainty)
Vr = 64.13 MW = power level at which scram is initiated for LEU and HEU
M(Vr) = margin relative to Vr, [%]

The margins relative to Vr for the LEU and HEU fuel configurations are summarized in Table 5.5. It is noted that the HEU margin to FNB using the Jens-Lottes correlation, 81%, is very close to the corresponding value of 82% obtained with the CFX code in an independent ILL CFD analysis [Ref. 17]. The LEU margin to ONB based on the Bergles-Rohsenow correlation is 46.7%. This value is 15% lower than the corresponding HEU margin to ONB, but indicates that a substantial margin to ONB exists for the nominal LEU RHF case analyzed.

Table [5.5]: Margin to Saturation, ONB, and FNB relative to Scram Power, Vr, in%

	LEU	HEU
M(Vr) (DTsat = 0) [%]	31.2	41.3
M(Vr) (DTonb, br = 0) [%]	46.7	54.8
M(Vr) (DTonb, jl = 0) [%]	71.0	81.0

5.5 Thermal-Hydraulic Conclusions

A script-based model for the CFD analysis of RHF with the STAR-CD code has been developed. This script allows the modification of geometric parameters, mesh size and physical parameters in order to study the sensitivity of the results to various perturbations. Preliminary analyses of the HEU RHF reactor were performed to evaluate the model performance. The maximum coolant temperature at the cladding surface is the best prediction of the coolant maximum temperature and the maximum temperature of the cladding cells at the interface with the coolant provides a reliable upper limit. The results of the HEU preliminary calculations were compared with corresponding results obtained independently with the CFX code and reasonably good agreement was obtained.

A model of the recommended LEU Relocated Poison Configuration fuel plate was developed and analyses of the RHF thermal-hydraulic characteristics were performed for nominal operating conditions. The maximum cladding surface temperature and the margins to saturation, ONB, and FNB for the LEU fuel were determined and compared with the corresponding values for the HEU fuel plate. The results show that the LEU margin to ONB, relative to the scram power level Vr, is approximately 15% lower than the corresponding margin for HEU fuel plate but remains still high at 46.7%, indicating that a substantial margin to ONB exists for the recommended LEU Relocated Poison Configuration case analyzed.

VI Summary of Differences between HEU and LEU Design

The goal of this section is to summarize the main results obtained in the previous parts of this report and emphasize the difference between the current HEU and the recommended LEU design. Figure 6.1 shows the scheme and the dimensions of an HEU plate and the recommended LEU design (plate + boron poison belt). Table 6.1 compiles the main parameters evaluated for both design.

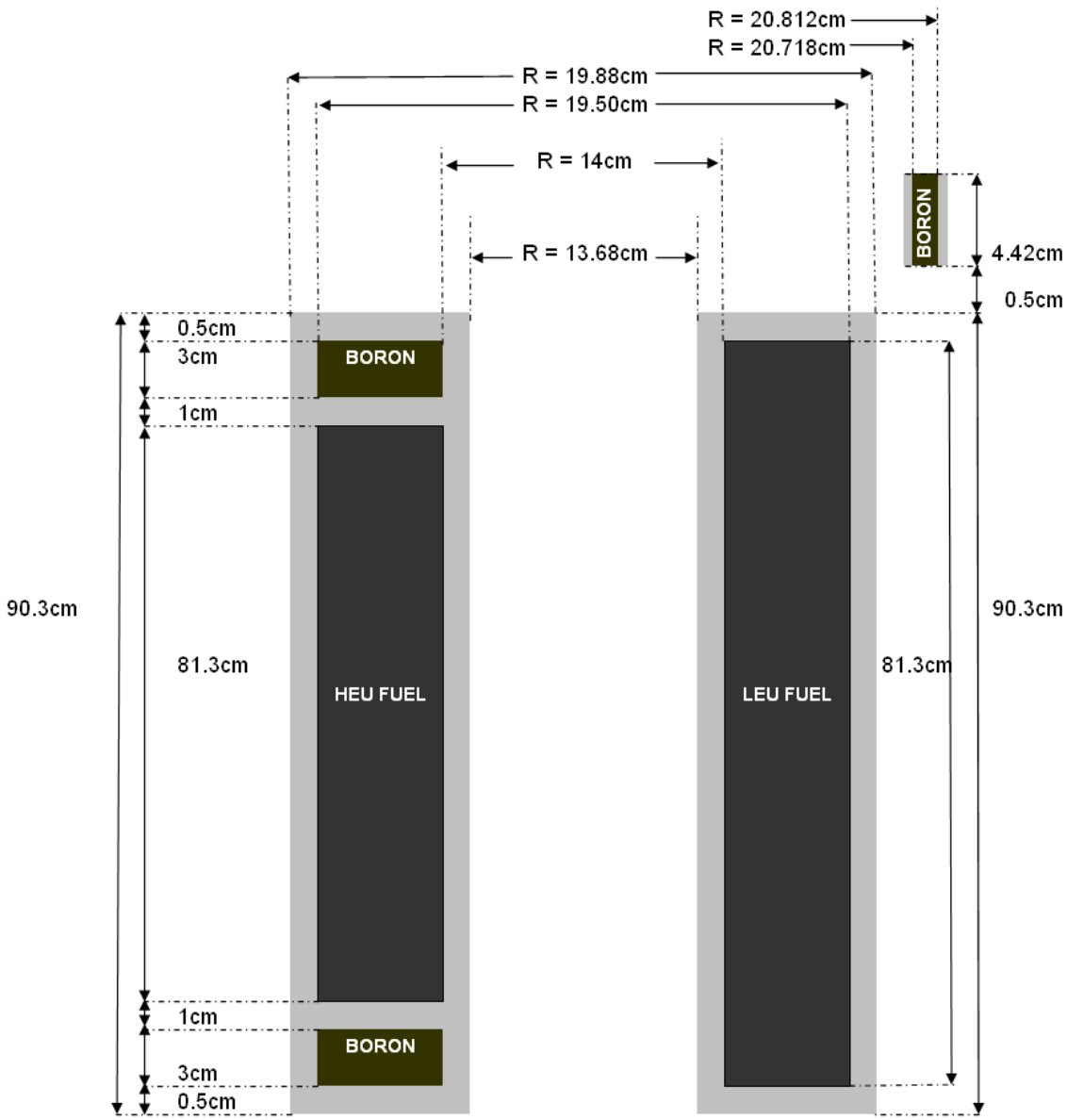

Figure [6.1]: On the left, scheme and dimensions of a current HEU plate. On the right, scheme and dimensions of the recommended LEU plate with the boron poison belt.

Table [6.1]: Main characteristics of current HEU and recommended LEU design

	HEU	**recommended LEU**
Number of plates	280	280
Plate thickness (mm)	1.270	1.270
Fuel Meat thickness (mm)	0.510	0.510
Fuel Meat length (cm)	81.30	89.30
^{235}U enrichment (%)	93.00	19.95
^{235}U density (g/cm^3)	1.096	1.525
Core mass ^{235}U (kg)	8.568	13.10
Core mass of poison (^{10}B) (g)	5.770	2.070
Beff BOC ± σ (pcm)	685 ± 28	657 ± 28
Beff EOC ± σ (pcm)	not calculated	658 ± 31
Control rod worth ± σ (pcm)	17,048 ± 32	15,289 ± 52
Shutdown margins accidental scenario ± σ (%Δk/k)		
SR 1 withdrawn	not calculated	1.220 ± 0.044
SR 2 withdrawn	not calculated	2.905 ± 0.036
SR 3 withdrawn	not calculated	1.249 ± 0.048
SR 4 withdrawn	not calculated	1.130 ± 0.037
SR 5 withdrawn	not calculated	0.942 ± 0.040
	HEU (57 MW)	**recommended LEU (57MW)**
Total power in the meat (MW)	53.9 ± 0.6	54.4 ± 0.6
Maximum heat flux (W/cm^2)	437 ± 3	470 ± 4
Margin to ONB relative to Vr (%) *using Bergles-Rohsenow correlation*	55	47
Margin to FNB relative to Vr (%) *using Jens-Lottes correlation*	81	71
Cycle length (days)	45	47.5
max. Brightness HCS (n/cm²/s/sterad)x10^{-10}	1.14	1.02
max. Brightness VCS (n/cm²/s/sterad)x10^{-10}	0.87	0.78
	HEU (52 MW) ***current condition of operation***	**recommended LEU (57MW)**
Cycle length (days)	49.5	47.5
max. Brightness in HCS (n/cm²/s/sterad) x 10^{-10}	1.04	1.02
max. Brightness in VCS (n/cm²/s/sterad) x 10^{-10}	0.79	0.78

VII Conclusions

This report documents the calculational basis for the ILL determination that it is technically feasible to convert the RHF to LEU fuel [Ref 19].

The analyses presented in this report show that the ILL reactor, the RHF, can be operated safely with the new LEU fuel element if the UMo fuel can be qualified and manufactured. Nevertheless, as has always been true for reactor conversion projects, full safety analyses need to be performed and regulatory approvals received before the reactor will be able to convert.

It is important to note that the UMo dispersion fuel is not yet qualified or commercially available. The partnership of the GTRI Reactor Conversion Program with the LEONIDAS Advanced Technology Group is a key step toward qualifying the UMo Dispersion Fuel and toward clarifying the specifications that will be supported for this new fuel. The positive results reported at this time are predicated on the best information available to date for fuel performance and feasibility.

The technical analyses that we have completed indicate that the use of the LEU Relocated Poison fuel element design should maintain the RHF performance at a high level. Indeed, we have shown in this report that the thermal safety margins and shutdown safety margins are maintained. The predicted cycle length with LEU is very close to the current HEU operation, so the proposed LEU design maintains an efficient and effective use of the facility. Finally, we have shown that the brightness in the cold sources decreases by only 1-2% relative to typical current HEU operations, so the conversion should not have a significant impact the experiments carried out in the Institute.

With the new design, the total amount of fuel has been increased without changing the external plate dimensions by relocating the burnable poison along the outer radius of the outer tube. AREVA CERCA, the fuel manufacturer, must determine the technical and economic feasibility of this new proposed fuel element.

Finally, we must also note that the economic feasibility of conversion cannot be established until commercial availability of the fuel has been developed, including credible fuel cost projections. ILL and GTRI must maintain close contact in order to pursue analyses and potential redesigns once key factors are better understood.

Acknowledgements

This report was produced by Argonne staff working in close collaboration with the ILL. In particular, the authors express their gratitude to Herve Guyon, Yoann Calzavara, and Frederic Thomas for sharing their expertise and efforts.

References

[1] S.C. MO, J.E. MATOS "Conversion feasibility studies for the Grenoble high flux reactor" XII RERTR International meeting, 1989

[2] M. RIPERT et al. "IRIS3 experiment – status and results of thickness increases" 10th Int. Topical meeting on RRFM; Sofia, 30 April – 3 May 2006.

[3] RHF Safety Analytic Report, released 2004

[4] G. CAMPIONI, A. ENTRINGER "Realisation d'etudes sur le RHF de Grenoble – calculs sur le Coeur standard" CEA SERMA report, SERMA/LPEC/RT/07-4183/A

[5] "MCNPX 2.6.0 User's Manual". Los Alamos National Laboratory. LA-CP-07-1473. 2008

[6] W. HAECK "VESTA User's Manual Version 2.0.0". Institut de Radioprotection et de Surete Nucleaire. DSU/SEC/T/2008-331 - Indice A. 2009

[7] "MCNP - A General Monte Carlo N-Particle Transport Code, Version 5". Los Alamos National Laboratory. Volume I LA-UR-03-1987 & Volume II LA-CP-03-0245. 2003 revised 2005.

[8] J.G. STEVENS "The REBUS-MCNP Linkage". Argonne National Laboratory. ANL/RERTR/TM-08-04. 2008

[9] Y. CALZAVARA, S. FUARD "Evaluation of measurements performed on the French high flux reactor (RHF)", RHF-HWR-RESR-001 CRIT, International Handbook of Evaluated Reactor Physics Benchmark Experiments, Nuclear Energy Agency (OECD), 2009.

[10] A. BERGERON "Conversion of RHF to a low enriched uranium fuel – Neutronic calculations with VESTA", IRSN report DSU/SEC/T/2009-346

[11] A. DOS SANTOS et al. "A proposal of a benchmark for Beff, Beff/Λ and Λ of thermal reactors fueled with slightly enriched uranium" Annals of Nuclear Energy 33 (2006) 848-855

[12] Y. CALZAVARA, A. BERGERON "Etude neutronique de l'impact d'un nouveau combustible en UMo sur les performances du RHF – Jalon Février 2010' ILL internal memo. 09/017

[13] Y. CALZAVARA. Private communications

[14] STAR-CD Version 3.20 Methodology Manual, CD-adapco, UK (2004)

[15] F. THOMAS, "Etude thermo-hydraulique d'une lame d'eau lourde reacteur", ILL report, September 2009

[16] W. JENS and P. LOTTES, “Analysis of heat transfer, burnout, pressure drop and density data for high-pressure water”, ANL-4267, 1951

[17] F. THOMAS,"Thermo-hydraulique d'une lame d'eau lourde", ILL presentation, March 2010

[18] A. BERGLES and W. ROHSENOW, "The Determination of Forced-Convection Surface-Boiling Heat Transfer", Journal of Heat Transfer, August 1964

[19] R. WAGNER and H. GUYON, letter to Dr. Parrish Staples, DIR-RW/pg 09/22, 1 October 2009

Nuclear Engineering Division
Argonne National Laboratory
9700 South Cass Avenue, Bldg. 208
Argonne, IL 60439-4842

www.anl.gov

Argonne National Laboratory is a U.S. Department of Energy
laboratory managed by UChicago Argonne, LLC